DISSERTATION

Hepatocellular carcinoma: establishing imaging biomarkers for non-invasive subtype differentiation with Gd-EOB-enhanced MRI

Hepatozelluläres Karzinom: Etablierung bildbasierter Biomarker für nicht-invasive Subtypendifferenzierung mittels Gd-EOB-verstärktem MRT

zur Erlangung des akademischen Grades
Doctor medicinae (Dr. med.)

vorgelegt der Medizinischen Fakultät

Charité – Universitätsmedizin Berlin

von

Sebastian Halskov

Erstbetreuer*in: PD Dr. med. T. A. Auer

Datum der Promotion: 30.06.2024

To my parents

Preface

Partial results presented in this dissertation form part of a research manuscript "*Gd-EOB MRI for HCC Subtype Differentiation in a Western Population according to the 5th Edition of the World Health Organization Classification"*, which has been submitted to European Radiology on 29.03.2023, accepted on 10.04.2023 and published on 28.04.2023. These findings have also been presented by Sebastian Halskov at the European Congress of Radiology 2023 in Vienna, Austria, in the presentation entitled *"The value of Gd-EOB MRI for HCC subtype differentiation in a western population according to the 5th edition of the World Health Organization (WHO) classification"*, for which the *"Best Research Presentation Abstract Award"* within the topic "Abdominal and Gastrointestinal" was awarded. A detailed description is provided in ***"13 Declaration of contributions to publications"***.

Table of Contents

1 List of abbreviations 8
2 List of figures 10
3 List of tables 12
4 Abstract 13
5 Abstract (German) 15
6 Introduction 17
6.1 Epidemiology 18
6.1.1 Primary liver cancer 18
6.1.2 Hepatocellular carcinoma 18
6.1.3 Risk factors for HCC 19
6.2 Hepatocarcinogenesis 23
6.2.1 Overview of mechanisms 23
6.2.2 Chronic inflammation leading to liver cirrhosis 24
6.2.3 Dysplastic transformation of hepatocytes 26
6.2.4 Role of the tumor microenvironment 28
6.2.5 Heterogeneity of HCC 29
6.3 Staging of HCC according to the Barcelona Clinic Liver Cancer strategy 30
6.4 Subtypes of HCC according to the WHO 31
6.4.1 Overview of subtypes 31
6.4.2 Potential of subtype classification 32
6.4.3 Current limitations 32
6.5 Diagnostics of HCC 33
6.5.1 Overview of diagnostics 33
6.5.2 Percutaneous liver biopsy 33
6.5.3 Principles of imaging of HCC 34
6.5.4 Magnetic resonance imaging 35
6.5.5 Contrast agents for MRI of the liver 36

6.5.6 Predicting histopathology and prognosis using Gd-EOB-enhanced MRI ... 38
6.5.7 Limitations of HSCA ... 39
6.5.8 Liver Imaging Reporting and Data System (LI-RADS) ... 39
6.5.9 Surveillance of high-risk patients ... 41
6.6 Literature review on WHO subtypes of HCC ... 42
6.6.1 Steatohepatitic HCC ... 42
6.6.2 Macrotrabecular massive HCC ... 43
6.6.3 Clear cell HCC ... 45
6.6.4 Chromophobe HCC ... 46
6.6.5 Scirrhous HCC ... 48
6.6.6 Fibrolamellar HCC ... 49
6.6.7 Lymphocyte-rich and granulocyte-rich HCC ... 51
6.7 Purpose of this study ... 53
7 Materials and methods ... 54
7.1 Study design ... 54
7.2 Patients ... 54
7.3 Reference standard: histopathological analysis of a surgical specimen ... 55
7.4 Index test: preoperative Gd-EOB enhanced abdominal MRI ... 56
7.5 Statistical analysis ... 59
8 Results ... 61
8.1 Patient characteristics ... 61
8.2 Lesion characteristics ... 66
8.2.1 Unspecific characteristics ... 66
8.2.2 Histopathological analysis ... 66
8.2.3 Radiological lesion characteristics ... 67
8.2.4 Multi-phase imaging: imaging features ... 70
8.2.5 Multi-phase imaging: enhancement ratios ... 70

8.2.6 Multi-phase imaging: signal intensity and heterogeneity, Gd-EOB uptake area 71
8.3 Predictors for NOS and subtypes of HCC 82
9 Discussion 89
9.1 Brief summary of results 90
9.2 Interpretation of results 90
9.2.1 Study cohort 90
9.2.2 Evaluation of the diagnostic accuracy of our tests 91
9.2.3 Subtype-specific interpretation of results 93
9.2.4 Intra-tumor heterogeneity 100
9.2.5 Added value of Gd-EOB-enhanced MRI? 100
9.2.6 Abbreviated MRI protocols for subtype differentiation 102
9.3 Strengths of the study 102
9.3.1 Choice of reference standard 102
9.3.2 Choice of imaging features 102
9.3.3 Size and geography of the cohort 103
9.3.4 Granularity of results 103
9.4 Limitations of the study 103
9.4.1 Surgical cohort 103
9.4.2 Observations per subtype 104
9.4.3 Absence of non-HCC lesions 104
9.4.4 Lack of molecular analysis in subtype determination 105
9.4.5 Internal validation of predictors 105
9.4.6 Selection of predictors and the need for external validation 105
9.4.7 Impact of multiple comparisons 106
9.4.8 Detection bias 107
9.5 Outlook 107

9.5.1 Implications for clinical practice: a new diagnostic strategy 107
9.5.2 Future research: potential role of liquid biopsy 109
10 Conclusion 110
11 References 111
12 Statutory declaration 122
13 Declaration of contributions to publications 123
14 Curriculum vitae 124
15 List of publications by Sebastian Halskov 126
16 Acknowledgements 127
17 Certification of statistics 128

1 List of abbreviations

AASLD	American Association for the Study of Liver Disease
ADC	Apparent diffusion coefficient
AFIP	Armed Forces Institute of Pathology
AFP	Alpha-fetoprotein
ALBI	Albumin-bilirubin index
AMRI	Abbreviated magnetic resonance imaging
APHE	Arterial phase hyperenhancement
ASH	Alcoholic steatohepatitis
AUC	Area under the curve
BCLC	Barcelona Clinic Liver Cancer
CC	Clear cell
CCA	Cholangiocellular carcinoma
CE	Contrast-enhanced
CEUS	Contrast-enhanced ultrasound
CH	Chromophobe
cHCC-CCA	Combined hepatocellular-cholangiocellular carcinoma
CP	Child-Pugh
CT	Computed tomography
DWI	Diffusion-weighted imaging
ECA	Extracellular contrast agents
ECM	Extracellular matrix
ECOG	Eastern Cooperative Oncology Group
FFAs	Free fatty acids
FIB	Fibrolamellar hepatocellular carcinoma
FNH	Focal nodular hyperplasia
FS	Fat saturation
Gd-BOPTA	Gadobenate dimeglumine
Gd-EOB	Gadolinium ethoxybenzyl dimeglumine
GR	Granulocyte-rich
HBP	Hepatobiliary phase
HBP	Hepatobiliary phase
HBV	Hepatitis B virus
HCA	Hepatocellular adenoma
HCC	Hepatocellular carcinoma
HCSA	Hepatocyte-specific contrast agents
HCV	Hepatitis C virus
HDV	Hepatitis D virus
HGDN	High-grade dysplastic nodule
HSC	Hepatic stellate cell
HSCA	Hepatocyte-specific contrast agents
IARC	International Agency for Research on Cancer
IOA	Interobserver agreement

IQR	Inter-quartile range
ITH	Intra-tumor heterogeneity
LGDN	Low-grade dysplastic nodule
LI-RADS	Liver Imaging Reporting and Data System
LR	Lymphocyte-rich
MELD	Model for End Stage Liver Disease
MRI	Magnetic resonance imaging
MTM	Macrotrabecular-massive
NAFLD	Non-alcoholic fatty liver disease
NASH	Non-alcoholic steatohepatitis
NOS	Not otherwise specified
NPV	Negative predictive value
PBC	Primary biliary cirrhosis
PLC	Primary liver cancer
PPV	Positive predictive value
PSC	Primary sclerosing cholangitis
RN	Regenerative nodule
ROC	Receiver operating characteristics
ROI	Region of interest
SC	Scirrhous
SD	Standard deviation
ST	Steatohepatitic
T1w	T1-weighted
T2w	T2-weighted
TERT	Telomerase reverse transcriptase
TME	Tumor microenvironment
US	Ultrasound
WHO	World Health Organization

2 List of figures

19 Figure 1: “The incidence and major etiological factors involved in hepatocarcinogenesis”
23 Figure 2: “‘Multiple-hit’ theory of clinical progression of NAFLD”
25 Figure 3: “Mechanisms of fibrogenesis”
28 Figure 4: “Mechanisms of malignant transformation”
35 Figure 5: “Schematic representation of multistep hepatocarcinogenesis from the perspective of blood supply to the nodule.”
37 Figure 6: “Hemodynamic and OATP expression changes during multistep hepatocarcinogenesis.”
43 Figure 7: Steatohepatitic HCC
44 Figure 8: Macrotrabecular massive HCC
46 Figure 9: Clear cell HCC
47 Figure 10: Chromophobe HCC
49 Figure 11: Scirrhous HCC
51 Figure 12: Fibrolamellar HCC
52 Figure 13: Lymphocyte-rich HCC
55 Figure 14: Results of evaluating 800 consecutive cases for inclusion
58 Figure 15: Scale for subjective rating of Gd-EOB uptake area in the HBP
64 Figure 16: Relative frequencies of steatosis, fibrosis and cirrhosis by subtype
64 Figure 17: Frequencies of risk factors in the study cohort on a per-lesion basis
65 Figure 18: Box-and-whisker plots of the logarithm of AFP by subtype
65 Figure 19: ROC curve of the logarithm of AFP for identifying MTM-HCC
66 Figure 20: Box-and-whisker plots of lesion size by subtype
67 Figure 21: Relative frequency of NOS and each subtype of HCC in the cohort
69 Figure 22: Frequency of tumor invasion of macrovascular invasion by subtype
69 Figure 23: Frequency of intralesional steatosis by subtype
74 Figure 24: Arterial phase hyperenhancement by subtype
74 Figure 25: Portal venous washout appearance by subtype
75 Figure 26: Frequency of non-rim APHE and non-peripheral PVP washout by subtype

75 Figure 27: Frequency of non-rim APHE, non-peripheral PVP washout and HBP hypointensity
76 Figure 28: 74-year-old man with liver fibrosis and no known risk factors for HCC
76 Figure 29: 61-year-old man with liver cirrhosis secondary to alcoholism and diabetes mellitus type II who later underwent liver transplantation
77 Figure 30: Frequency of capsule enhancement in the arterial phase by subtype
77 Figure 31: Enhancement ratio lesion-to-liver during the arterial phase
78 Figure 32: Enhancement ratio lesion-to-liver during the post-arterial phases
78 Figure 33: Predominant signal intensities in the arterial phase by subtype
79 Figure 34: Predominant signal intensities in the portal venous phase by subtype
79 Figure 35: Predominant signal intensities in the venous phase by subtype
80 Figure 36: Predominant signal intensities in the HBP by subtype
80 Figure 37: Gd-EOB uptake area on a 5-point scale by subtype
81 Figure 38: Examples of lesions showing high enhancement in more than 50% of their area in the HBP

3 List of tables

20 Table 1: Risk factors for the development of HCC by category

24 Table 2: Examples of mechanisms of hepatocarcinogenesis

27 Table 3: Stages of dedifferentiation from regenerative nodules to progressed HCC, according to The International Consensus Group for Hepatocellular Neoplasia

31 Table 4: “Characteristics of Variant Hepatocellular Carcinoma (HCC) Subtypes”

40 Table 5: Major imaging features suggesting HCC in Gd-EOB-enhanced MRI according to CT/MRI LI-RADS v2018

57 Table 6: Recorded imaging parameters in Gd-EOB enhanced MRI with possible outcomes and remarks on their measurement

59 Table 7: 5-point scale for subjective rating of intralesional signal intensity in HCC lesions

63 Table 8: Patient characteristics and risk factors in cases included in the study

68 Table 9: Unspecific lesion characteristics among lesions of each subtype

72 Table 10: Imaging features in dynamic T1w-FS phases of Gd-EOB-enhanced MRI in lesions of each subtype

72 Table 11: Mean ratio between lesion enhancement and liver enhancement in each phase of dynamic T1w-FS imaging

73 Table 12: Subjective rating of enhancement patterns and signal intensities in multi-phase T1w-FS imaging in Gd-EOB-enhanced MRI

83 Table 13: Diagnostic accuracy of predictors for NOS-HCC

84 Table 14: Diagnostic accuracy of predictors for FIB-HCC

85 Table 15: Diagnostic accuracy of predictors for ST-HCC

86 Table 16: Diagnostic accuracy of predictors for MTM-HCC

87 Table 17: Diagnostic accuracy of predictors for CH-HCC

87 Table 18: Diagnostic accuracy of predictors for SC-HCC

88 Table 19: Diagnostic accuracy of predictors for CC-HCC

4 Abstract

Background: Hepatocellular carcinoma (HCC) exhibits highly diverse phenotypes, thus complicating diagnostics and prediction of response to therapy. The World Health Organization (WHO) now defines eight subtypes, potentially advancing precision oncology in HCC. However, diagnosing these subtypes typically requires invasive procedures. To explore a non-invasive alternative, we investigated whether imaging features in magnetic resonance imaging (MRI) enhanced with gadoxetic acid (Gd-EOB) are associated with these subtypes.

Methods: We retrospectively included 240 consecutive patients with 262 histopathologically confirmed HCC lesions who underwent surgical resection or liver transplantation at our center from January 2010 to January 2022 and received preoperative Gd-EOB MRI. Two pathologists assigned subtypes to the specimens. Subsequently, two radiologists assessed qualitative and quantitative imaging features in Gd-EOB MRI, and we analyzed their distribution among subtypes. Diagnostic tests were formulated for each subtype, and their performance was evaluated.

Results: The typical enhancement pattern for HCC is common in “Not otherwise specified” (NOS) HCC (88/168, 52%) and uncommon in macrotrabecular massive (MTM) (3/15, 20%), scirrhous (SC) (2/9, 22%) and chromophobe (CH) HCC (1/8, 13%) (**p=0.035**). MTM-HCC was associated with macrovascular invasion (5/16, 31%) (**p=0.033**) and high AFP (median, 397 µg/l (74-5370))(**p<0.001**). Steatohepatitic (ST) HCC was associated with intralesional steatosis (28/32, 88%)(**p<0.001**) and diabetes type II (20/33, 61%)(**p=0.027**). Intralesional steatosis was also associated with clear cell (CC) HCC (4/13, 31%). Fibrolamellar (FIB) HCC was associated with young age (median 44 years, 19-66)(**p<0.001**), female gender (4/5, 80%)(**p=0.023**) and absence of liver pathology and risk factors for HCC (5/5, 100%)(**p=0.002**). For prediction of MTM-HCC in our cohort, macrovascular invasion with AFP >48 µg/l and atypical enhancement has 25% sensitivity (SEN), 99% specificity (SPE), 75% positive predictive value (PPV), and 25 positive likelihood ratio (PLR). For ST-HCC, intralesional steatosis with diabetes type II has 54% SEN, 96% SPE, 67% PPV and 13.5 PLR. For FIB-HCC, age <60 with no risk factors has 80% SEN, 100% SPE and 100% PPV. High intralesional Gd-EOB uptake area over 50%, while not significantly different across all subtypes, was exclusive to NOS-HCC (16/174, 9%), CC-HCC (3/13, 23%) and ST-HCC (3/33, 9%)(**p=0.031** in post-hoc analysis).

Conclusion: Gd-EOB-enhanced MRI is of value in suggesting or ruling out specific subtypes, notably MTM-HCC and ST-HCC. A valuable clinical application could be to identify patients who would benefit from biopsy. Hepatobiliary phase iso- to hyperintensity is uncommon and indicates subtypes with a better prognosis. Further research is essential to better characterize NOS-HCC and uncommon subtypes, validate predictors, and to investigate the clinical impact of strategies incorporating WHO subtypes of HCC.

5 Abstract (German)

Hintergrund: Das hepatozelluläre Karzinom (HCC) stellt sich äußerst vielfältig dar, wodurch Diagnostik und die Vorhersage des therapeutischen Ansprechens erschwert werden. Die Weltgesundheitsorganisation (WHO) definiert nun acht Subtypen, die den Weg für eine präzisere Onkologie bereiten könnten, aber invasive Diagnostik voraussetzen. Wir untersuchten, ob Bildmerkmale in der mit Gadoxetsäure (Gd-EOB) verstärkten Magnetresonanztomographie (MRT) mit Subtypen assoziiert sind.

Methoden: Wir haben retrospektiv 240 aufeinanderfolgende Patienten mit 262 histologisch gesicherten HCCs eingeschlossen, die sich an unserem Zentrum zwischen Januar 2010 und Januar 2022 einer chirurgischen Resektion oder Lebertransplantation unterzogen und bei denen präoperative Gd-EOB MRT-Bildstudien vorlagen. Subtypen wurden durch zwei Pathologen zugeordnet. Qualitative und quantitative Bildmerkmale wurden durch zwei Radiologen erhoben und zwischen den Subtypen verglichen. Wir entwickelten diagnostische Tests für die Subtypen und evaluierten deren diagnostische Genauigkeit.

Ergebnisse: Das HCC-typische Anreicherungsmuster trat häufiger in „Nicht genauer angegeben“ (NOS) HCC (88/168, 52%) auf und seltener in makrotrabekulär massivem (MTM) (3/15, 20%), szirrhösem (SC) (2/9, 22%) und chromophobem (CH) HCC (1/8, 13%) (**p=0.035**). MTM-HCC war mit makrovaskulärer Infiltration, (5/16, 31%) (**p=0.033**) und hohem AFP-Wert assoziiert (Median, 397 µg/l (74-5370)) (**p<0.001**). Steatohepatitisches (ST) HCC war mit intraläsionaler Steatose (28/32, 88%) (**p<0.001**) und Diabetes Typ II assoziiert (20/33, 61%) (**p=0.027**). Fibrolamelläres (FIB) HCC war mit jungem Alter (Median 44 Jahre, 19-66) (**p<0.001**), weiblichem Geschlecht (4/5, 80%) (**p=0.023**) und Abwesenheit von Risikofaktoren für HCC assoziiert (5/5, 100%) (**p=0.002**). Zur Bestimmung von MTM-HCC hatte die Kombination aus Makrogefäßinfiltration, AFP >48 µg/l und atypischem Anreicherungsmuster 25% Sensitivität (SEN), 99% Spezifizität (SPE), 75% positiv prädiktiven Wert (PPV) und 25 positives Likelihood Ratio (PLR). Für ST-HCC hatten intraläsionale Steatose mit Diabetes Typ II 54% SEN, 96% SPE, 67% PPV und 13.5 PLR. Für FIB-HCC hatten Alter <60 ohne Risikofaktoren 80% SEN, 100% SPE und 100% PPV. Hohe intraläsionale Gd-EOB-Aufnahmefläche über 50%, obwohl nicht signifikant unterschiedlich, trat ausschließlich bei NOS-HCC (16/174, 9%), CC-HCC (3/13, 23%) und ST-HCC (3/33, 9%) auf (**p=0.031** in der Post-hoc-Analyse).

Konklusion: Gd-EOB-verstärkte MRT ist für die Bestimmung der HCC-Subtypen von Mehrwert, insbesondere für MTM-HCC und ST-HCC. Dadurch könnten u.a. Patienten identifiziert werden, die von einer Biopsie profitieren. Iso- bis Hyperintensität in der hepatobiliären Phase ist selten und identifiziert Subtypen mit einer besseren Prognose. Weitere Forschung ist erforderlich, um NOS-HCC und seltene Subtypen genauer zu charakterisieren, Prädiktoren zu validieren und die klinische Auswirkung von Strategien, die auf den WHO-Subtypen beruhen, zu untersuchen.

6 Introduction

Hepatocellular carcinomas (HCCs), the most common type of primary liver cancer, are increasingly prevalent in much of the world. Unfortunately, the prognosis of patients with HCC remains poor with a 5-year survival rate of only 20%. An important reason for this is that most cases are diagnosed at an advanced stage, limiting access to curative therapies. The high heterogeneity of HCC poses significant challenges to clinicians, making accurate diagnosis difficult and complicating therapeutic stratification and the development of targeted therapies.

In its 5th edition of the Classification of Tumors of the Digestive System (2019), the World Health Organization (WHO) recognized the diversity of HCC by defining eight subtypes, covering as many as 35% of all HCC lesions. This is a marked increase in comparison to the three subtypes previously defined in the 4th edition. Each subtype is characterized by distinct histopathological morphology, molecular-genetic profile, and biological behavior. The WHO Classification can potentially refine therapeutic algorithms by facilitating prognosis prediction and treatment response assessment. Additionally, it may augment diagnostic accuracy by characterizing atypical variants.

However, the WHO Classification relies on morphological and molecular criteria, necessitating tissue sample extraction, which carries inherent risks for the patient. These risks could potentially be mitigated with modern non-invasive radiological imaging techniques, which have already been able to predict histopathological properties of HCC. Magnetic resonance imaging (MRI) with hepatocyte-specific contrast agents is particularly promising as it can visualize both vascularity and hepatocyte function. This modality could prove to be a valuable tool in the non-invasive armamentarium for identifying HCC subtypes.

Therefore, the objective of this study was to contribute to the establishment of radiological biomarkers by retrospectively correlating imaging features in gadoxetic-acid-enhanced MRI with each subtype defined by the WHO. This includes reproducing imaging features previously reported in CT and MRI enhanced with extracellular agents. This should permit non-invasive subtype differentiation as a basis for the development of more accurate diagnostics and more effective therapeutic algorithms.

6.1 Epidemiology

6.1.1 Primary liver cancer

Primary liver cancer (PLC), as a cancer type, ranks fourth globally in terms of incidence, with an estimated 905,700 new cases each year. Additionally, it stands as the second leading cause of cancer-related mortality worldwide with 830,000 deaths per year[1], expected to rise to 1 million annual deaths by 2030[2]. The incidence of PLC continues to rise on a global level but is developing heterogeneously between regions[3]. As an illustration, in Germany, the age-standardized ratio (ASR) for incidence is projected to increase by 2% annually from 2018 to 2030. On the other hand, in Egypt, a country with a historically high burden of PLC, the ASR is expected to decrease by 1.7% annually during the same period[3]. In the USA, ASR is currently increasing by 4% per year in men and 3% in women[4], but declined by 2% annually among men under 50 years of age between 2014 and 2018, potentially foreshadowing trends in older age groups[4].

6.1.2 Hepatocellular carcinoma

Hepatocellular carcinoma (HCC) is the predominant type of PLC, accounting for 75%-85% of all histopathologically confirmed cases. Following HCC, intrahepatic cholangiocellular carcinomas (CCAs) represent 10-15% of cases, combined hepatocellular-cholangiocellular carcinomas (cHCC-CCAs) make up 5%, and there are rarer malignant entities such as hepatocellular adenoma (HCA)[5].

The incidence and mortality rates of HCC are two to three times higher in men compared to women, which is likely attributed to a higher prevalence of known risk factors for HCC in men[6]. The 5-year relative survival rate is very low at 20% for all stages combined, despite improvements in the management of the disease[4].

There is considerable geographic variation in the incidence of HCC (**Figure 1**). Developed countries have witnessed a decline in chronic hepatitis infections, mainly due to the widespread adoption of vaccines against the hepatitis B virus (HBV) and improved antiviral therapy against hepatitis C virus (HCV). Conversely, in regions like Asia and sub-Saharan Africa, the burden of disease remains persistently high due to the contamination of wheat and nuts with fungal aflatoxins and relatively high prevalence of HBV. Furthermore, the escalating global incidence of HCC is increasingly attributed to

metabolic risk factors, such as metabolic syndrome and type II diabetes mellitus, which have become a growing concern worldwide [7].

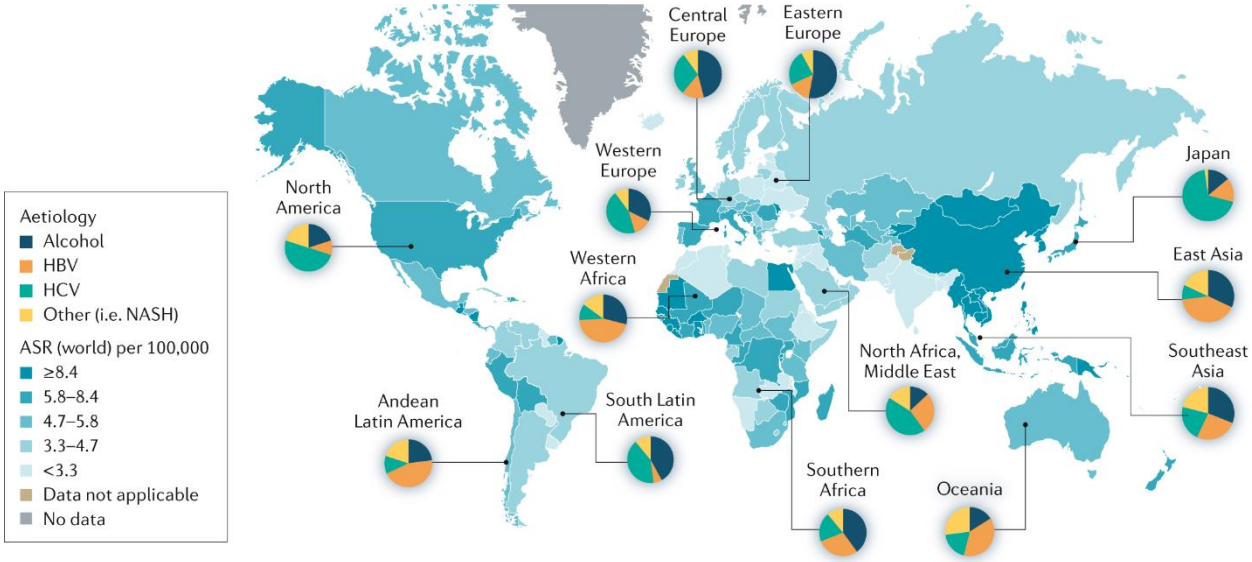

Figure 1: "The incidence and major etiological factors involved in hepatocarcinogenesis", depicting the considerable geographic variation in the prevalence of risk factors for HCC[8].

6.1.3 Risk factors for HCC

The major drivers of HCC incidence include chronic infections with HBV or HCV, chronic alcohol abuse, exposure to aflatoxins in contaminated foods and traits of metabolic dysfunction like obesity and diabetes. Less prevalent risk factors include conditions such as haemochromatosis, Wilson's disease, alpha-1 antitrypsin deficiency, primary sclerosing cholangitis (PSC) and primary biliary cirrhosis (PBC)[9, 10]. An overview of risk factors is given in **Table 1**.

Risk factors for the development of HCC by category	
Category	**Examples**
Patient characteristics	Male gender, higher age
Hepatotoxic	Alcohol, aflatoxins, drugs
Infectious	Hepatitis B, B/D or C virus infection, schistosomiasis
Metabolic	Diabetes, metabolic syndrome
Genetic	Haemochromatosis, M. Wilson, diabetes
Autoimmune	Autoimmune hepatitis, PBC, PSC
Liver pathologies	Liver steatosis, ASH/NASH, liver cirrhosis

Table 1: Risk factors for the development of HCC by category. PBC = primary biliary cirrhosis. PSC = primary sclerosing cholangitis. ASH/NASH = alcoholic/non-alcoholic steatohepatitis.

6.1.3.1 Alcoholism

Alcohol is classified as a group 1 carcinogen, defined as “carcinogenic to humans”, by the International Agency for Research on Cancer (IARC), with this risk factor accounting for 30% of HCC cases worldwide[11]. This is particularly problematic as, due to poor patient compliance that impairs participation in surveillance programs, HCC is often detected at a late stage in patients abusing alcohol, where curative therapeutic regimens may no longer be available[11].

The hepatotoxicity of alcohol involves numerous direct and indirect mechanisms that have been studied extensively. One such mechanism is the formation of aldehydes, which are the initial metabolites of alcohol metabolism. Additionally, reactive aldehydic products resulting from lipid peroxidation can also lead to the formation of protein adducts that hinder DNA repair processes[12]. Oxidative stress secondary to the formation of reactive oxidative species (ROS) results in the accumulation of structural and functional changes in DNA that, in turn, lead to cell cycle arrest or apoptosis[11]. Alterations in lipid metabolism promote liver steatosis, which may progress to alcoholic steatohepatitis (ASH) and subsequently, alcoholic liver cirrhosis[13], a severe liver disease associated with a 2.9% annual incidence for HCC in a European cohort[14].

6.1.3.2 Hepatitis B virus

HBV is a double-stranded DNA virus that infects the liver and is associated with the development of HCC, liver cirrhosis, and hepatic decompensation[15]. The initial acute infection is asymptomatic in two thirds of patients but may progress to a chronic infection as a result of insufficient viral clearance or immune escape[16, 17]. As progression occurs in 95% of infections in infancy or early childhood in comparison to 5% of infections in adulthood, age is the greatest risk factor for chronic infection[17].

Transmission of HBV occurs through exposure to infected blood and bodily secretions and can also occur vertically, from an infected mother to her neonate during birth[18]. In regions with low incidence, like Northern America and Europe, transmission commonly takes place during early adulthood, often through the reuse of contaminated syringes among intravenous drug users and unprotected sexual intercourse. Conversely, in regions with high incidence, such as southeast Asia, HBV infections frequently occur perinatally or in early childhood[18].

Historically, HBV has contributed significantly to the incidence of HCC, with 250-260 million people worldwide chronically infected with HBV[18]. An estimated 15-40% will go on to develop serious liver diseases including cirrhosis and PLC, leading to 0.5-1.2 million deaths annually[19]. In patients with chronic HBV infection, several risk factors contribute to the development of HCC. These include male gender, advanced age, HBe antigen positivity, specific HBV genotypes such as B or C, and elevated levels of alanine aminotransferase and serum HBV DNA[20, 21]. HCC associated with HBV infection has an extremely poor prognosis with a median survival of less than 16 months[22]. Coinfection with Hepatitis D virus (HDV) further exacerbates the risk for serious liver disease[23].

6.1.3.3 Hepatitis C virus

Hepatitis C virus (HCV) is an RNA virus associated with the development of liver fibrosis, cirrhosis, HCC, and extrahepatic manifestations such as cryoglobulinemia and non-Hodgkin lymphoma[24, 25]. Due to its ability to develop various immune escape mechanisms, the initial infection of HCV progresses to a chronic infection in 50-80% of cases in adults, a significantly higher rate compared to HBV. The specific interactions

between the virus and the host immune system that result in this progression are not yet fully understood and remain an area of ongoing research[25, 26].

Similar to HBV, HCV is a major public health burden with 92-149 million chronically infected individuals worldwide, of which half are in China, Pakistan, India, Egypt, and Russia[27]. Typically transmission occurs parenterally through exposure to blood by exchange of syringes among injection drug users or iatrogenically during medical procedures. Mother-to-infant and sexual transmission play lesser roles, and no cause can be discerned in as many as 40% of cases[25]. Direct-acting antiviral drugs (DAAs) such as NS5B inhibitors signify a major breakthrough in the treatment of HCV, leading to a sustained virological response with improved liver histology and clinical outcomes and late relapse rates under 1%[28].

6.1.3.4 Aflatoxins

Aflatoxins refer to mycotoxins produced by species of Aspergillus such as *A. flavus* that contaminate food, primarily nuts, rice, spices, grains and maize[29]. Around 4.5 billion people are estimated to be chronically exposed to aflatoxins, especially where food is stored under inappropriate storage conditions with exposure to high temperatures and air humidity[30, 31]. They are strongly carcinogenic, classed as group 1 carcinogens by the IARC, by forming genotoxic epoxides and DNA adducts and modifying the TP53 gene[32, 33].

6.1.3.5 Non-alcoholic fatty liver disease

Non-alcoholic fatty liver disease (NAFLD) is characterized by the excessive accumulation of fat in the liver, where steatosis is observed in at least 5% of hepatocytes in histological analysis or 5.6% in magnetic resonance imaging (MRI) spectroscopy or quantitative fat/water selective MRI. To diagnose NAFLD, other potential secondary causes for hepatic fat accumulation, such as significant alcohol consumption, must be ruled out[34].

NAFLD is strongly linked to obesity, insulin resistance, dyslipidemia, and cardiovascular diseases, contributing to a global prevalence of 25.4%, with expectations of further increase in the future[35]. Histologically, these metabolic risk factors promote the

accumulation of free fatty acids (FFAs) in hepatocytes. According to the “multiple hit” theory of NAFLD progression, this hepatocyte steatosis serves as the “first hit”. FFAs, being highly reactive, expose hepatocytes to subsequent “hits”, including oxidative stress, chronic inflammation, and apoptosis. Consequently, simple hepatic steatosis may advance to non-alcoholic steatohepatitis (NASH), characterized by signs of hepatocyte injury. NASH predisposes patients to developing liver fibrosis, cirrhosis and, eventually, HCC development (**Figure 2**)[36].

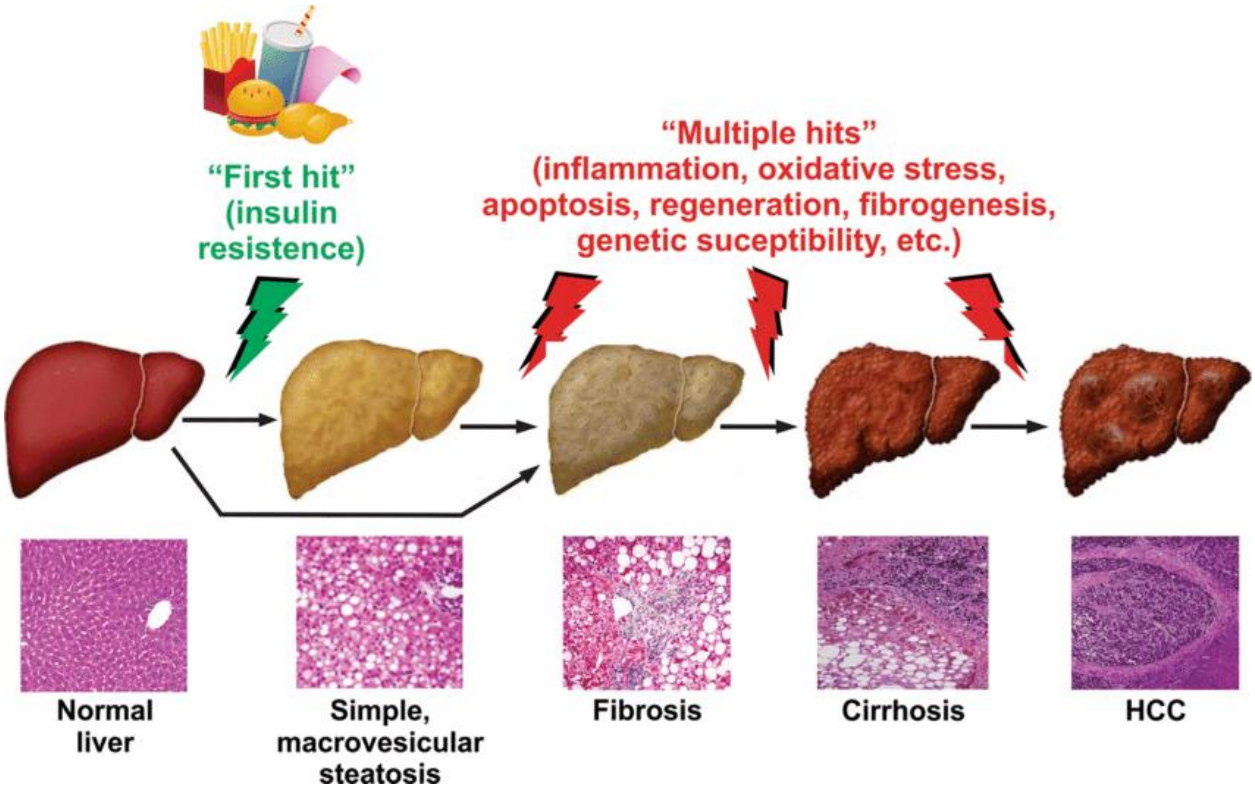

Figure 2: “‘Multiple-hit’ theory of clinical progression of NAFLD”, where insulin resistance followed by various mechanisms of injury leads to the progression to HCC through hepatic steatosis, fibrosis and cirrhosis.[36]

In parallel with the obesity epidemic, NAFLD is the fastest-growing cause of HCC in the USA, France and the UK[37], and the third most common cause of HCC in the United States[38].

6.2 Hepatocarcinogenesis

6.2.1 Overview of mechanisms

As exemplified in the previous chapter, HCC can develop due to a wide array of insults. In the majority of cases, HCC develops in a cirrhotic liver on the background of chronic

inflammation, but as many as 20% of HCCs may develop in a non-cirrhotic liver[39]. Some etiologies may induce HCC through multiple mechanisms. For instance, HBV serves as an independent risk factor for cirrhosis. Additionally, it acts as a mutagenic agent by integrating its viral DNA into host cell DNA and releasing the protein HBx, which disrupts cell cycle control, DNA repair and apoptosis. As a consequence, approximately 30% of HBV-associated HCCs develop in the absence of cirrhosis[40]. HCC may also develop from HCA, particularly in males, and when a mutation of the ß-catenin gene has occurred[41]. **Table 2** provides an overview of these mechanisms.

Key mechanisms of cirrhosis development or malignant transformation	
Mechanism	**Examples**
Exposure to hepatotoxic agents	Alcohol, drugs, aflatoxins
Collateral damage due to chronic immune response	HBV, HCV, autoimmune hepatitis
Accumulation of metabolites or metallic ions	NASH, hereditary haemochromatosis, M. Wilson
Biliary or venous congestion	Destruction of bile ducts by PBC or PSC, cirrhose cardiaque, Budd Chiari syndrome
Genetic alteration	HBV, aflatoxins
Malignant transformation of a precursor lesion	HCA with ß-catenin mutation

Table 2: Examples of mechanisms of hepatocarcinogenesis. HBV = hepatitis B virus. HCV = hepatitis C virus. PSC = primary sclerosing cholangitis. PBC = primary biliary cirrhosis. NASH = non-alcoholic steatohepatitis. HCA = hepatocellular adenoma.

6.2.2 Chronic inflammation leading to liver cirrhosis

When the liver is injured, it initiates a wound-healing response characterized by the activation of biological cascades. This process leads to the deposition of fibrotic scar tissue in the extracellular matrix (ECM) and the formation of new blood vessels (neoangiogenesis) as shown in **Figure 3**. In cases of chronic liver disease, this sustained response can result in the gradual accumulation of fibrosis, which may progress to cirrhosis, where the typical lobular structure of the liver is lost[42, 43]. Moreover, significant vascular remodeling takes place, involving the creation of intrahepatic shunts connecting the hepatic arterial and portal venous systems,

sinusoidal capillarization, vascular thrombosis, and, ultimately, the development of portal hypertension with potentially life-threatening complications. Considering these vascular alterations, cirrhosis can be considered a vascular disease[44]. Since mechanisms for degrading fibrous tissue in the ECM become exhausted, the scarring that occurs in cirrhosis has been considered irreversible. However, this view is challenged by new therapeutic agents that modulate hepatic stellate cells, the main source of fibrous scar tissue, to induce regression of fibrosis and early-stage cirrhosis[45].

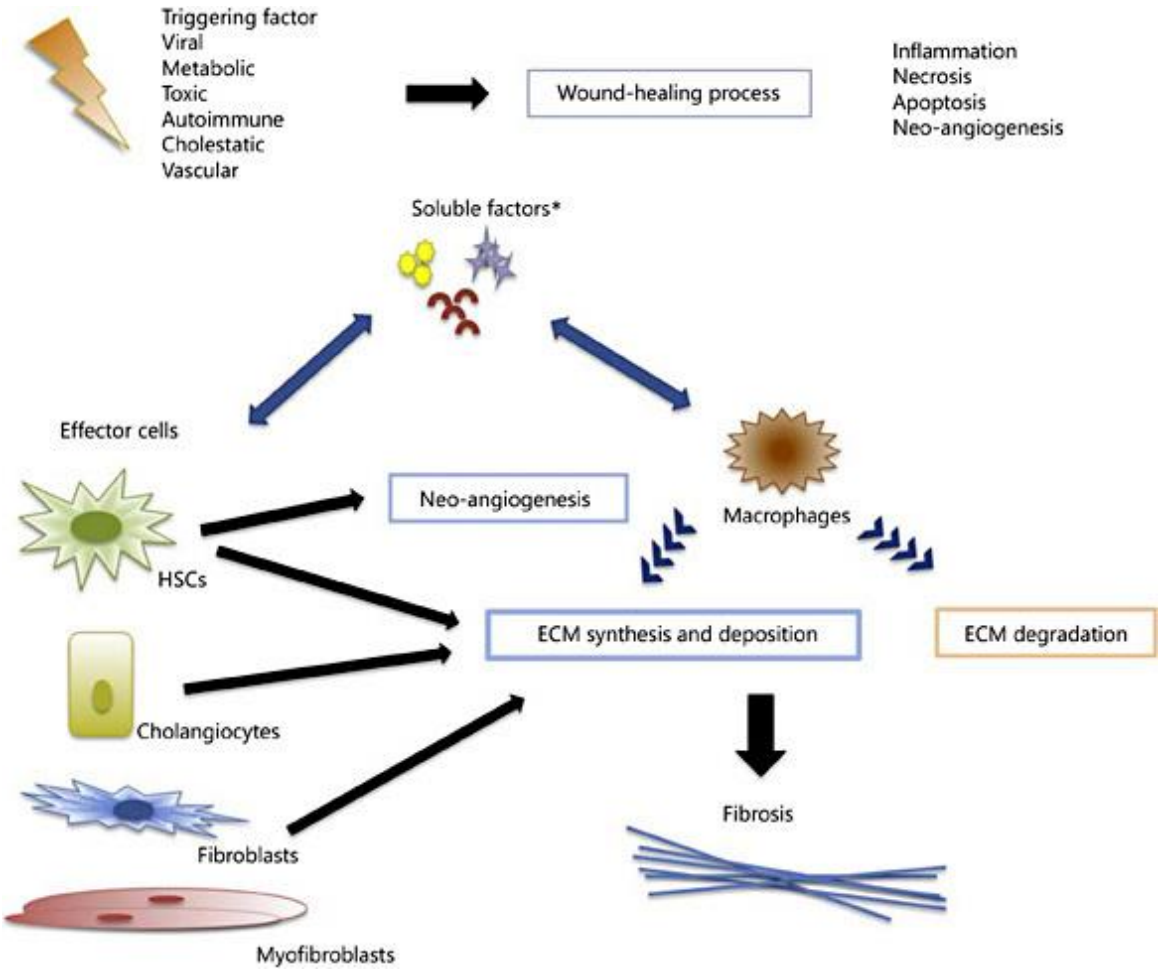

Figure 3: "Mechanisms of fibrogenesis"[42]. Wound-healing processes in response to a variety of triggering factors lead to the release of soluble factors. These induce effector cells to deposit additional extracellular matrix (ECM) and initiate neoangiogenesis. Macrophages are involved in both deposition and degradation of ECM. An excess of deposition leads to the accumulation of fibrosis. HSCs = hepatic stellate cells.

While liver cirrhosis usually represents the final stage of a decades-long disease process it may also develop within weeks or months due to drug injury, infection with

HCV, and after liver transplantation[43]. Although cirrhosis represents the ultimate shared outcome of various insults, the occurrence, prognosis, and biological behavior of resultant HCC differ depending on the underlying cause of cirrhosis. In a Swedish nationwide population-based cohort study, the 10-year cumulative incidence of HCC exhibited considerable variation, ranging from 4.3% in women with alcohol-related liver disease to 26.6% in men with viral hepatitis[46]. This fact assumes significance given the geographic variability in the prevalence of risk factors for HCC, as it may limit the transferability of research outcomes between regions.

6.2.3 Dysplastic transformation of hepatocytes

Hepatocarcinogenesis is considered a complex multistep process, during which hepatocytes undergo dedifferentiation as they accumulate mutations in various genes. These genes include CTNNB1, which is associated with the β-catenin pathway, the p53 gene, which plays a role in tumor suppression, as well as genes involved in JAK/STAT and AKT/PI3K signaling pathways[47]. Telomerase reverse transcriptase (TERT) promoter mutations are particularly significant, as they are not only found in 59% of HCCs[48] but are also among the earliest recurrent somatic alterations in premalignant lesions and cirrhotic livers, where they contribute to the immortalization of premalignant cells by inhibiting senescence and apoptosis[49].

The International Consensus Group for Hepatocellular Neoplasia defines 5 stages of hepatocarcinogenesis according to histological criteria (Table 3), beginning with regenerative nodules (RN)[50]. RNs can be regarded as pre-malignant lesions with a relatively low risk of developing into malignancy[51]. They may further progress into dysplastic nodules, which are categorized into low-grade and high-grade dysplastic nodules (LGDN and HGDN). The latter, HGDN, poses a significant risk of malignant transformation and can exhibit unpaired arteries that lack accompanying portal venous and biliary vessels, making it challenging to differentiate from early, well-differentiated stages of hepatocellular carcinoma (HCC) [50].

Malignant transformation can be observed as the emergence of an expansive nodule within a larger nodule, resulting in a nodule-in-nodule appearance in histological or imaging examinations [50]. HCC can advance and acquire the ability for microvascular

invasion, tumor thrombosis of the portal vein, and metastasis. However, when HCC arises in a non-cirrhotic liver, it often bypasses most of these stages and directly develops into progressed HCC. (Figure 4)[52].

Lesion	Characteristics
Regenerative nodule (RN)	• The proliferation of hepatocytes, depositing fibrous extracellular matrix.
Low-grade dysplastic nodule (LGDN)	• No cellular atypia, making morphological differentiation from RN difficult. • The risk of malignant transformation is comparable to that of a RN.
High-grade dysplastic nodule (HGDN)	• May develop unpaired arteries. • Difficult to distinguish from well-differentiated HCC due to no clear histological cut-off.
Early HCC	• Invades the stroma. • Accelerated neoangiogenesis. • Usually smaller than 1.5 cm.
Progressed HCC	• Has the capacity for microvascular invasion and metastasis. • Typically has a tumor capsule. • Initially expansive growth. May dedifferentiate further to exhibit a permeative growth pattern into the surrounding stroma

Table 3: Stages of dedifferentiation from regenerative nodules to progressed HCC, according to The International Consensus Group for Hepatocellular Neoplasia[50].

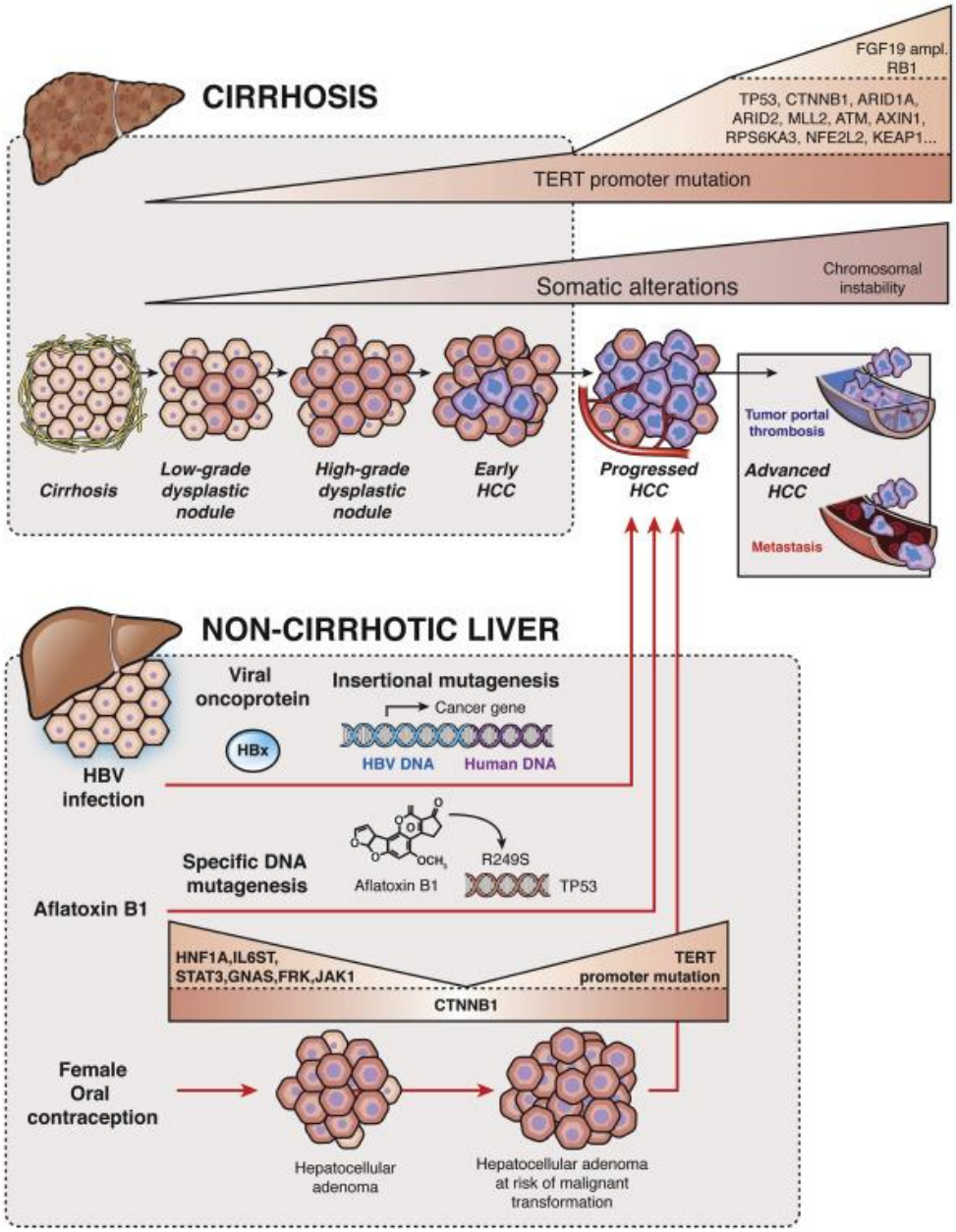

Figure 4: "Mechanisms of malignant transformation". HCC that arises in a cirrhotic liver typically undergoes a sequence of dedifferentiation steps, accumulating somatic alterations and chromosomal instability. In non-cirrhotic livers, HCC may arise by various mechanisms, including direct mutagenic effects by HBV or aflatoxins, and malignant transformation from HCA.[52]

6.2.4 Role of the tumor microenvironment

The tumor microenvironment (TME) can be characterized as a dynamic system comprising immune, vascular, and stromal components, as well as the ECM, which includes cells and their mediators, such as cytokines[53]. It denotes a development of the model for carcinogenesis due to an accumulation of sequential mutations, into one

where the complex interactions between the tumor cells and their microenvironment are considered. These interactions can either promote or suppress carcinogenesis and are influenced by external factors, contributing to the significant heterogeneity observed in HCC[54].

One of the most prominent constituents of the TME is cancer-associated fibroblasts, which make up a diverse group of cells within the stromal component. These fibroblasts are activated by chronic inflammation or hypoxia and can play a significant role in promoting the growth, invasiveness, and immune evasion of cancer cells through various mechanisms. These mechanisms include the release of growth or proangiogenic factors, cytokines, and proteases[55]. Moreover, they can present cancer antigens together with major histocompatibility class II proteins to inhibit a T-cell mediated anti-HCC immune response[56]. Consequently, the stromal compartment plays a crucial role in driving the initiation, growth, and progression of cancer, particularly in the context of chronic inflammation.

The immune compartment represents another important constituent of the TME, since many cell types in the liver are susceptible to cytokines[57]. IL-6, produced by Kupffer cells (liver-residing macrophages), is typically considered hepatoprotective as it supports hepatocyte regeneration in response to hepatocyte death[58]. Nevertheless, persistently elevated levels of IL-6 can paradoxically worsen liver injury and have been linked to the development of HCC[59, 60]. IL-6 secretion is also induced by HBV[61], providing a further mechanism for the causation of HCC by HBV through interaction with the TME. Furthermore, estrogens inhibit IL-6 production and may be part of the explanation for the considerable gender disparity observed in HCC incidence[62]. Finally, due to chronic exposure of immune cells to tumor antigens, chronic inflammation promotes immune tolerance of the cancer, with T-cells exhibiting markers of exhaustion[63].

6.2.5 Heterogeneity of HCC

Heterogeneity is a hallmark of HCC and exists on an inter-patient, intra-patient and intra-tumor level[64]. This heterogeneity may partially be explained by tumor-extrinsic factors, primarily the diversity of etiologies that predispose to HCC, where each shapes

the TME and as a consequence, the phenotypic output of liver tumors in a unique manner[49]. Tumor-intrinsic factors are also known to play an important role, as hepatocarcinogenesis involves the accumulation of diverse, random somatic mutations, resulting in unique cancer genomes for each lesion[49].

Furthermore, in chronic liver disease, conditions promoting hepatocarcinogenesis exist throughout the liver. This can give rise to multiple heterogeneous primary tumors in various loci and states of malignant transformation[65]. This is known as the “field-effect” and is a common cause for late recurrences after surgical resection or local ablation of an HCC lesion, occurring more than 2 years after the initial therapy[66]. In a genetic analysis of 356 HCC specimens after partial hepatectomy, Ding et al. found that only 52% of recurrent HCCs derived from the clonal lineage of the initial tumor[67].

Finally, intra-tumor heterogeneity (ITH) is a common feature of solid tumors, including HCC[68], as tumor cells and the TME are exposed to natural selection processes that result in the coexistence of multiple competing cell lines within a tumor[49]. High ITH is recognized as an independent marker for poor prognosis and a major contributor to the evolution of polyclonal drug resistance[69].

Viewed collectively, these factors contribute to the considerable heterogeneity observed in HCC. This has important implications for clinical practice, including challenges in diagnosing HCC with atypical morphology, developing tumor biomarkers, predicting the most effective therapy, and developing targeted therapies against druggable targets[70, 71]. Thus, there is an urgent need for accurate, pretherapeutic characterization of HCC lesions to enable the development of personalized medicine for HCC.

6.3 Staging of HCC according to the Barcelona Clinic Liver Cancer strategy

The Barcelona Clinic Liver Cancer (BCLC) strategy is a frequently used staging system that stratifies patients into 5 categories by integrating tumor burden, hepatic function, and the general condition of the patient according to the Eastern Cooperative Oncology Group (ECOG) performance status[72]. Evidence-based therapy recommendations are provided for each category, with surgical and ablative approaches being recommended

for earlier stages, liver transplantation and trans-arterial chemoembolization (TACE) for intermediate stages, and systemic therapy or best supportive care for advanced stages.

The BCLC has faced criticism for notable inter-patient heterogeneity within its categories, in particular in the intermediate categories BCLC-B and BCLC-C[73, 74]. This becomes especially relevant since some patients with intermediate-stage HCC may potentially benefit from a curative approach. Recent updates of the BCLC have addressed this concern by eliminating the Child-Pugh grade and subdividing BCLC-B into three categories. Nevertheless, the essential question remains whether further granularity and individualization can be attained, such as by incorporating histopathological and molecular markers indicating tumor aggressiveness.

6.4 Subtypes of HCC according to the WHO

6.4.1 Overview of subtypes

In its 5th edition of the Classification of Digestive System Tumors released in 2019, the World Health Organization (WHO) has integrated the results of extensive molecular profiling studies with histopathological and clinical characteristics. This has led to the identification of a total of 8 subtypes of HCC, collectively accounting for as much as 35% of all cases of HCC[5], a marked rise from the previously defined 3 main subtypes. **Table 4** provides an overview of these subtypes.

Subtype	Prognosis[a]	Frequency Among All HCCs (%)[b]	Histopathologic Characteristics	Clinical Considerations
Steatohepatitic	Similar	5–20	Cell ballooning, inflammation, pericellular fibrosis, and Mallory-Denk bodies	NAFLD, NASH, or metabolic syndrome
Clear cell	Better	3–7	Cytoplasmic accumulation of glycogen with clear cell morphology (> 80% of the tumor)	
MTM	Worse	5	Macrotrabecular (> 6 cells thick) architecture in > 50% of tumor, with satellite nodules and macrovascular and/or microvascular invasion	Hepatitis B, high serum α-fetoprotein level
Scirrhous	Unclear	4	Dense fibrous stroma (> 50% of the tumor)	
Chromophobe	Similar	3	Smooth, clear (chromophobic) cytoplasm, abrupt focal nuclear anaplasia	
Fibrolamellar	Similar[c]	1	Well-differentiated neoplastic cells with deeply eosinophilic and granular cytoplasm; thick, fibrous lamellae	Young age, no liver disease
Neutrophil-rich	Worse	< 1	Marked infiltrates by neutrophils	
Lymphocyte-rich	Better	< 1	Prominent lymphocytic infiltrate, predominance of cytotoxic CD8+ lymphocytes	

Table 4: "Characteristics of Variant Hepatocellular Carcinoma (HCC) Subtypes", indicating basic properties of the 8 subtypes of HCC according to the 5th Edition of the WHO Classification of Digestive System Tumors[75]. NAFLD = non-alcoholic fatty liver disease. NASH = non-alcoholic steatohepatitis. MTM = macrotrabecular-massive. [a]

Relative to NOS-HCC. [b] Approximately two thirds of all HCCs are NOS-HCC. [c] In patients without liver cirrhosis.

6.4.2 Potential of subtype classification

The WHO Classification addresses the considerable inter- and intrapatient heterogeneity of HCC and may hold significant promise for both diagnostics and therapeutics.

Firstly, the WHO Classification may lead to improved recognition of HCC with atypical morphology in histopathology or radiological imaging by characterizing further phenotypes of HCC.

Additionally, the existing therapeutic algorithms can be further improved by considering variations in prognosis and biological behavior among different HCC subtypes. For example, macrotrabecular massive HCC is linked to macrovascular and biliary tract invasion, peritumoral satellite nodules, and early recurrence after resection, leading to a poorer prognosis[76]. Moreover, the molecular tests of certain subtypes reveal potential targets for targeted therapies, such as the fusion product DNAJB1-PRKACA in FIB-HCC[77] and the activators of neoangiogenesis Ang2 and VEGFA in MTM-HCC[78].

6.4.3 Current limitations

The integration of the WHO Classification into clinical routines is impeded by the fact that it only defines histological and molecular diagnostic criteria. It, therefore, necessitates invasive diagnostics through biopsy or surgical resection, which is at odds with current clinical guidelines. These permit the diagnosis of HCC to be made non-invasively in patients with liver cirrhosis when a lesion is larger than 2 cm and shows a typical enhancement pattern for HCC[79, 80]. In these patients, the benefits of subtype identification based on the WHO classification would have to be weighed against the inherent risks of the biopsy.

Moreover, biopsies provide only a limited amount of tissue, which does not reflect the whole lesion and may be inadequate for diagnosing subtypes that require specific histopathological criteria to be fulfilled by a certain percentage of the lesion's volume. While standardized multi-region sampling techniques may address this concern, they

are complex procedures that may be challenging to implement into clinical routines[81]. Thus, there exists an unmet clinical need to predict the WHO subtypes of HCC non-invasively.

The subsequent section of this paper will explore current techniques utilized in HCC diagnostics and the potential for non-invasive prediction of histopathological features and phenotypes. The section will culminate with a review of the literature concerning the clinical, pathological, and radiological characteristics of each HCC subtype.

6.5 Diagnostics of HCC

6.5.1 Overview of diagnostics

The diagnostic workup of HCC involves a diverse range of tools, including laboratory tests, radiological examinations, and histopathological examinations. Notably, HCC stands apart from other malignant cancers as its diagnosis does not necessitate histopathological confirmation in cases where the lesion measures larger than 2cm, contrast-enhanced imaging demonstrates the typical enhancement pattern for hypervascular HCC, and the patient has a high pretest probability for HCC due to liver cirrhosis[79, 80]. Several options are available in cases where lesions are indeterminate, including follow-up imaging to assess the growth of the lesion, imaging with a different modality or contrast agent, or performing percutaneous liver biopsy[79, 80].

6.5.2 Percutaneous liver biopsy

6.5.2.1 Indications and strengths of biopsy

Percutaneous, ultrasound-guided liver biopsy followed by histopathological analysis may be performed where imaging does not permit a confident diagnosis of a focal liver lesion as HCC. It yields valuable information for guiding the diagnosis and therapy decisions of HCC, including the histopathological grade of differentiation according to Edmondson Steiner[82]. Poor differentiation is an independent predictor for aggressive growth and recurrence[83, 84]. Immunohistochemical analysis can provide valuable additional information. For example, a panel of 3 markers consisting of HSP70, glypican-3, and glutamine synthetase excels at differentiating early HCC from premalignant nodules, a diagnostic challenge with high clinical relevance[85].

6.5.2.2 Limitations of biopsy

Liver biopsy, as an invasive procedure, comes with significant drawbacks that limit its application in routine diagnostic workups of HCC, especially considering the current trend towards less invasive medical practices. Complications associated with liver biopsies include pain in 20% of cases, needle tract seeding in 1-5%[86], bleeding in 0.8-1.7% and death in 0-0.14%[87]. A biopsy cannot easily be repeated to monitor the progression of a suspicious nodule or confirmed HCC. Finally, samples from percutaneous liver biopsy may only reflect a small portion of the tumor and thus its intra-tumor heterogeneity.

Hence, it would be advantageous to non-invasively forecast the histological, molecular, and genetic characteristics of HCC by correlating with biomarkers. Notably, imaging biomarkers indicating generally aggressive biological behavior have already been identified, such as large size, multifocality, macrovascular invasion, and bile duct invasion[88, 89]. However, in order to develop precision medicine, it will be critical to thoroughly characterize these associations and to identify additional biomarkers[88].

6.5.3 Principles of imaging of HCC

6.5.3.1 Classical imaging features

Imaging plays a central role in HCC diagnostics as hepatocarcinogenesis leads to distinctive changes in vascularization, which can be visualized using contrast-enhanced (CE) imaging with ultrasound, computed tomography or magnetic resonance. Notably, the emergence of unpaired arteries is most evident in progressed HCC and is linked to an augmented arterial blood supply compared to the surrounding liver parenchyma[50]. This gives the lesion a hypervascular appearance through a rapid uptake of contrast agent in the arterial phase, which is known as arterial phase hyperenhancement (APHE). Washout in the portal venous or delayed phases is a further hallmark of progressed HCC, as the portal venous blood supply to the lesion is degraded, while surrounding cirrhotic tissue is comparatively slow to enhance and slow to wash out[90, 91]. The combination of APHE and washout is crucial because certain HGDN may already have started exhibiting APHE, but usually lack washout as their portal venous perfusion is still intact[92].

6.5.3.2 HCC with atypical imaging features

HCC may, however, reveal an atypical enhancement pattern on imaging in 40% of cases[93], particularly in well- and poorly-differentiated lesions[94, 95]. In HGDN and well-differentiated early HCC, a hypovascular stage may precede hypervascularity. During this stage, the normal vascular structure is deranged, but significant neo-angiogenesis has not yet taken place (**Figure 5**)[96-98]. This, in turn, hinders early detection of HCC, an issue with significant clinical ramifications as curative therapeutic options are primarily indicated in early HCC[79].

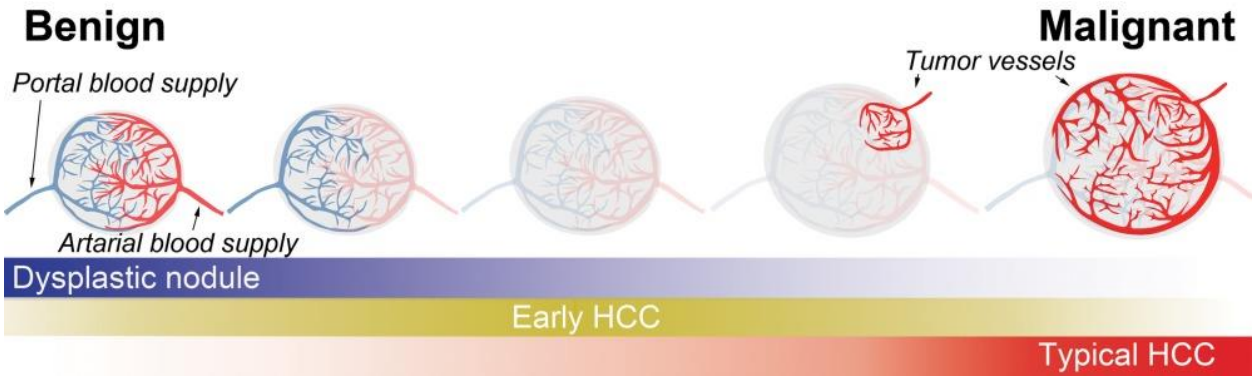

Figure 5: "Schematic representation of multistep hepatocarcinogenesis from the perspective of blood supply to the nodule." Arterial blood supply decreases during malignant transformation to early HCC, where it may be hypovascular, but the lesion typically later becomes hypervascular through parasitized arterial tumor vessels[97].

In cases of poorly differentiated HCC, certain regions within the lesion may undergo further dedifferentiation, leading to partial hypovascularity. Kenichiro et al. conducted a study involving 226 HCCs and observed that the majority (85%) of lesions exhibiting heterogeneous enhancement in the arterial phase were poorly differentiated[99]. Poor differentiation is important to recognize prior to a therapeutic decision, as it is an independent predictor for recurrence after therapies such as liver transplantation[100, 101].

6.5.4 Magnetic resonance imaging

Contrast-enhanced magnetic resonance imaging (CE-MRI) is a first-line tool in the diagnostic workup of a liver nodule that is suspicious for HCC. Although contrast-enhanced computed tomography (CE-CT) can also visualize the characteristic imaging features of HCC with higher temporal and spatial resolution, CE-MRI offers superior tissue contrast and additional imaging sequences and contrast agents, which can aid in

further characterizing lesions and assessing hepatocyte function[102]. Diffusion-weighted imaging (DWI) has excellent sensitivity for detecting small HCC lesions, which is one of the weaknesses of CE-CT in HCC diagnostics[103].

6.5.5 Contrast agents for MRI of the liver

6.5.5.1 Classes of contrast agents

Three main classes of gadolinium-based contrast agents are available. They have in common that they primarily shorten T1 relaxation times, thereby resulting in increased T1 signal intensity referred to as “enhancement”. However, their distribution differs according to their respective pharmacokinetic properties[104]. Blood pool agents remain in the intravascular space and are primarily established for angiography. Extracellular contrast agents (ECA) – such as gadoteric acid (Dotarem®, Guerbet, Aulnay-sous-Bois, France) and gadobutrol (Gadovist®, Bayer HealthCare, Berlin, Germany) – distribute throughout the extracellular space, including both blood pool and interstitial space.

Hepatocyte-specific contrast agents (HSCA) – such as gadobenate dimeglumine (Gd-BOPTA, Multihance®, Bracco, Milan, Italy) and gadolinium ethoxybenzyl dimeglumine (Gd-EOB, Primovist® in Europe and Eovist® in the USA, Bayer HealthCare) – not only distribute throughout the extracellular space, but are also subject to hepatobiliary transport as they undergo both renal and hepatic elimination[104]. Hepatobiliary transport entails uptake via organic anion transporters such as OATP1B1 and B3 on the sinusoidal membrane, followed by biliary excretion via multidrug-resistance associated proteins such as MRP2 on the canalicular membrane[105].

6.5.5.2 Hepatobiliary phase imaging

The signal intensity in T1-weighted dynamic phases enhanced with hepatospecific contrast agents (HSCA) provides valuable information not only about the vascular perfusion of liver parenchyma but also about the presence and gene expression profile of hepatocytes. Focal liver lesions that lack normal hepatocytes may exhibit a lower uptake of HSCA, leading to a hypointense appearance compared to the surrounding liver parenchyma in the hepatobiliary phase (HBP), which occurs 20 minutes after intravenous injection of a bolus[106]. HBP hypointensity is considered a hallmark of HCC

due to the characteristic changes in gene expression that occur during hepatocarcinogenesis (Figure 6)[107].

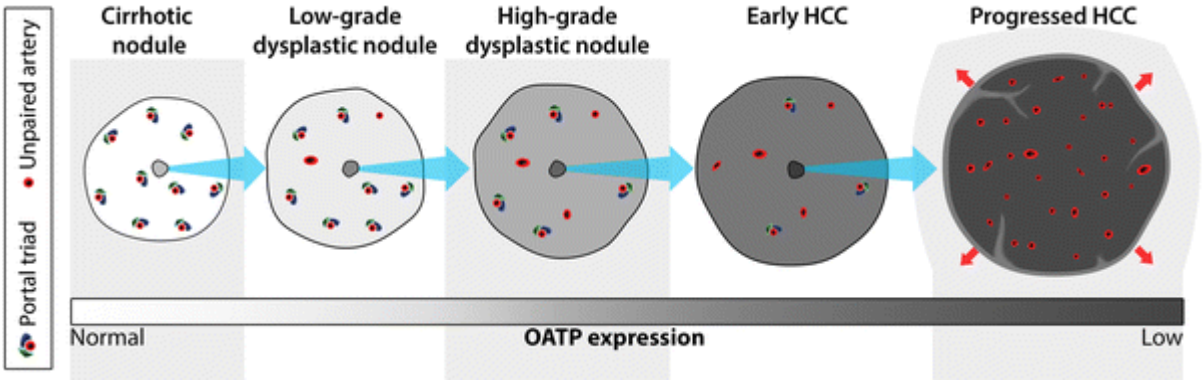

Figure 6: "Hemodynamic and OATP expression changes during multistep hepatocarcinogenesis.", adapted from Choi et al. 2014[107]. A progressive decrease in expression of OATP during hepatocarcinogenesis is accompanied by an increasingly hypointense appearance on hepatobiliary phase imaging.

This imaging feature has high per-lesion sensitivity for HCC[108] and is also highly specific if employed following the exclusion of benign and non-HCC lesions based on multiparametric assessment[109]. Compared to ECA, imaging with HSCA has improved sensitivity for detecting small HCC lesions under 2 cm, albeit with HCSA primarily being studied in Asian countries[110].

6.5.5.3 Lesions with iso- or hyperintense signal in hepatobiliary phase imaging

Focal liver lesions, including HCC, can exhibit iso- or even hyperintensity due to various mechanisms. These mechanisms may involve the preservation or overexpression of OATP1B1 and B3, activation of β-catenin, fat sparing in a steatoic liver and the presence of a fibrotic stroma[106].

An overexpression of OATP1B1 and B3 leads to a greater uptake of Gd-EOB from the sinusoidal space[111]. This finding is present in as many as 100% of focal nodular hyperplasias (FNH) and FNH-like nodules[112], and in 0-83% of HCAs depending on their subtype. It is most common in the β-catenin-activated subtype of HCA[113] as ß-catenin leads to overexpression of OATP1B3[114]. Subjectively rated signal intensity in HBP imaging has been found to be useful for differentiating between FNH and HCA with an AUC of 0.848-0.920[115, 116] and non-invasively diagnosing some subtypes of

HCA[117]. β-catenin-activated HCA is more likely to undergo malignant transformation into HCC[118], making Gd-EOB-enhanced MRI a valuable tool for identifying patients with high-risk forms of HCA[111]. A similar potential may exist for predicting subtypes of HCC.

Another factor contributing to the iso- or hypointensity in the hepatobiliary phase (HBP) is the presence of fibrotic stroma with slow uptake of Gd-EOB, which persists until the HBP. This appears as delayed central enhancement in a targetoid shape during dynamic phases, a characteristic that is considered atypical for HCC and highly specific for non-HCC types of primary liver cancer, such as cholangiocellular carcinoma (CCA)[119, 120].

Notably, 10-15% of HCCs have been reported to appear iso- or hyperintense in the HBP as a consequence of the histopathological and molecular properties described above[106]. Given that hyperintense HCC has been associated with longer time to recurrence, this imaging feature appears to be clinically relevant [121] and lower rates of vascular invasion[122].

6.5.6 Predicting histopathology and prognosis using Gd-EOB-enhanced MRI

HCC is an aggressive tumor entity with rates of recurrence after partial hepatectomy or liver transplantation of approximately 54% and 13%, respectively[123, 124]. The histopathological properties of the resected HCC lesion affect overall survival and recurrence after R0 liver resection, including microvascular invasion (MVI)[125], vessels encapsulating tumor clusters (VETC)[126] and a poor histopathological grade[84]. It is important to preoperatively predict these properties to identify the optimal therapy for each patient in light of the risk of recurrence.

Peritumoral microvascular invasion (MVI), where surrounding small vessels contain tumor embolisms, is a sign of aggressive growth[127]. There appear to be limited signs in MRI with satisfactory diagnostic performance for predicting MVI. A recent meta-analysis found that only peritumoral arterial phase enhancement was suited for this, with an AUC of 0.72. However, combining this sign with other features like peritumoral hypointensity in HBP and an irregular non-smooth margin could potentially enhance the diagnostic

performance for predicting MVI[128]. Sensitivity and interobserver variability may be improved further by employing radiomics in order to evaluate combinations of quantitative imaging features[129].

6.5.7 Limitations of HSCA

The use of HSCA is a subject of controversial discussion. HSCA has a higher likelihood of causing transient arterial-phase motion-related artifacts during the arterial phase when compared to ECA. This can potentially lead to image quality issues and hinder the accurate detection of areas with APHE in patients with liver cirrhosis[130, 131]. However, this may be compensated for by performing multiple single-breath-hold arterial phase acquisitions, where it is likely that at least one acquisition is well-timed[132]. Diagnostic accuracy studies should pay special consideration to this artifact given the critical importance of APHE for the non-invasive diagnosis of HCC.

Further limitations of HSCA are their relatively lower vascular enhancement in both the arterial and venous phases. To overcome this issue, adjusting the dose of the contrast agent upward may be considered [133]. Although HSCA is associated with higher costs compared to ECA, it has been found to be cost-effective in both the USA and China for the diagnostic workup of suspicious liver lesions. This is primarily attributable to a reduced need for confirmatory diagnostic procedures when compared CEUS, CE-CT, or ECA-enhanced MRI[134].

Finally, contrast in the HBP relies on the differences in HSCA uptake between liver parenchyma and liver lesions. Parenchymal uptake may be insufficient to be of diagnostic quality in patients with advanced liver cirrhosis, such as liver transplant candidates. Adequate HBP has been defined as unequivocally higher HBP signal intensity of liver parenchyma relative to hepatic blood vessels[135].

6.5.8 Liver Imaging Reporting and Data System (LI-RADS)

6.5.8.1 Overview

LI-RADS is a widely used standard for “terminology, technique, interpretation, reporting, and data collection of liver imaging”[135]. It is available for US, CEUS, CT and MRI. US LI-RADS v2017 is primarily used in surveillance of patients at high risk for developing

HCC to determine the surveillance interval and whether follow-up examinations with other modalities are necessary. CEUS LI-RADS v2017 and CT/MRI LI-RADS v2018 categorize lesions based on the probability of malignancy and of being HCC. This is based on major as well as ancillary imaging features that suggest either benignity, malignancy or specifically HCC, thereby providing a useful reference for research into imaging features of HCC. Our study will make use of imaging features as defined in LI-RADS.

6.5.8.2 Major imaging features

Major imaging features suggesting HCC in Gd-EOB enhanced MRI according to CT/MRI LI-RADS v2018 are shown in **Table 5**.

Feature	**Description**
Non-rim APHE	The lesion unequivocally enhances more than the liver, becoming hyperintense during the arterial phase.
Non-peripheral washout	The lesion loses enhancement relative to the liver, becoming hypointense in the portal venous or delayed phase.
Enhancing “capsule”	A thick, sharp and uniform border around the lesion, enhancing in the portal venous, delayed or transition phase.
Size of the lesion	The largest edge-to-edge diameter measured in the phase and sequence with the clearest margins of the lesion. The arterial phase and diffusion weighted imaging (DWI) are not well suited as they can lead to overestimation or an unreliable measurement. A lesion larger than 20 mm is likelier to be HCC or a non-HCC malignancy.
Threshold growth	An increase in the size of the lesion by more than 50% in less than 6 months.

Table 5: Major imaging features suggesting HCC in Gd-EOB-enhanced MRI according to CT/MRI LI-RADS v2018[135]. APHE = arterial phase hyperenhancement.

The targetoid appearance, characterized by a distinct contrast between the periphery and the center of the lesion, may suggest malignancy of non-hepatocellular origin, particularly intrahepatic CCA or cHCC-CCA. This manifestation can present as rim arterial-phase hyperenhancement, peripheral "washout," delayed central enhancement in dynamic phases, or targetoid appearance in DWI or HBP[135].

6.5.9 Surveillance of high-risk patients

6.5.9.1 Ultrasound for surveillance

Current clinical guidelines recommend entering patients at high risk for developing HCC into screening programs, where abdominal US is used as the primary imaging modality and may be followed up by CE-CT or MRI[79, 136]. Detection at an early stage improves survival as curative therapeutic options may still be available[137]. In patients with obesity and liver cirrhosis, the sensitivity of ultrasound (US) for detecting early stages of HCC is low due to increased absorption of ultrasound by the patient's tissues and the presence of a heterogeneous, nodular background in liver cirrhosis. In a meta-analysis of 32 studies, surveillance US was able to detect 84% of HCCs in patients with cirrhosis before clinical presentation, but its sensitivity for detecting early HCC was only 45%[138]. To potentially increase sensitivity, tumor biomarkers like AFP may be combined with US, but this may come at the expense of specificity[138].

6.5.9.2 Abbreviated MRI protocols for surveillance

MRI has considerably higher sensitivity than US in a surveillance setting, but comes with increased cost and long examination times. Abbreviated MRI (AMRI) protocols consisting of diffusion-weighted, T2-weighted and/or T1-weighted imaging with or without enhancement by hepatocyte-specific contrast agents (HCSA), may be a suitable alternative in a surveillance setting. In a meta-analysis, Kim et al. found the pooled sensitivity and specificity of AMRI for detecting HCC of any stage to be 86% and 96%, respectively. Employing HSCA to enhance T1w images improved sensitivity significantly (87% vs 82%) but also led to a reduction in specificity (93% vs 98%)[139].

When investigating whether MRI can differentiate between HCC subtypes, it would also be worthwhile to assess whether any potential imaging biomarkers can be evaluated within AMRI protocols in a surveillance setting.

6.6 Literature review on WHO subtypes of HCC

6.6.1 Steatohepatitic HCC

Steatohepatitic HCC (ST-HCC) is the most prevalent subtype with a relative frequency of 5-20% and a better prognosis than NOS[5]. It is strongly associated with metabolic syndrome, NAFLD and NASH, and exhibits histopathological similarities to hepatocytes in steatohepatitic livers, including large droplet steatosis, ballooning of malignant hepatocytes, Mallory-Denk bodies, inflammation, and pericellular fibrosis[5, 140]. In combination with its infiltrative, rather than expansile growth pattern, this can make it challenging to distinguish ST-HCC from the background liver[141]. ST-HCC may also occur in patients without any of the abovementioned risk factors, which Yew et al. suggest is an indication that the steatohepatitic phenotype may in some cases manifest as a result of tumor-specific pathways and genetic alterations, rather than interactions with NAFLD[142]. While ST-HCC has first been described in patients with HCV[140], the absence of HCV infection has been reported to be a predictor for ST-HCC among histopathologically confirmed HCC[143].

Imaging studies have primarily associated this subtype with the “fat in mass” feature[75, 143, 144], an expected correlate of the intralesional steatosis that is a histopathological criterion for this subtype. This feature is marked by hyperechogenicity on US or a low, lipid-like density on pre-contrast CT[145]. Comparison with the spleen has been suggested as an internal reference standard to avoid confounding of steatosis estimates by other factors such as iron content[146]. MRI is regarded as the most sensitive and specific technique, offering qualitative estimates through dual echo chemical shift imaging or fully quantitative estimates via the proton density fat fraction (PDFF). These measurements show robust correlations with both biochemically determined triglyceride concentration and magnetic resonance spectroscopy.[145]

“Fat in mass” is, however, not specific to ST-HCC and may also be observed in CC-HCC and early HCC. The distinction from early HCC is aided by the fact that ST-HCC frequently expresses major features of HCC according to LI-RADS, including non-rim APHE, non-peripheral washout and capsule enhancement[75]. Around 80% of lesions belonging to this subtype demonstrate the typical enhancement pattern on MRI,

resulting in only 0-4% of lesions being classified as LR-M according to CT/MRI LI-RADS v2018, as reported by Canella et al[144, 147]. Additionally, ST-HCC has been associated with smaller lesion sizes compared to other HCC types in preoperative imaging[143]. An example of ST-HCC from our study cohort is shown in **Figure 7**.

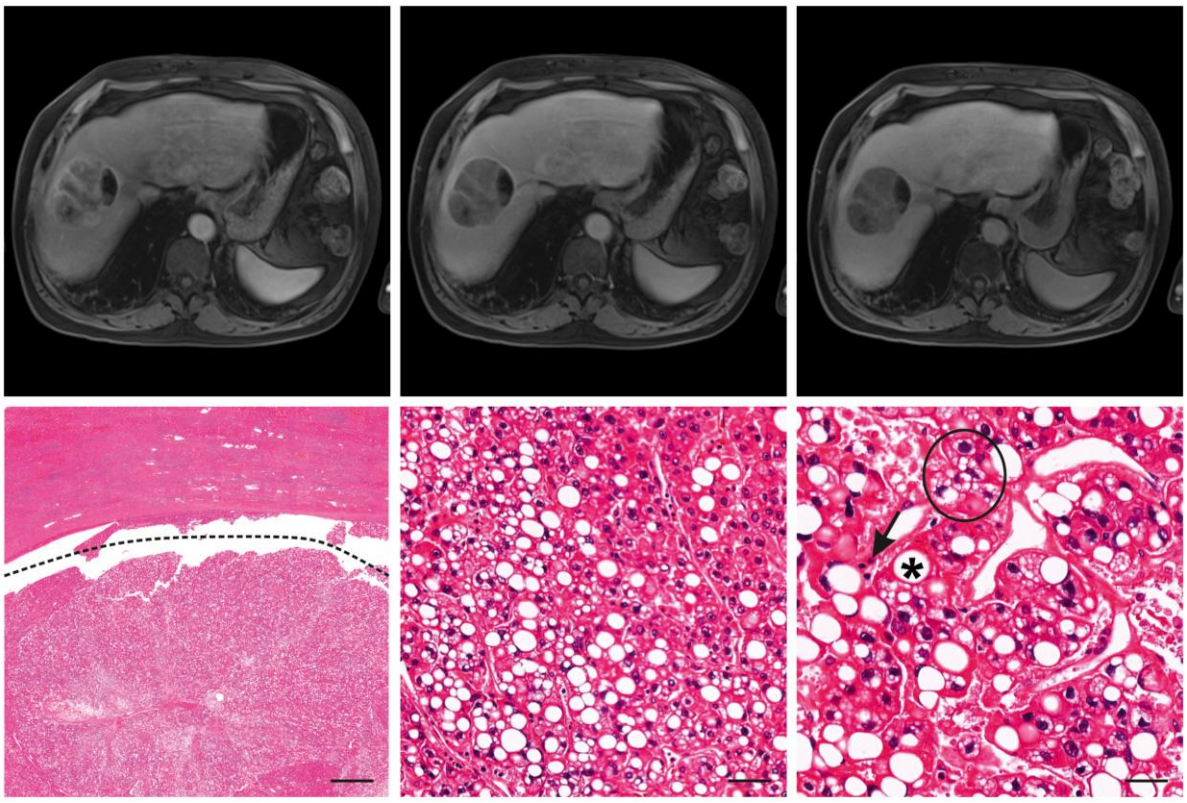

Figure 7: Steatohepatitic HCC

57-year-old man with diabetes type II and liver cirrhosis secondary to a chronic, therapy-resistant hepatitis C infection.

Top row: a 66 mm solitary HCC lesion in segment VIII with a strongly hypointense peripheral area that shows a large signal intensity drop between in-phase/opposed-phase imaging indicating steatosis. The lesion shows capsule enhancement and arterial phase hyperenhancement, followed by "washout" in the portal venous phase and Gd-EOB uptake deficiency in the hepatobiliary phase.

Bottom row: Tumor cells contain fat vacuoles (*) and are ballooned (circle). There is marked pericellular fibrosis and chronic inflammation (arrow).

6.6.2 Macrotrabecular massive HCC

Macrotrabecular massive HCC (MTM-HCC) is associated with a large size over 5 cm upon diagnosis, HBV infection, high AFP, satellite nodules and micro- and

macrovascular invasion, all of which are recognized as predictors of poor prognosis and higher rates of recurrence. Its prognosis is worse than other types of HCC, even if accounting for the higher prevalence of clinical, biological, and pathological features of aggressiveness[5, 22, 78, 148]. Its aggressiveness may derive from Ang2 and VEGFA overexpression[78], increasing the tumor's blood supply and vascular permeability and thereby promoting hepatocarcinogenesis, growth, infiltration and metastasis[149, 150]. This indicates the clinical relevance of this subtype, for which optimal treatment strategies may involve inhibitors of neoangiogenesis.

Despite its activation of neoangiogenesis, MRI imaging studies have associated this subtype with hypovascular components and T2 hyperintensity, which when combined represent areas of necrosis, indicating rapid growth[144, 151-153]. According to LI-RADS, necrosis is a feature favoring non-HCC malignancy. Furthermore, MTM-HCC has been associated on CT/MRI with high intra-tumor heterogeneity[152], the presence of an intratumor artery, arterial phase peritumoral enhancement, a non-smooth tumor margin[151, 154] and intratumor hemorrhage[155]. An example of MTM-HCC from our study cohort is shown in **Figure 8**.

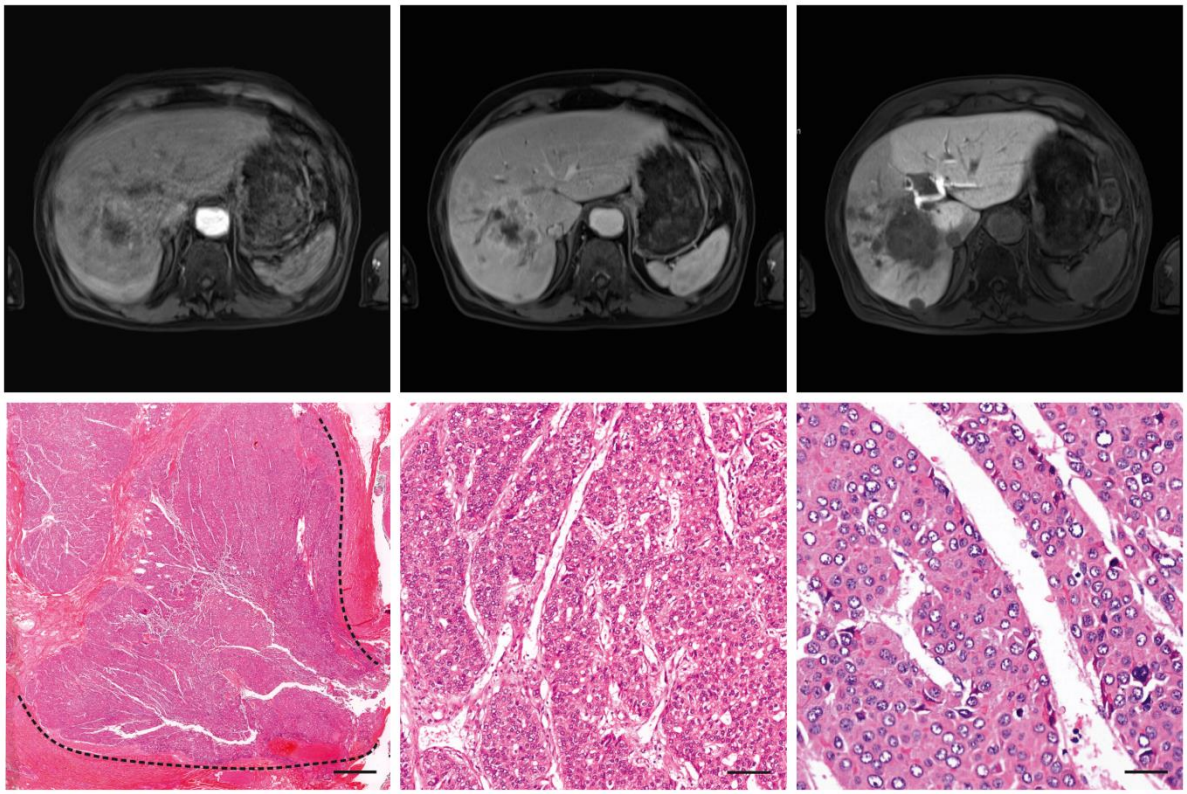

Figure 8: Macrotrabecular massive HCC

63-year-old man with liver cirrhosis secondary to a history of alcoholism. Gd-EOB-enhanced MRI was performed after elevated alpha-fetoprotein and weight loss were found during routine check-up.
Top row: 48 mm lesion in the right lobe with satellite lesions and a non-smooth tumor margin, (left) arterial phase peritumoral enhancement and substantial hypovascular areas, (middle) absence of portal venous phase washout and occlusion of the right branch of the portal vein and (right) hypointensity in the HBP, also revealing a perfusion deficit in the right liver lobe.
Bottom row: This tumor grows predominantly (>50%) in thick trabeculae that consist of sheets thicker than 6-10 tumor cells. In this case, most areas show low-grade nuclear atypia, where visible.

6.6.3 Clear cell HCC

Clear cell HCC (CC-HCC) is an uncommon subtype of HCC with a prevalence between 3-7%[5]. Like clear cell renal carcinoma, it is believed to arise from a preneoplastic lesion that exhibits excessive glycogen accumulation due to aberrant activation of insulin signaling. During malignant transformation, triggered by activation of AKT/mTOR proto-oncogenes, it is characterized by clear and/or acidophilic ground glass appearance, where glycogen may be partially replaced by fat depending on the phenotype. A metabolic shift from gluconeogenesis to the pentose phosphate pathway and glycolysis provides the cancer with abundant energy[156, 157]. Accordingly, it has been associated with a large tumor size, besides a higher patient age at diagnosis and non-viral liver cirrhosis[158, 159]. Despite its propensity for growth, CC-HCC has been linked to an improved prognosis and longer time to recurrence than NOS-HCC[160, 161].

Imaging studies have reported CC-HCC to exhibit signs of intralesional steatosis, which is marked by a signal drop in opposed-phase T1w imaging[162] or low attenuation on unenhanced CT[163]. Pseudocapsule formation has been observed more frequently in this subtype, but this imaging characteristic might not be effectively visualized in Gd-EOB-enhanced MRI due to the early uptake of the contrast agent by hepatocytes, which can obscure the appearance of the pseudocapsule[164]. Otherwise, clear HCC has been reported to have a similar appearance to NOS-HCC on imaging[162, 164]. Nevertheless, a higher proportion of clear cells was associated with a higher likelihood of an atypical

enhancement pattern[159]. An example of CC-HCC from our study cohort is shown in **Figure 9**.

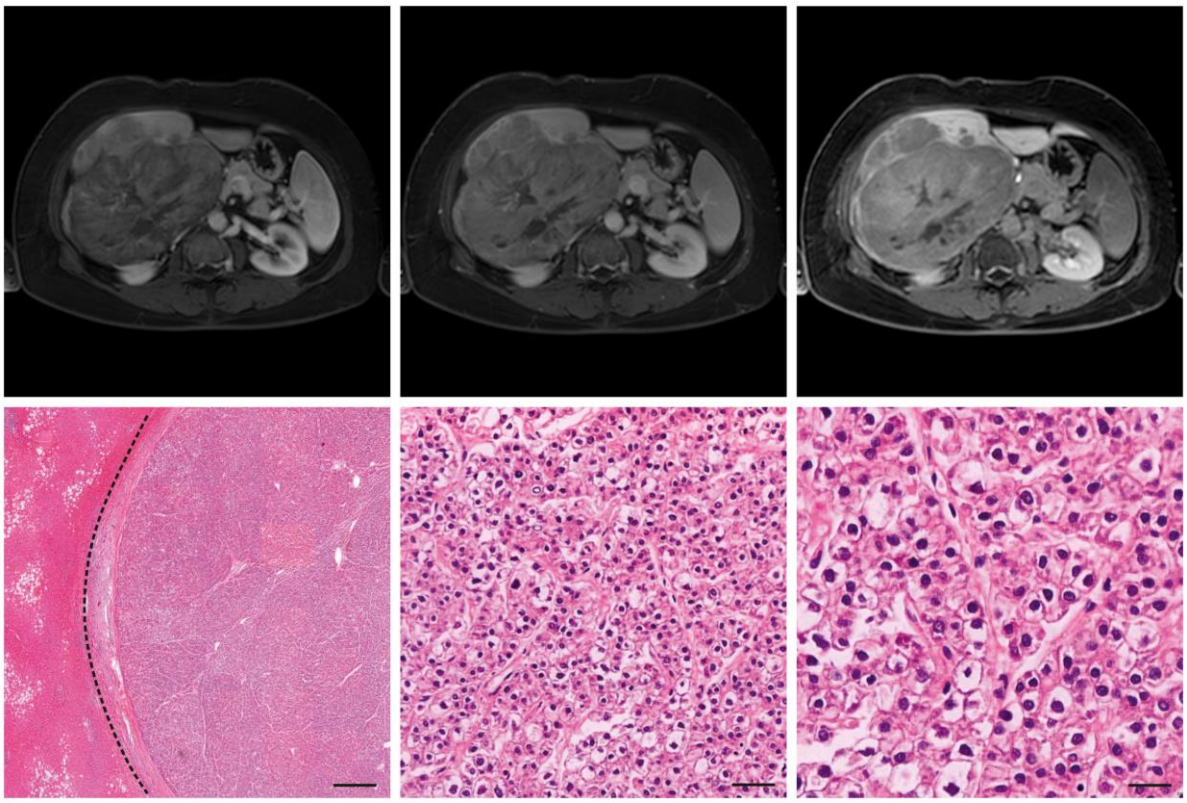

Figure 9: Clear cell HCC

57-year-old woman with liver steatosis and no other risk factors for HCC. MRI was performed after the patient presented with fatigue, weight loss and slight fever.

<u>Top row:</u> a large 210 mm HCC lesion with central necrosis and satellite lesions occupies much of the right liver lobe. The lesion gradually enhances from the (left) arterial phase, through the (middle) portal venous phase until (right) the hepatobiliary phase, remaining hypointense relative to liver parenchyma in all dynamic phases: an atypical enhancement pattern.

<u>Bottom row:</u> Tumor cells show abundant clear cytoplasm and bland round nuclei. Clear cell changes are present in at least 80% of the tumor.

6.6.4 <u>Chromophobe HCC</u>

Chromophobe HCC (CH-HCC) is a relatively rare subtype of HCC with a relative frequency of 3%[5], histologically characterized by smooth chromophobic cytoplasm that may be slightly eosinophilic or basophilic, abrupt focal nuclear anaplasia among cells with bland nuclear cytology, and scattered microscopic pseudocysts. There is a strong association with the alternative lengthening of telomeres (ALT) phenotype, present in

92% of CH-HCCs compared to 8% of unselected HCCs. ALT represents an additional mechanism of telomer maintenance, granting cell immortality independently of telomerase[165]. Clinically it has been associated with female predominance and a comparable prognosis to NOS-HCC[5, 165, 166].

The imaging features of CH-HCC are poorly described in the literature. Wood et al., who first described this subtype in 2013, reported five out of six CH-HCC lesions to have a typical enhancement pattern, slight hyperintensity in T2w images, no intra or extracellular fat, and a thick pseudocapsule on MRI[165]. The sixth lesion demonstrated progressive enhancement and large central necrosis. An example of CH-HCC from our study cohort is shown in **Figure 10**.

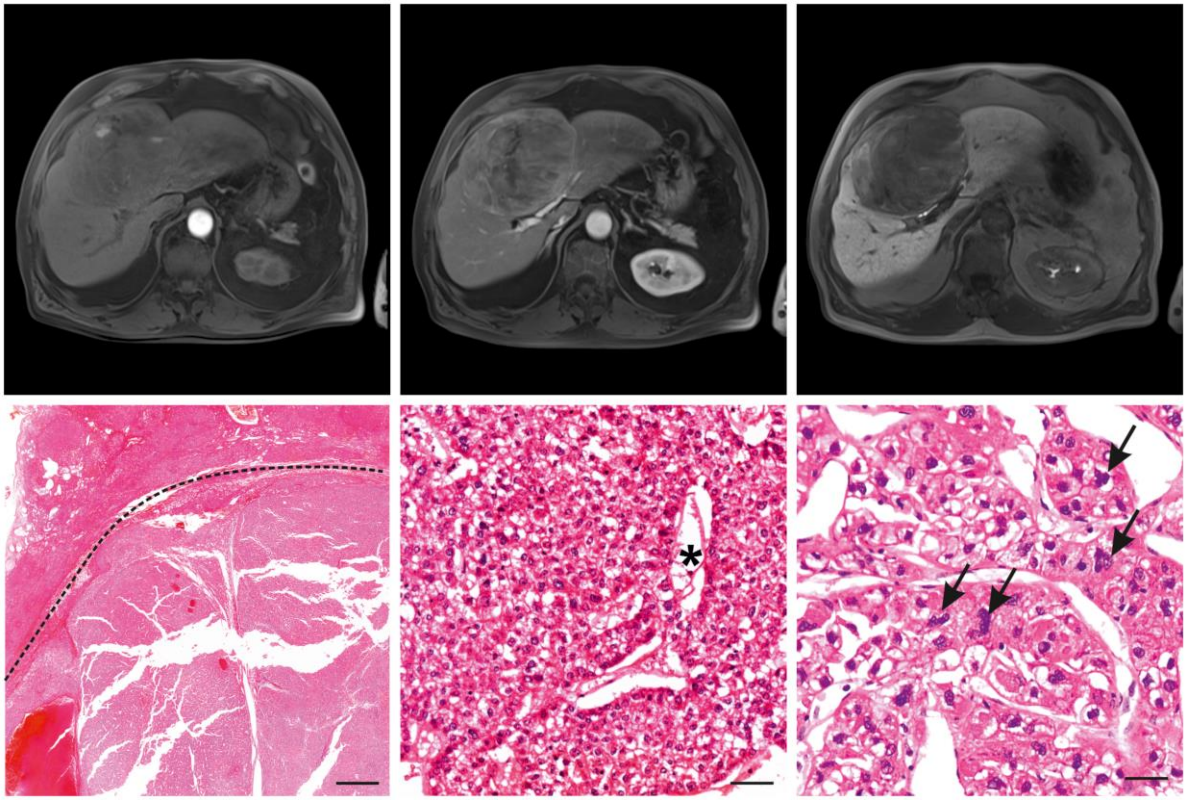

Figure 10: Chromophobe HCC

74-year-old man with liver fibrosis, insulin-dependent diabetes type II and a history of alcoholism.

<u>Top row:</u> solitary HCC lesion in segment IV, 123 mm in diameter, showing multiple minor hemorrhages and (left) slight arterial phase enhancement. (middle) The lesion enhances heterogeneously and progressively in the portal venous phase (right) and becomes predominantly hypointense in the HBP.

<u>Bottom row:</u> The tumor cells contain a smooth chromophobic, slightly eosinophilic

cytoplasm and mostly small nuclei with low-grade changes and small inconspicuous nucleoli. Cyst-like spaces are found inbetween the tumor cells (*). However, tumor cells show marked nuclear anaplasia in some areas (arrows).

6.6.5 Scirrhous HCC

Scirrhous HCC is a less common subtype of HCC characterized by having fibrous stroma in more than 50% of the tumor area. Unlike NOS-HCC, it is not commonly associated with a cirrhotic liver, which can make its diagnosis as HCC according to the diagnostic criteria of the American Association for the Study of Liver Disease (AASLD) less likely[167]. Another notable feature of scirrhous HCC is its predominant location near the liver capsule, where there is less portal venous perfusion, leading to hypoxia. This hypoxic environment triggers fibrogenesis and neoangiogenesis[167, 168]. It is also associated with a low serum AFP level and less frequent HBV association[167, 168]. The prognosis of this subtype in comparison to NOS-HCC remains unclear as studies with small cohorts have reported heterogeneous estimates for survival[5, 167, 169]. In one such study, survival was poorer despite a lower rate of recurrence[169].

Other focal liver lesions may similarly contain a high amount of fibrous stroma including mass-forming CCA, FIB-HCC and metastasis. As fibrotic areas are characterized by prolonged enhancement and delayed washout in contrast-enhanced imaging studies[170], high rates of misdiagnosis have been observed in imaging studies of scirrhous HCC, reaching up to 36%[167, 168]. When differentiating CCA from scirrhous HCC, target appearance in the HBP appears to favor CCA[171] while an area of central T2 hypointensity, capsule in the portal venous phase and intralesional septation favor scirrhous HCC[172]. Numerous further imaging features have been associated with the scirrhous subtype, including retraction of the liver surface, rim APHE, lack of necrosis and hemorrhage, tumor in vein, bulging appearance, and a central scar[168, 169, 173]. An example of scirrhous HCC from our study cohort is shown in **Figure 11**.

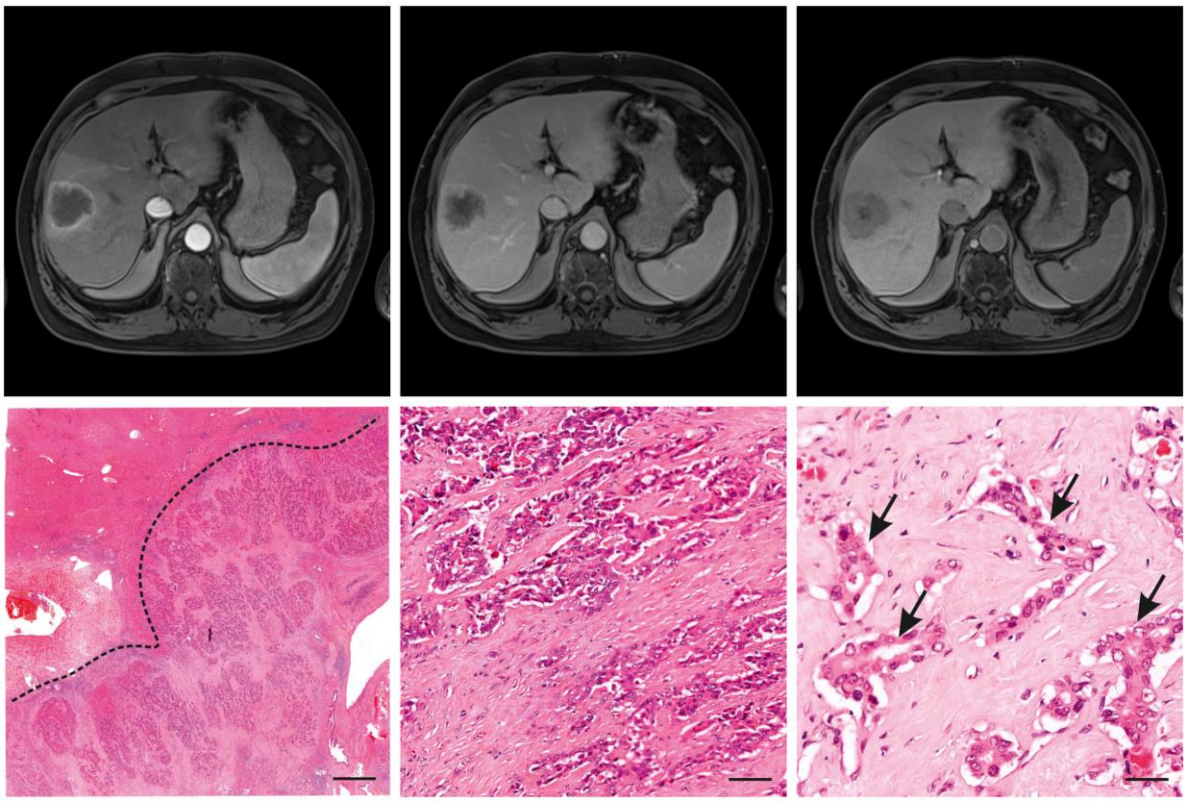

Figure 11: Scirrhous HCC

60-year-old man with a chronic hepatitis B and D coinfection and liver cirrhosis.

<u>Top row:</u> a 53 mm solitary HCC lesion in segment VII shows (left) rim APHE, (middle) followed by peripheral "washout" and gradual targetoid enhancement in the portal venous phase. The lesion shows a Gd-EOB uptake deficiency in the hepatobiliary phase with a central scar.

<u>Bottom row:</u> This tumor shows abundant fibrous stroma consisting of thick fibrous septa that separate nests of poorly differentiated tumor cells. A fibrous tumor capsule is absent. Fibrosis is present in at least 50% of the tumor.

6.6.6 <u>Fibrolamellar HCC</u>

Fibrolamellar HCC (FIB-HCC) is a very rare subtype with a relative frequency <1%[5]. Histologically it is characterized by lamellar bands of fibrosis, large polygonal cells with abundant eosinophilic cytoplasm, large vesiculated nuclei, and large nucleoli[174]. FIB-HCC is known to occur primarily in young patients between 10 and 30 years old, without gender bias and in the absence of underlying liver pathology[175]. The etiology of FIB-HCC remains ambiguous. Nevertheless, a driver mutation DNAJB1-PRKACA has been found in nearly all lesions. This is a fusion product of exons of the HSP40 and protein kinase A genes, which is capable of upregulating oncogenic pathways[176, 177]. Bauer et

al. found that DNAJB1-PRKACA can be targeted by peptide-based immunotherapy, which has led to a relapse free survival of one patient for more than 21 months[77]. This underscores the significance of detecting this subtype.

Overall, the prognosis of FIB-HCC is better than NOS-HCC, but becomes comparable after accounting for the lack of underlying liver disease[178]. In terms of clinical management, early detection and surgical resection or liver transplantation, depending on resectability, are key. Unlike other HCC, FIB-HCC is not responsive to chemotherapy, but hepatic artery embolization may be considered as an alternative to surgical resection[175].

Imaging studies primarily describe FIB-HCC as a large lesion without satellite nodules, with 82-100% showing heterogeneous APHE, portal venous phase washout and HBP hypointensity[179-182]. A central scar in 50-80% of cases is a distinctive feature. FNHs also frequently show a central scar, but remain hyperintense into the portal venous and HBP[180, 182, 183]. Further important differential diagnoses comprise focal liver lesions containing significant fibrotic areas: cholangiocellular carcinoma, scirrhous HCC, and some liver metastases[167]. An example of FIB-HCC from our study cohort is shown in **Figure 12**.

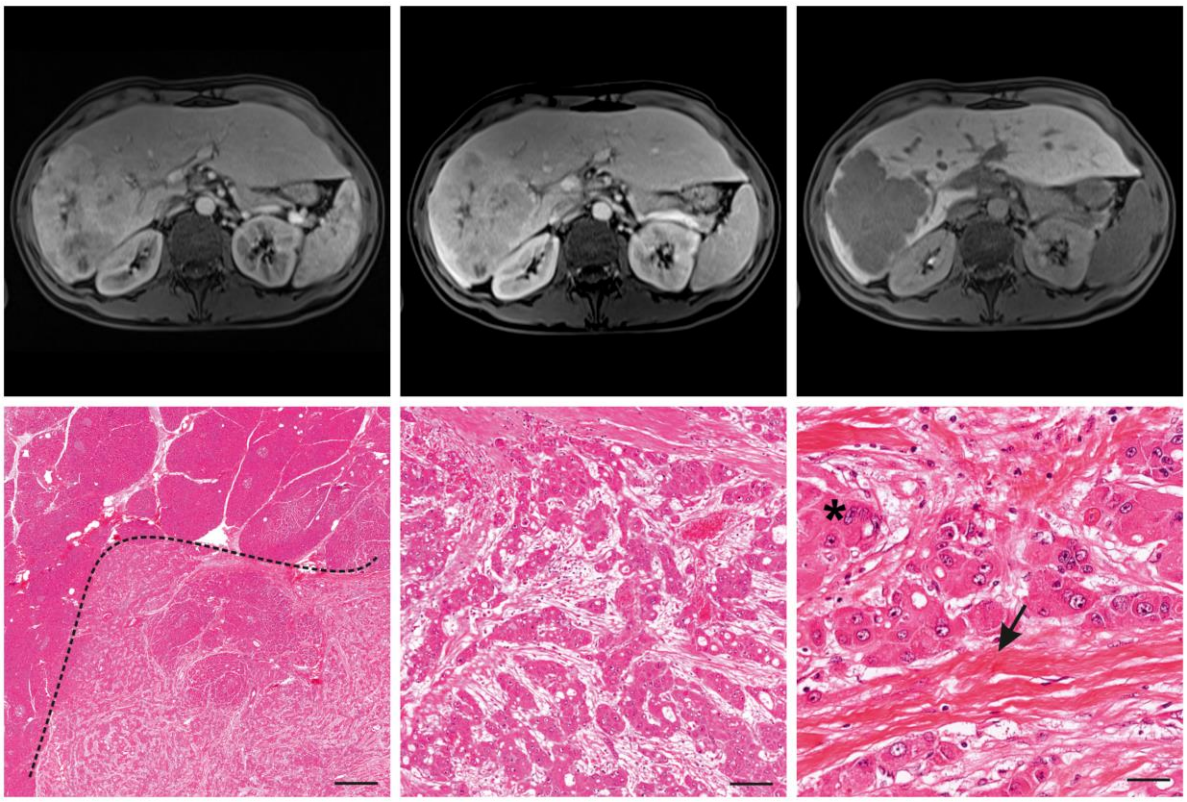

Figure 12: Fibrolamellar HCC

44-year-old woman with no underlying liver pathology and no known risk factors for HCC. Bipulmonary metastases of HCC were also present.
Top row: a 117 mm solitary HCC lesion in the right liver lobe, displacing adjacent hepatic vessels, with (left) heterogeneous APHE and a central scar, (middle) followed by "washout" in the portal venous phase and (right) homogeneous Gd-EOB uptake deficiency in the hepatobiliary phase.
Bottom row: The tumor has a trabecular appearance and consists of sheets or cords of large polygonal cells with abundant eosinophilic, oncocytic cytoplasm, owing to plenty of mitochondria (*). Nuclei show coarse chromatin and macronucleoli. In the interstitial space, there are dense collagen bundles arranged in parallel lamellae (arrow).

6.6.7 Lymphocyte-rich and granulocyte-rich HCC

In most HCC cases, mild inflammatory changes are observed. However, in some instances where the number of inflammatory cells surpasses that of tumor cells, the diagnosis of lymphocyte-rich HCC (LR-HCC) or granulocyte-rich HCC (GR-HCC) may be established[184]. Both are exceedingly rare, limited to case reports and case series in the literature, with a paucity of established molecular markers. In fact, questions are

raised as to whether GR-HCC is a subtype in its own right or merely a subset of HCCs that aberrantly produce granulocyte colony stimulating factor[184]. The prognosis of LR-HCC is reported to be better than that of NOS-HCC, possibly due to active engagement of the tumor by the immune system. Conversely, GR-HCC is associated with a worse prognosis[5]. These subtypes have elicited interested as potential targets for immune checkpoint inhibitors, which have led to good disease control in case reports[185].

The limited available data on these subtypes suggests that both LR-HCC and GR-HCC share imaging morphology with NOS-HCC. However, some authors have reported nodular cystic morphology within mural enhanced components in GR-HCC[186]. Laboratory markers of inflammation such as IL-6 and C-reactive protein may play an important role in these subtypes' non-invasive detection, but may result in a misdiagnosis as inflammatory or infectious disease[186]. An example of LR-HCC from our study cohort is shown in **Figure 13**.

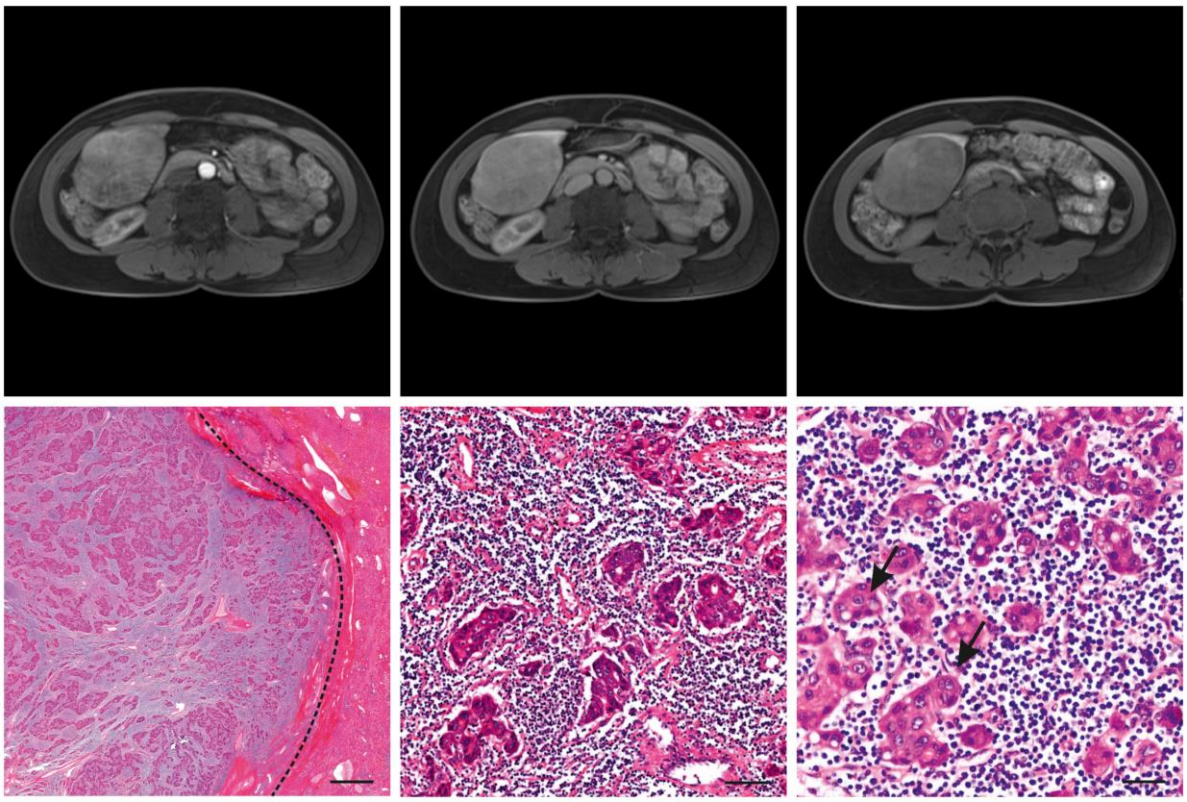

Figure 13: Lymphocyte-rich HCC

59-year-old woman with liver fibrosis and no known risk factors for HCC. The MRI was performed after a suspicious intrahepatic lesion was found during abdominal ultrasound of a renal cyst.

<u>Top row:</u> a solitary 86 mm HCC lesion appended caudally to the right liver lobe. It

shows inhomogeneous arterial phase hyperenhancement followed by portal venous phase "washout" and homogeneous Gd-EOB uptake deficiency in the hepatobiliary phase.
<u>Bottom row:</u> This rare tumor consists of islets of pleomorphic tumor cells with atypical nuclei that are surrounded by a large number of lymphocytes. Lymphocytes outnumber and focally invade tumor cells.

6.7 Purpose of this study

As previously mentioned, the diverse phenotypes of HCC present considerable challenges in diagnosing the disease promptly and selecting the most appropriate treatment. Existing guidelines and staging systems primarily consider tumor burden, liver function, hypertension-related complications, and overall patient condition, but they do not account for tumor biology. As a result, there may still be significant heterogeneity within each patient category. This is particularly relevant for early and intermediate stages of HCC, where curative therapies like surgical resection could be beneficial for patients with less aggressive forms of the disease but are not always readily chosen. The introduction of the 8 subtypes of HCC defined by the 5th edition of the WHO Classification of Tumors of the Digestive System holds promise for personalized therapeutic stratification. However, their implementation in clinical practice is impeded by the need for invasive diagnostics, which are currently not part of the recommended diagnostic workup for a large portion of the patient population.

The advancements in modern imaging techniques have already yielded imaging biomarkers that can predict patient prognosis and certain histopathological properties of HCC. Among these techniques, MRI combined with hepatocyte-specific contrast agents shows particular promise due to its ability to provide high tissue contrast, high per-lesion sensitivity, and visualization of both vascularity and hepatocyte function. Hence, it holds potential as a valuable non-invasive tool for differentiating HCC subtypes. Improved characterization of the imaging features of HCC subtypes may also lead to an overall enhancement in the diagnostic accuracy of detecting HCC. The objective of this study, therefore, was to contribute to the development and validation of imaging biomarkers in Gd-EOB-enhanced MRI for each subtype of HCC.

7 Materials and methods

7.1 Study design

This study is a single-center retrospective and explorative investigation aimed at evaluating potential morphologic imaging characteristics in Gd-EOB enhanced MRI that could serve as predictors for histopathological subtypes of hepatocellular carcinoma, as defined by the 5th edition of the WHO Classification of Digestive System Tumors. As the data was collected retrospectively, the institutional review board waived the need for informed consent (internal registration number: EA1/323/20). The study protocol adheres to the ethical guidelines outlined in the 2002 Declaration of Helsinki.

7.2 Patients

All consecutive patients who underwent surgical treatment for confirmed hepatocellular carcinoma (HCC) at the Charité Department of General, Visceral and Transplantation Surgery between January 2010 and January 2022 and received preoperative Gd-EOB-enhanced abdominal MRI were eligible for inclusion. Patients were identified from a prospectively maintained list of patients who underwent surgical resection or liver transplantation for liver malignancies. Exclusion criteria were prior systemic chemotherapy before surgical resection or absence of histopathological confirmation of HCC. Relevant clinical data and results of laboratory and immunohistochemical tests were extracted from our institutional database, in part with IT assistance from the Health Data Platform (Berlin Institute of Health).

Out of 800 cases initially evaluated, 249 cases involving 240 patients met the inclusion criteria and were included in this study. Seven patients were included in two cases each and one patient was included in three cases due to recurrence of surgically treated HCC. Notably, five of these patients (63%) had HCC lesions with different subtypes compared to their previous cases. A total of 382 histopathologically confirmed, surgically resected HCC lesions were identified. 262 lesions were included in analysis after excluding 16 lesions with an indeterminate subtype, 104 lesions from cases with multiple lesions of the same subtype and 1 lesion of the LR-HCC subtype due to its statistical irrelevance. **Figure 14** summarizes the results of the inclusion/exclusion procedure.

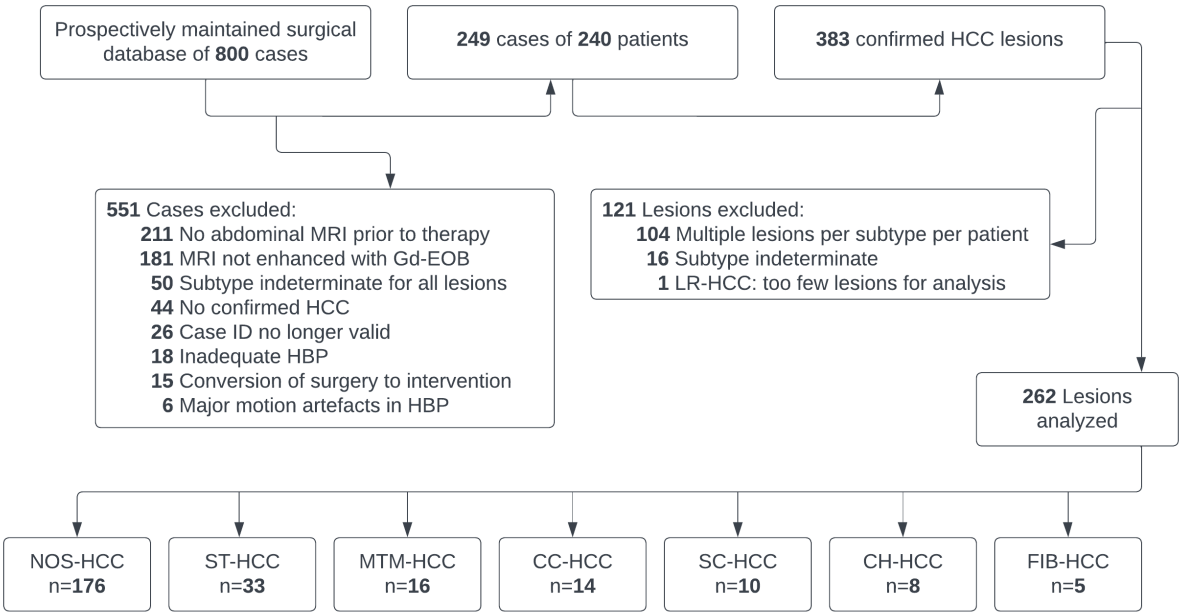

Figure 14: Results of evaluating 800 consecutive cases for inclusion in this study.

7.3 Reference standard: histopathological analysis of a surgical specimen

Two pathologists, David Horst and Jana Ihlow, conducted the review of the histological material independently and in a blinded manner, without access to the clinical and radiological data. Their objective was to determine the subtype of each lesion based on the criteria and guidance published by the WHO and Armed Forces Institute of Pathology (AFIP)[187]. The degree of differentiation according to Edmondson Steiner and the presence of steatosis, fibrosis or cirrhosis were also determined. Lesions with an indeterminate subtype were excluded from analysis.

In this study, we opted for histopathological analysis of a surgical specimen after resection or liver transplantation as the reference standard for diagnosing HCC. This choice was made because histopathological analysis is considered the gold standard for accurate HCC diagnosis. Unlike tissue core samples, the analysis of the entire volume of the lesion in surgical specimens allows for the quantification of the proportion of cells exhibiting histological features consistent with each HCC subtype. This approach is crucial as the WHO defines specific cut-off thresholds for the diagnosis of several HCC subtypes, making comprehensive evaluation necessary for accurate classification.

7.4 Index test: preoperative Gd-EOB enhanced abdominal MRI

The index test is Gd-EOB enhanced abdominal MRI of treatment-naïve lesions. All preoperative MRI studies were performed either at the Charité Department of Radiology or at external diagnostic centers, using 1.5 T or 3.0 T body-phased-array coils. The standard imaging protocol at the Charité Department of Radiology included pre-contrast T1-weighted (T1w) and T2-weighted (T2w) sequences with or without fat saturation (FS), T1w sequences in in-phase/opposed-phase technique and diffusion-weighted imaging sequences. Gd-EOB was applied intravenously at 0.025mmol/kg body weight at a flow rate of approximately 1–2 mL/s, followed by a 40-mL saline flush. Dynamic multi-phase T1-weighted sequences with fat saturation were acquired during breath-hold with fixed delays after contrast administration (arterial phase 15s, portal venous phase 50s, delayed / transitional phase 120s, hepatobiliary phase 20 minutes).

In this study, the largest HCC lesion in each patient was qualitatively and quantitatively analyzed in preoperative Gd-EOB-enhanced MRI. The analysis was performed by Sebastian Halskov in consensus with two board-certified radiologists, Timo A. Auer and Dominik Geisel, both having 7 and 13 years of experience, respectively. The radiologists were blinded to the results of the histopathological analysis during the evaluation. Lesions were excluded from the analysis if they were smaller than 6 mm in the MRI or located outside the liver. The most recent Gd-EOB enhanced MRI study showing the lesion in a treatment-naïve state was selected, allowing for a time interval of up to one year between the MRI and surgical resection.

Potential imaging biomarkers for analysis in this study were identified through a literature review that included national and international clinical practice guidelines for the management of hepatocellular carcinomas[79, 80, 135, 188]. The LI-RADS Lexicon as of June 2021 was used as a reference for defining imaging features[135]. The recorded imaging parameters are presented in Table 6.

Imaging parameter	Possible values	Comments
Lesion size	Maximal diameter in millimeters	Measured in the hepatobiliary phase to avoid overestimation.
Lesion location	Liver segment(s) (I to VIII)	
Type of surgery	Anatomical/Atypical/Liver transplantation	
Arterial phase hyperenhancement	Rim/Non-rim/None	Unequivocally greater enhancement than surrounding liver.
Pseudocapsule in arterial phase	Yes/No	Distinct narrow, uniform and sharp rim of greater enhancement relative to liver in the arterial phase around most of the lesion.
Portal venous phase washout	Peripheral/Non-peripheral/None	Drop in signal intensity in the portal venous phase compared to the arterial phase.
Nodule-in-nodule appearance	Yes/No	Distinct smaller nodule(s) contained within the lesion.
Macrovascular invasion	Yes/No	Lesion infiltrates the lumen of the portal or hepatic vein(s), indicated by an occluded or obscured vein in contiguity with the lesion. May lead to distal vascular signal loss particularly in the portal venous phase.
Diffusion restriction	Yes/No	High signal intensity in high B-value DWI with corresponding low signal intensity in apparent diffusion coefficient (ADC) map.
Apparent diffusion coefficient	Quantitative measure	Measured with 2D regions of interest in the ADC map.
Intralesional steatosis	Yes/No	Lesional signal drop in opposed-phase T1w imaging.
Parenchymal steatosis	Yes/No	Parenchymal signal drop in opposed-phase T1w imaging.
MR-morphologic liver iron load	Elevated/Normal	Abnormally low parenchymal signal in T2w imaging.
Intralesional hemorrhage	None/Minor/Major	Focal hyperintensity in precontrast T1w imaging, blurred border.
Intralesional necrosis	None/Minor/Major	Non-enhancing areas that do not appear hyperintense in T2w imaging (suggesting fibrosis).
Mosaic architecture	T1/T2/Both/None	Heterogeneous signal intensity in precontrast T1w or T2w imaging.
Enhancement pattern in dynamic phase sequences	Central/Rim/Homogeneous/Heterogeneous	Enhancing areas may appear targetoid (enhancement of the center or rim of the lesion), uniform or heterogeneous.
Signal intensity	See	Subjectively rated in precontrast T1w, dynamic T1w and T2w imaging, based on the predominant signal intensity by area.

Table 6: Recorded imaging parameters in Gd-EOB enhanced MRI with possible outcomes and remarks on their measurement, using the LI-RADS Lexicon as of June 2021 as a reference for defining imaging features[135].

The evaluation of intralesional signal intensity, Gd-EOB uptake area, and heterogeneity in the hepatobiliary phase was performed using 5-point subjective scales. Intralesional signal intensity was rated according to the predominant signal intensity by area (Figure 15). Intralesional Gd-EOB uptake area and heterogeneity were rated based on the estimated percentage of the lesion's area with isointense or hyperintense signal, or heterogeneous signal, respectively: 0 (0-5%); 1 (5-25%), 2 (25-50%), 3 (50-75%) and 4 (75-100%) (Figure 15).

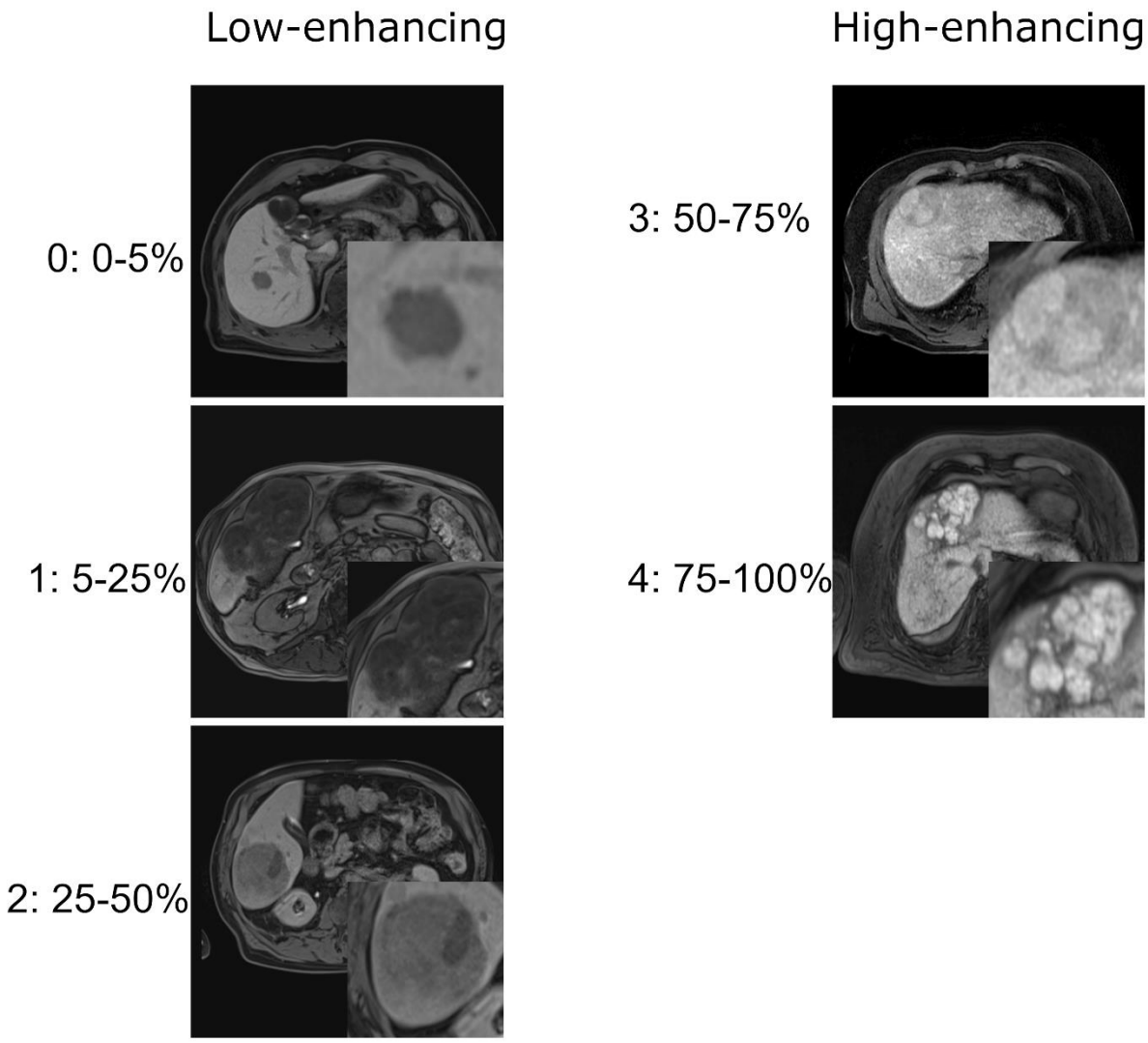

Figure 15: Subjective rating of Gd-EOB uptake area in the HBP. Lesions were rated on a 5-point scale by two readers according to the proportion of the lesion area which is iso- to hyperintense to liver parenchyma in the HBP. Scores from 0 to 2 represent lesions that are predominantly hypointense, which we named "Low-enhancing". Scores from 3 to 4 represent predominantly iso- to hyperintense lesions, which we named "High-enhancing". An example lesion is shown for each score.

Intralesional signal intensity	Definition
0: Hypointense	Markedly lower intensity than liver parenchyma
1: Isointense to hypointense	Slightly lower intensity than liver parenchyma
2: Isointense	Same intensity as liver parenchyma
3: Isointense to hyperintense	Slightly higher intensity than liver parenchyma
4: Hyperintense	Markedly higher intensity than liver parenchyma

Table 7: 5-point scale for subjective rating of intralesional signal intensity in HCC lesions

To quantify signal intensity and enhancement of the lesion relative to liver parenchyma, two-dimensional circular regions of interest (ROIs) were placed in the precontrast T1w FS sequence and in each dynamic phase sequence. Lesional ROIs were placed in enhancing areas, if any. Parenchymal ROIs were placed near each lesion at approximately 1-2 cm in areas with homogeneous signal and no apparent blood vessels. Muscle ROIs were placed in ipsilateral autochthonous back muscles. All ROIs were placed in the same position in each phase. Enhancement was defined as the difference in signal intensity to the precontrast phase. The ratio between lesion and liver enhancement was calculated for each phase with the following formula:

$$\frac{\textit{Dynamic phase lesion signal intensity - Precontrast lesion signal intensity}}{\textit{Dynamic phase liver signal intensity - Precontrast liver signal intensity}}$$

7.5 Statistical analysis

XLSTAT Statistical and Data Analysis Solution (Addinsoft, Long Island, NY, USA) was used to perform all statistical analyses. Descriptive statistics were carried out for all variables. Proportional distributions of categorical and ordinal variables among subtypes were compared with Fisher's exact test or a Monte Carlo estimation. Statistical comparisons for continuous variables were conducted using ANOVA if normal distribution and homoscedasticity were assumed. Nonparametric continuous variables were log-transformed if this resulted in a normal distribution. Central tendencies of nonparametric continuous variables were compared with the Kruskal-Wallis test. Receiver operating characteristic (ROC) curve analysis was employed to determine the AUC and the optimal threshold of continuous variables for identifying specific subtypes, with no preference given to sensitivity or specificity. Sensitivity, specificity, positive predictive values (PPV), and negative predictive values (NPV) were calculated for potential predictors of subtypes. Interobserver agreement (IOA) for subtype assignment

and subjective rating of Gd-EOB uptake area were assessed using Cohen's kappa and interpreted on a 6-point scale: 0.00-0.20 (no agreement), 0.21-0.39 (minimal agreement), 0.40-0.59 (weak agreement), 0.60-0.79 (moderate agreement), 0.80-0.90 (strong agreement), and above 0.90 (almost perfect agreement). A two-sided p-value of less than 0.05 was considered statistically significant.

To prevent overrepresentation of metastatic HCCs, if multiple lesions of the same subtype were present in a patient, only the largest lesion was included in the statistical analysis. Measures and dynamic phases with indeterminate or missing data, as well as those affected by severe motion artifacts, were excluded from the analysis.

8 Results

8.1 Patient characteristics

Patient characteristics including clinical, laboratory and pathological characteristics are presented in **Table 8***: Observed counts of patient characteristics and risk factors in cases included in the study, sorted by lesion subtypes present in each case. IQR = interquartile range. NOS = not otherwise specified. ECOG = Eastern Cooperative Oncology Group. AFP = alpha-fetoprotein. Pathology: N = None. S = steatosis. F = fibrosis. C = cirrhosis.*. As 19 patients had multiple lesions with different subtypes, and 8 patients were included in multiple cases with different lesions, all counts are given on a lesion level (n=262) rather than a patient level (n=240).

The median age was 66 years with an interquartile range (IQR) of 59-72. 72% (188/262) of patients were male. 23% (59/262) of lesions were removed during liver transplantation, including 36% of ST-HCC lesions (12/33). 61% (158/262) of lesions occurred in patients with liver cirrhosis, 25% (65/262) in fibrosis, 9% (22/262) in steatosis and 5% (13/262) in the absence of any liver pathology (Figure 16). At least one known risk factor for HCC was present in 84% (220/262) of patients, with diabetes type II and alcoholism being the most common at 37% (98/262) and 31% (80/262), followed by chronic HBV and HCV infection at 17% (44/262) and 24% (63/262) (Figure 17). The median interval between imaging and surgery was 34 days (12-58).

Significant differences were observed for age, sex, log-AFP, liver pathology, diabetes type II and the absence of known risk factors. Patients with FIB-HCC were younger (median age of 44 years vs. 66 years, **p < 0.001**) and more often female (80% (4/5)) vs. 28% (74/262), **p = 0.023**). Median AFP was higher for patients with MTM-HCC (397 µg/l), CH-HCC (208 µg/l) and FIB-HCC (30 µg/l) than for the cohort as a whole (8 µg/l) and became significantly different after log-transformation (**p < 0.001**) (Figure 18). AUC for identifying MTM-HCC in ROC curve analysis was 0.824 (Figure 19).

The distribution of underlying liver pathology was found to be significantly different among the subtypes. Specifically, all patients (5/5) with FIB-HCC had no liver pathology, in contrast to only 5% (13/262) of the entire sample. Liver cirrhosis was slightly more frequent in patients with NOS lesions (66% or 114/262) compared to 61% (158/262) of

the total sample (**p = 0.001**). Furthermore, diabetes type 2 was more common in patients with ST-HCC (61% or 20/33) compared to 37% (98/262) of the total sample (**p = 0.027)**. None of the patients with FIB-HCC had any risk factors for HCC (0% or 0/5) compared to 84% (220/262) of the total sample (**p = 0.002**)

PATIENT CHARACTERISTICS	Whole cohort (n=262)	NOS-HCC (n=176)	FIB-HCC (n=5)	MTM-HCC (n=16)	CC-HCC (n=14)	ST-HCC (n=33)	SC-HCC (n=10)	CH-HCC (n=8)	p-value
Age (y) median (IQR)	66 (59-72)	66 (59-73)	44 (19-66)	63 (54-71)	68 (57-78)	65 (54-72)	64 (58-71)	71 (67-74)	<0.001*
Sex	M: 72% (188/262) F: 28% (74/262)	M: 74% (130/176) F: 26% (46/176)	M: 20% (1/5) F: 80% (4/5)	M: 56% (9/16) F: 44% (7/16)	M: 57% (8/14) F: 43% (6/14)	M: 85% (28/33) F: 15% (5/33)	M: 80% (8/10) F: 20% (2/10)	M: 50% (4/8) F: 50% (4/8)	0.023*
Recurrence	16% (43/262)	17% (30/176)	20% (1/5)	13% (2/16)	21% (3/14)	18% (6/33)	10% (1/10)	0% (0/8)	0.913
Liver transplantation	23% (59/262)	23% (41/176)	0% (0/5)	13% (2/16)	7% (1/14)	36% (12/33)	20% (2/10)	13% (1/8)	0.286
Increased PV pressure	64% (65/262)	69% (46/176)	0% (0/5)	33% (2/16)	50% (4/14)	80% (8/33)	50% (2/10)	75% (3/8)	0.741
Ascites	7% (19/261)	7% (12/176)	0% (0/5)	13% (2/16)	7% (1/14)	6% (2/33)	10% (1/10)	14% (1/7)	0.772
AFP (µg/l) median (IQR)	8 (4-82)	8 (5-81)	30 (9-15846)	397 (74-5370)	5 (3-6)	6 (3-11)	5 (3-24)	208 (5-3167)	<0.001*
ECOG performance status	0: 50% (50/101) 1: 45% (45/101) 2+: 6% (6/101)	0: 55% (37/67) 1: 42% (28/67) 2+: 3% (2/67)	0: 50% (1/2) 1: 50% (1/2) 2+: 0% (0/2)	0: 50% (3/6) 1: 33% (2/6) 2+: 17% (1/6)	0: 25% (2/8) 1: 63% (5/8) 2+: 13% (1/8)	0: 30% (3/10) 1: 50% (5/10) 2+: 20% (2/10)	0: 50% (2/4) 1: 50% (2/4) 2+: 0% (0/4)	0: 50% (2/4) 1: 50% (2/4) 2+: 0% (0/4)	0.413
Child-Pugh Grade (from report)	A: 81% (78/96) B: 11% (11/96) C: 7% (7/96)	A: 82% (58/71) B: 13% (9/71) C: 6% (4/71)	-	A: 86% (6/7) B: 0% (0/7) C: 14% (1/7)	A: 75% (3/4) B: 0% (0/4) C: 25% (1/4)	A: 78% (7/9) B: 22% (2/9) C: 0% (0/9)	A: 75% (3/4) B: 0% (0/4) C: 25% (1/4)	A: 100% (1/1) B: 0% (0/1) C: 0% (0/1)	0.451
Liver pathology	N: 5% (13/258) S: 9% (22/258) F: 25% (65/258) C: 61% (158/258)	N: 3% (5/174) S: 9% (15/174) F: 23% (40/174) C: 66% (114/174)	N: 100% (5/5) S: 0% (0/5) F: 0% (0/5) C: 0% (0/5)	N: 6% (1/16) S: 6% (1/16) F: 38% (6/16) C: 50% (8/16)	N: 17% (2/12) S: 8% (1/12) F: 33% (4/12) C: 42% (5/12)	N: 0% (0/33) S: 9% (3/33) F: 24% (8/33) C: 67% (22/33)	N: 0% (0/10) S: 10% (1/10) F: 30% (3/10) C: 60% (6/10)	N: 0% (0/8) S: 13% (1/8) F: 50% (4/8) C: 38% (3/8)	0.001*
RISK FACTORS									
Diabetes type 2	37% (98/262)	35% (62/176)	0% (0/5)	19% (3/16)	43% (6/14)	61% (20/33)	30% (3/10)	50% (4/8)	0.027*
Alcoholism	31% (80/262)	30% (53/176)	0% (0/5)	44% (7/16)	21% (3/14)	30% (10/33)	30% (3/10)	50% (4/8)	0.517
Chronic Hepatitis B	17% (44/262)	18% (31/176)	0% (0/5)	19% (3/16)	7% (1/14)	15% (5/33)	40% (4/10)	0% (0/8)	0.389
Chronic Hepatitis C	24% (63/262)	27% (47/176)	0% (0/5)	31% (5/16)	7% (1/14)	21% (7/33)	10% (1/10)	25% (2/8)	0.493
Hepatocellular adenoma	3% (7/262)	2% (4/176)	0% (0/5)	6% (1/16)	7% (1/14)	3% (1/33)	0% (0/10)	0% (0/8)	0.522
PBC	1% (5/262)	1% (4/176)	0% (0/5)	0% (0/16)	0% (0/14)	0% (0/33)	0% (0/10)	6% (1/8)	0.444
Other	4% (11/262)	5% (9/176)	0% (0/5)	0% (0/16)	0% (0/14)	3% (1/33)	10% (1/10)	0% (0/8)	0.822
None	16% (42/262)	15% (26/176)	100% (5/5)	13% (2/16)	21% (3/14)	9% (3/33)	20% (2/10)	13% (1/8)	0.002*

Table 8: Observed counts of patient characteristics and risk factors in cases included in the study, sorted by lesion subtypes present in each case. IQR = interquartile range. NOS = not otherwise specified. ECOG = Eastern Cooperative Oncology Group. AFP = alpha-fetoprotein. Pathology: N = None. S = steatosis. F = fibrosis. C = cirrhosis.

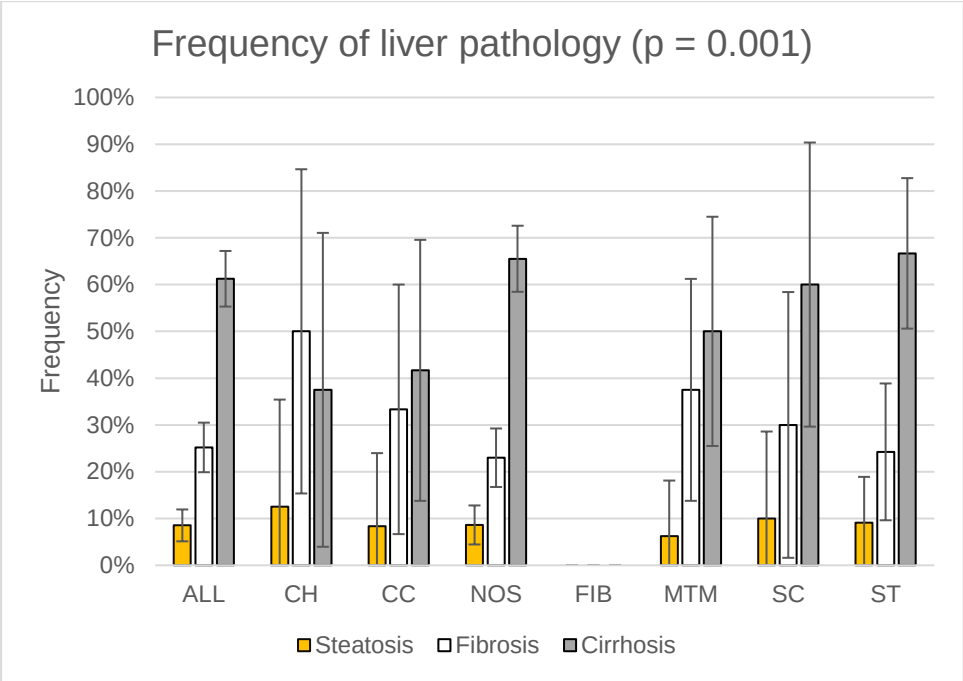

Figure 16: Relative frequencies of steatosis, fibrosis and cirrhosis by subtype of HCC. No liver pathology was present in patients with FIB-HCC. Error bars represent 95% confidence intervals.

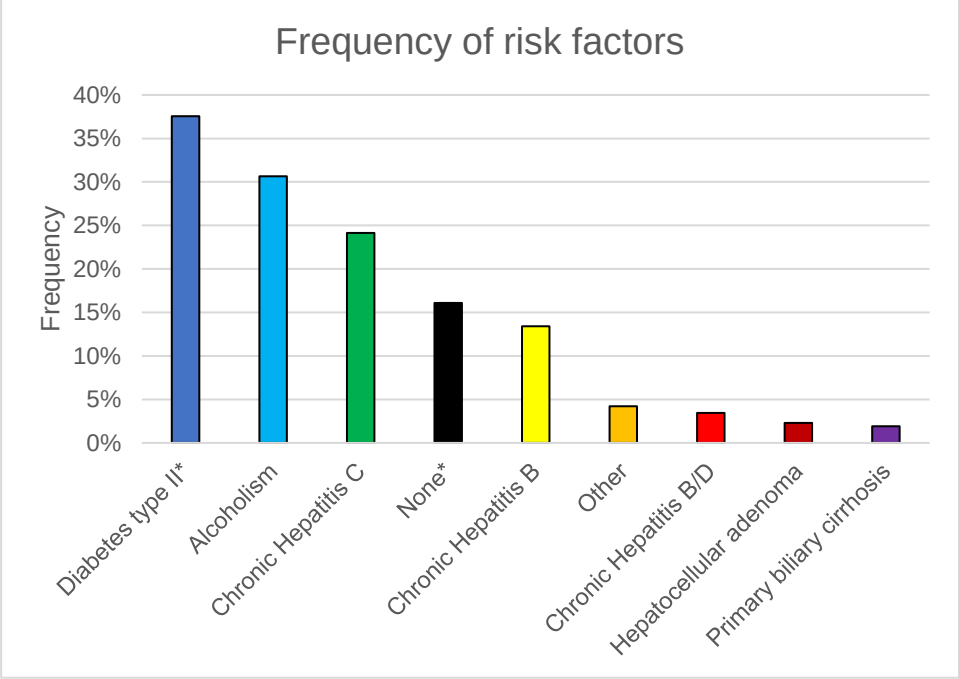

*Figure 17: Frequencies of risk factors in the study cohort on a per-lesion basis. The category "Other" comprises α1-antitrypsin deficiency, haemochromatosis, M. Wilson, tyrosinaemia, autoimmune hepatitis, steroid diabetes, choledocholithiasis and diabetes mellitus type I, all with counts no higher than 3. The category "None" signifies that no risk factors are known. *A significant difference was found for the distribution of this risk factor among subtypes. DM II = diabetes mellitus type II. HCV = hepatitis C virus. HBV = hepatitis B virus. HCA = hepatocellular adenoma. PBC = primary biliary cirrhosis.*

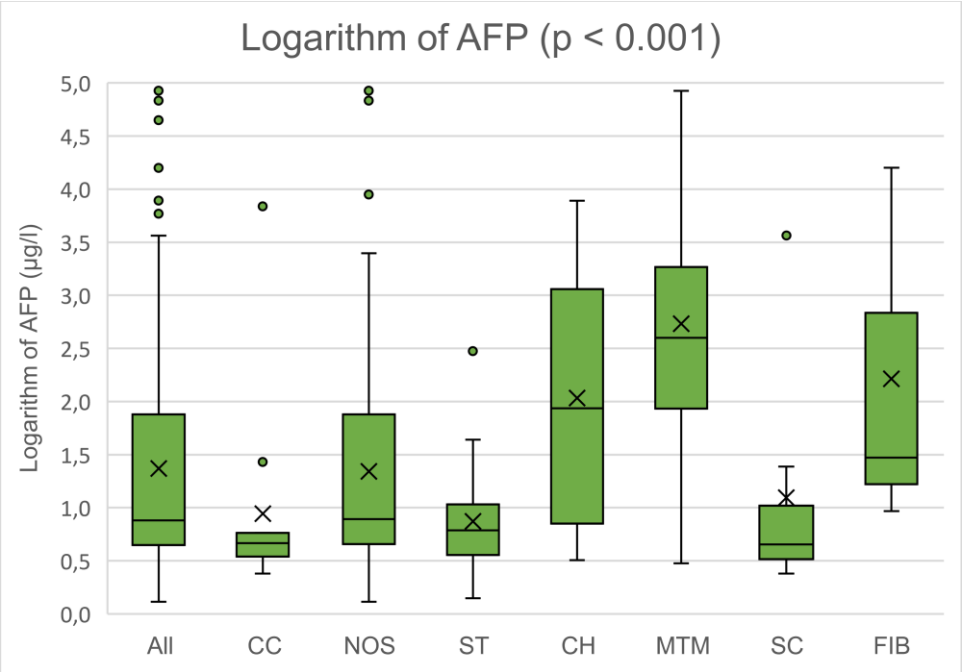

Figure 18: Box-and-whisker plots of the logarithm of AFP by subtype. Circles represent outliers. Crosses represent mean values of log AFP for each group.

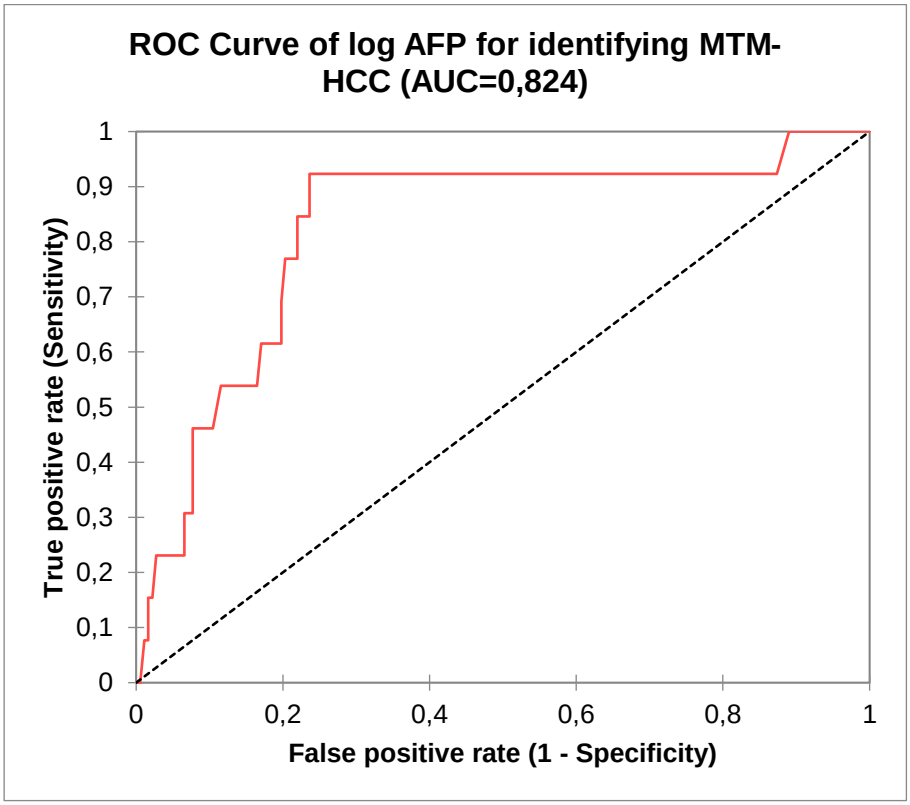

Figure 19: ROC curve of the logarithm of AFP for identifying MTM-HCC among histopathologically confirmed HCC, represented by a step function.

8.2 Lesion characteristics

8.2.1 Unspecific characteristics

Table 9 presents the unspecific characteristics of the lesions. The median lesion size was 33 mm, with an interquartile range (IQR) of 20 to 55 mm (as illustrated in Figure 20). Among the cases, 61% (160/262) had exactly 1 lesion, 32% (84/262) had 2 to 4 lesions, and 7% (18/262) had 5 or more lesions. This latter group included lesions that were not histopathologically confirmed as HCC but had a similar MRI-morphologic appearance to those lesions that were histopathologically confirmed as HCC.

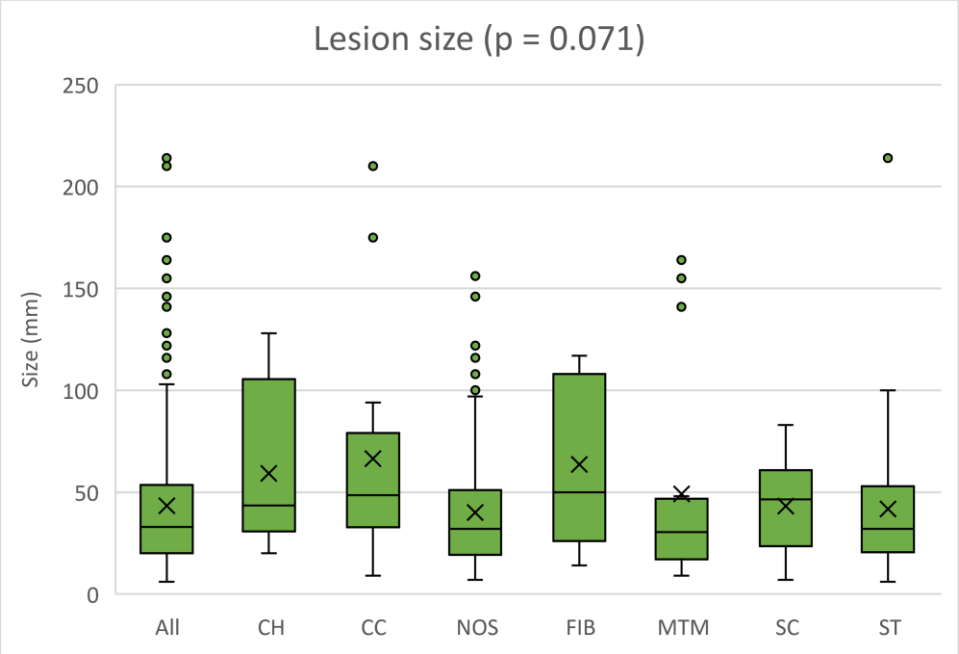

Figure 20: Box-and-whisker plots of lesion size by subtype, defined as the greatest diameter in any plane in Gd-EOB-enhanced MRI. Arterial phases and diffusion-weighted imaging were not used for measurements to avoid overestimation. Circles represent outliers. Crosses represent mean lesion size for each group.

8.2.2 Histopathological analysis

Among the 262 analyzed lesions, 33% (86/262) were categorized into one of the eight subtypes defined by the WHO, while the remaining lesions were classified under the NOS category (as depicted in Figure 21). Only one lesion was identified as the LR-HCC subtype, and no lesions were classified as GR-HCC subtype, leading to the exclusion of these subtypes from statistical analysis. For all other subtypes and NOS-HCC, 5 or more lesions were found. The IOA for subtype assignment was almost perfect, as indicated by a Cohen's k value of 0.95, with disagreements observed in only 2.7% (7/262) of lesions.

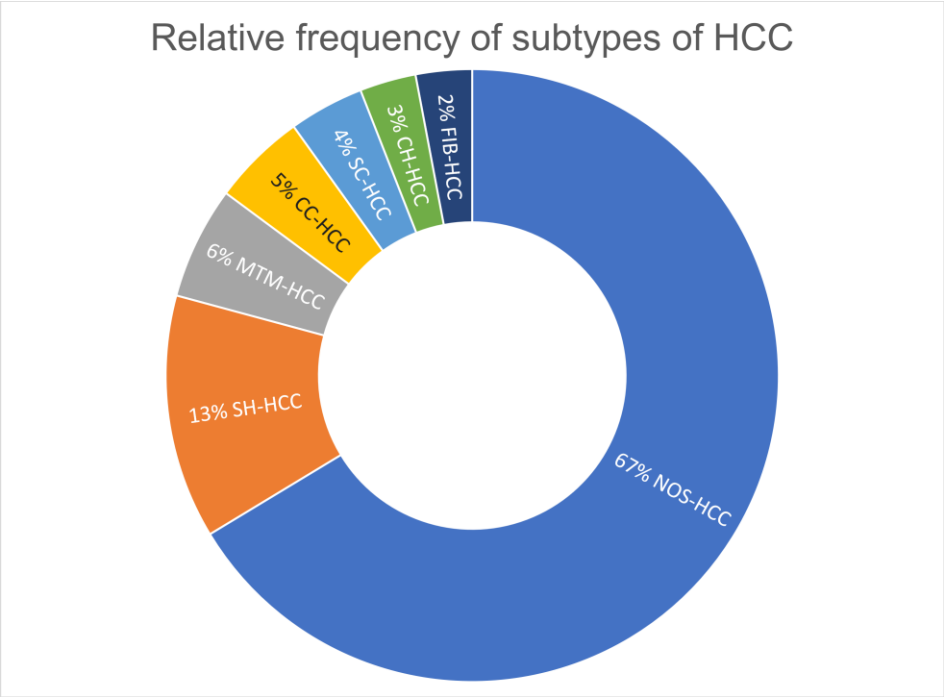

Figure 21: Pie chart showing the relative frequency of NOS and each subtype of HCC in the study cohort after histopathological analysis. The single lymphocyte-rich HCC lesion was excluded due to statistical irrelevance.

In 32% (83/262) of lesions, there were areas that appeared to be of a different subtype compared to the subtype assigned to the lesion. This phenomenon was observed in 34% (89/262) of NOS-HCC, 25% (4/16) of MTM-HCC, 29% (4/14) of CC-HCC, 39% (13/33) of ST-HCC and 30% (3/10) of SC-HCC. The majority of lesions (68%, 178/262) had an Edmondson Steiner grade of 2, while the remaining lesions were distributed between grades 1 and 3, accounting for 13% (34/262) and 19% (50/262), respectively.

8.2.3 Radiological lesion characteristics

Table 9 presents the compiled the results of radiological analysis of non-dynamic phase imaging. Statistically significant differences were found for macrovascular invasion (Figure 22) and intralesional steatosis (Figure 23). Macrovascular invasion occurred more often with MTM-HCC lesions (31% (5/16) compared to 8% (21/262) in the whole cohort, **p = 0.033**), whereas the great majority of ST-HCC showed intralesional steatosis (88% (28/32) compared to 27% (68/250), **p < 0.001**). 94% (15/16) of MTM-HCCs had a T2 signal intensity classed as '3: iso- to hyperintense' or '4: hyperintense' in comparison to 75% (194/262) for the entire cohort. However, no significant difference was found in T2 signal intensity scores between all subtypes (**p = 0.657**).

UNSPECIFIC LESION CHARACTERISTICS	Whole cohort (n=262)	NOS-HCC (n=176)	FIB-HCC (n=5)	MTM-HCC (n=16)	CC-HCC (n=14)	ST-HCC (n=33)	SC-HCC (n=10)	CH-HCC (n=8)	p-value
Size (mm) median (IQR)	33 (20-55)	32 (19-51)	50 (26-108)	31 (17-47)	49 (33-79)	32 (21-53)	47 (24-61)	44 (31-106)	0.071
Differentiation (Edm. St.)	1: 13% (34/256) 2: 68% (174/256) 3: 19% (48/256)	1: 14% (24/173) 2: 67% (116/173) 3: 19% (33/173)	1: 0% (0/4) 2: 50% (2/4) 3: 50% (2/4)	1: 0% (0/16) 2: 63% (10/16) 3: 38% (6/16)	1: 25% (3/12) 2: 67% (8/12) 3: 8% (1/12)	1: 21% (7/33) 2: 70% (23/33) 3: 9% (3/33)	1: 0% (0/10) 2: 80% (8/10) 3: 20% (2/10)	1: 0% (0/8) 2: 88% (7/8) 3: 13% (1/8)	0.203
Nodule-in-nodule appearance	18% (48/262)	18% (32/176)	20% (1/5)	25% (4/16)	14% (2/14)	15% (5/33)	10% (1/10)	38% (3/8)	0.749
Macrovascular invasion	8% (21/262)	7% (12/176)	20% (1/5)	31% (5/16)	7% (1/14)	3% (1/33)	0% (0/10)	13% (1/8)	0.033*
Intralesional hemorrhage	23% (59/262)	22% (38/176)	20% (1/5)	19% (3/16)	29% (4/14)	24% (8/33)	20% (2/10)	38% (3/8)	0.925
Intralesional steatosis	27% (69/251)	18% (30/169)	20% (1/5)	27% (4/15)	31% (4/13)	88% (28/32)	11% (1/9)	13% (1/8)	<0.001*
Necrosis	25% (64/261)	23% (41/175)	20% (1/5)	38% (6/16)	29% (4/14)	27% (9/33)	10% (1/10)	25% (2/8)	0.804
Diffusion restriction	71% (130/182)	71% (92/130)	100% (2/2)	80% (8/10)	67% (6/9)	67% (14/21)	100% (4/4)	67% (4/6)	0.277
ADC median (IQR)	986 (867-1104)	954 (865-1084)	656 °	963 (748-1213)	1038 (987-1148)	998 (786-1140)	1028 (815-1106)	1063 (983-1247)	0.716
T1 signal intensity	0: 29% (77/262) 1: 34% (88/262) 2: 24% (64/262) 3: 10% (26/262) 4: 3% (7/262)	0: 27% (48/176) 1: 33% (58/176) 2: 25% (44/176) 3: 13% (22/176) 4: 2% (4/176)	0: 60% (3/5) 1: 40% (2/5) 2: 0% (0/5) 3: 0% (0/5) 4: 0% (0/5)	0: 56% (9/16) 1: 38% (6/16) 2: 6% (1/16) 3: 0% (0/16) 4: 0% (0/16)	0: 29% (4/14) 1: 43% (6/14) 2: 29% (4/14) 3: 0% (0/14) 4: 0% (0/14)	0: 21% (7/33) 1: 27% (9/33) 2: 36% (12/33) 3: 9% (3/33) 4: 6% (2/33)	0: 30% (3/10) 1: 30% (3/10) 2: 20% (2/10) 3: 10% (1/10) 4: 10% (1/10)	0: 38% (3/8) 1: 50% (4/8) 2: 13% (1/8) 3: 0% (0/8) 4: 0% (0/8)	0.424
T2 signal intensity	0: 0% (1/262) 1: 5% (13/262) 2: 20% (53/262) 3: 55% (143/262) 4: 20% (52/262)	0: 1% (1/176) 1: 5% (8/176) 2: 22% (39/176) 3: 56% (99/176) 4: 16% (29/176)	0: 0% (0/5) 1: 0% (0/5) 2: 0% (0/5) 3: 80% (4/5) 4: 20% (1/5)	0: 0% (0/16) 1: 0% (0/16) 2: 6% (1/16) 3: 44% (7/16) 4: 50% (8/16)	0: 0% (0/14) 1: 7% (1/14) 2: 14% (2/14) 3: 57% (8/14) 4: 21% (3/14)	0: 0% (0/33) 1: 6% (2/33) 2: 24% (8/33) 3: 45% (15/33) 4: 24% (8/33)	0: 0% (0/10) 1: 10% (1/10) 2: 20% (2/10) 3: 60% (6/10) 4: 10% (1/10)	0: 0% (0/8) 1: 13% (1/8) 2: 13% (1/8) 3: 50% (4/8) 4: 25% (2/8)	0.657

Table 9: Observed counts of unspecific lesion characteristics among lesions of each subtype. NOS = not otherwise specified. IQR = interquartile range. Edm. St. = Edmondson Steiner. ADC = apparent diffusion coefficient. ° IQR for ADC could not be computed for FIB-HCC as DWI was only available for 2 lesions.

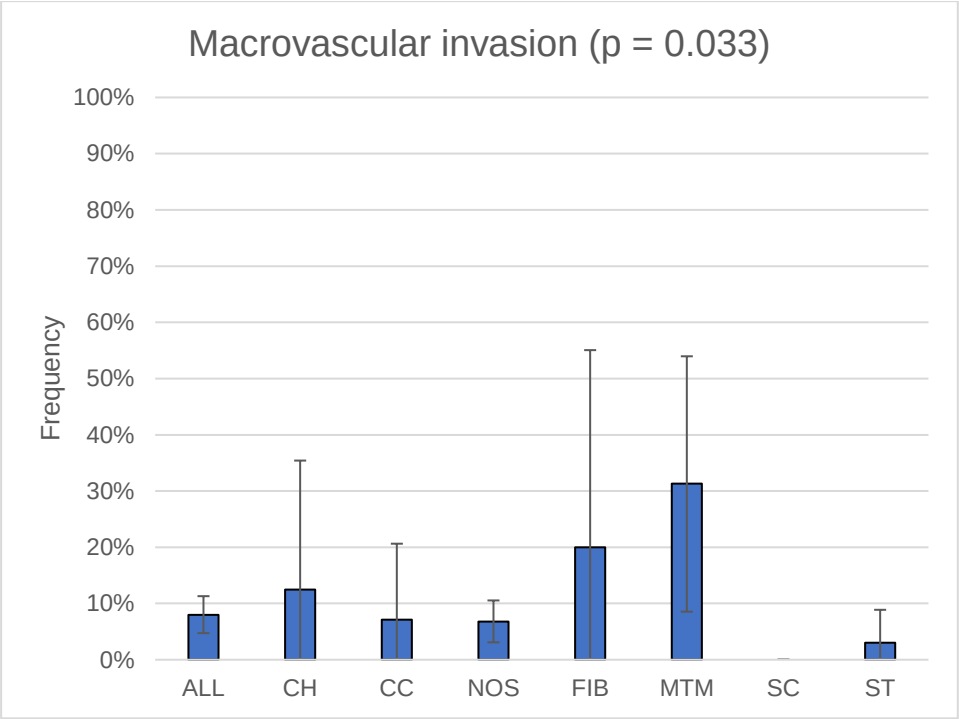

Figure 22: Frequency of tumor invasion of the main branches of the portal vein and/or hepatic veins by subtype of HCC. Error bars represent 95% confidence intervals.

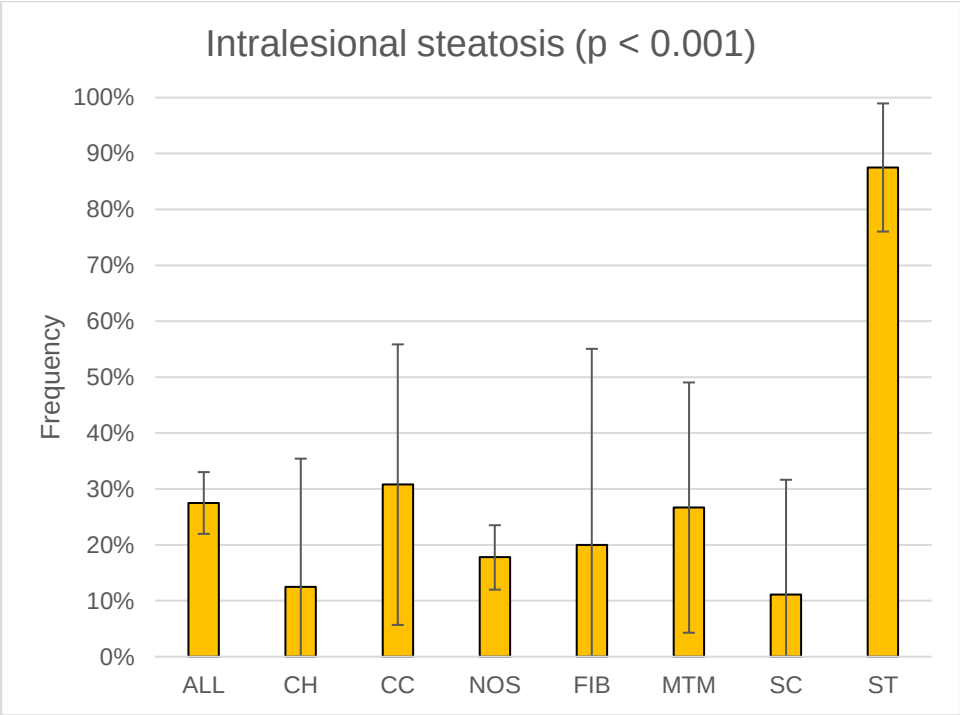

Figure 23: Frequency of intralesional steatosis by subtype of HCC. Error bars represent 95% confidence intervals.

8.2.4 Multi-phase imaging: imaging features

The results of analysis of qualitative imaging features are compiled in Table 10. While neither APHE (**p = 0.087**) (Figure 24) nor portal venous washout (**p = 0.234**) (Figure 25) differed significantly, the combination of non-rim APHE and washout was significantly different. This pattern was present in 46% (114/247) of the cohort, but was lower in all subtypes except ST-HCC and FIB-HCC (**p = 0.035**). It was particularly infrequent in MTM-HCC (20%, 3/15), SC-HCC (22%, 2/9) and CH-HCC (13%, 1/8) (Figure 26). When combining this pattern with HBP hypointensity, the difference was no longer significant across all subtypes **(p = 0.085**). However, it became significant when combining all subtypes, as 36% (21/58) of cases had this combination compared to 52% (75/168) of NOS-HCCs (**p = 0.008**) (Figure 27). Examples of typical and atypical enhancement patterns are shown in Figure 28 and Figure 29, respectively. Pseudocapsule enhancement was close to significant as it was nearly twice as frequent in MTM-HCC (64%, 9/14) and CH-HCC (63%, 5/8) compared to the whole cohort (33%, 78/239) (**p = 0.069**) (Figure 30). Washout was almost exclusively non-peripheral, with exceptions being ST-HCC 9% (2/23) and NOS-HCC 2% (2/125).

8.2.5 Multi-phase imaging: enhancement ratios

The results of analysis of dynamic phase enhancement ratios have been compiled in Table 11. Enhancement ratios in the arterial (Figure 31) and post-arterial phases (

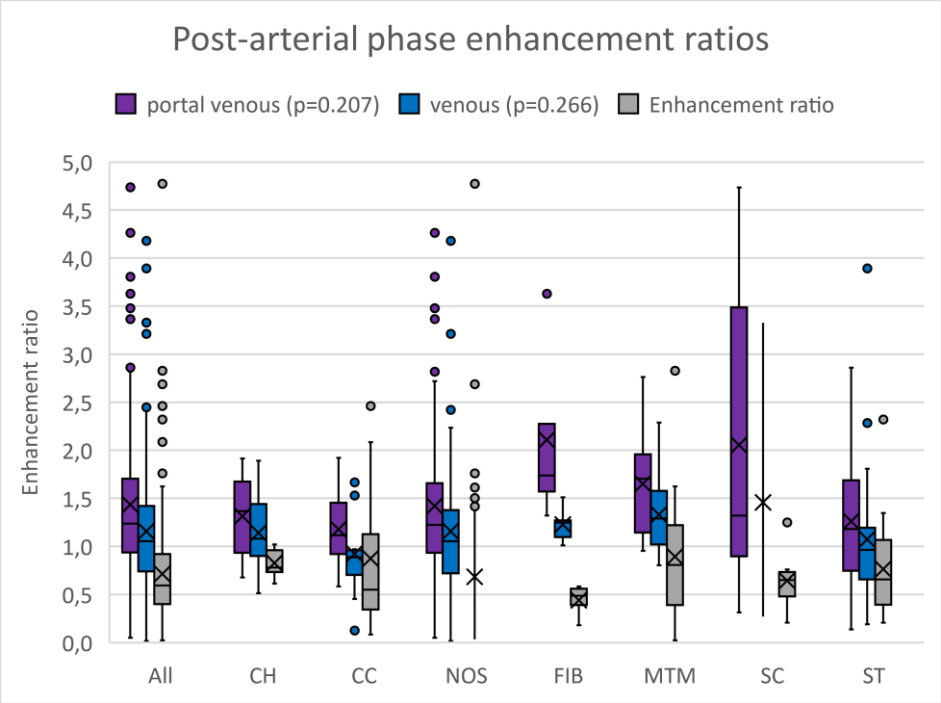

Figure 32) were not found to be significantly different. Arterial phases were excluded more frequently from 2D ROI placement due to transient respiratory motion artifacts (81/262, 31%) than other phases (24-36/262, 9-14%) (**p < 0.001** in post-hoc analysis).

8.2.6 Multi-phase imaging: signal intensity and heterogeneity, Gd-EOB uptake area

The results of subjective ratings of signal intensity, signal heterogeneity, and Gd-EOB uptake area have been summarized in Table 12. There was no statistically significant difference observed across all subtypes in these parameters. Among the HCC lesions, 8.9% (23/258) exhibited high enhancement, which we defined as a subjective score of 3 or higher, indicating an uptake area greater than 50%. This was exclusive to NOS-HCC (9.2%, 16/174), ST-HCC (9.1%, 3/33) and CC-HCC (23.1%, 3/13) (**p = 0.031** in post-hoc analysis, Figure 38). IOA for subjective rating of Gd-EOB uptake area was moderate with a Cohen's k of 0.76.

DYNAMIC PHASE IMAGING FEATURES	Whole cohort (n=262)	NOS-HCC (n=176)	FIB-HCC (n=5)	MTM-HCC (n=16)	CC-HCC (n=14)	ST-HCC (n=33)	SC-HCC (n=10)	CH-HCC (n=8)	p-value
Capsule enhancement	33% (78/240)	31% (51/163)	25% (1/4)	64% (9/14)	21% (3/14)	25% (7/28)	22% (2/9)	63% (5/8)	0.069
APHE (R: rim, N: non-rim)	R: 15% (37/248) N: 53% (132/248)	R: 13% (22/168) N: 59% (99/168)	R: 25% (1/4) N: 50% (2/4)	R: 33% (5/15) N: 27% (4/15)	R: 7% (1/14) N: 43% (6/14)	R: 10% (3/30) N: 57% (17/30)	R: 44% (4/9) N: 33% (3/9)	R: 13% (1/8) N: 13% (1/8)	0.087
PVP washout (P: periph., N: nonperiph.)	P: 2% (4/257) N: 70% (179/257)	P: 1% (2/174) N: 72% (125/174)	P: 0% (0/5) N: 60% (3/5)	P: 0% (0/16) N: 81% (13/16)	P: 0% (0/14) N: 57% (8/14)	P: 7% (2/30) N: 70% (21/30)	P: 0% (0/10) N: 60% (6/10)	P: 0% (0/8) N: 38% (3/8)	0.234
Non-rim APHE and nonperiph. PVP washout	46% (114/247)	52% (88/168)	50% (2/4)	20% (3/15)	36% (5/14)	45% (13/29)	22% (2/9)	13% (1/8)	0.035*
Non-rim APHE, nonperiph. PVP washout and HBP hypointensity	39% (96/247)	45% (75/168)	50% (2/4)	13% (2/15)	36% (5/14)	31% (9/29)	22% (2/9)	13% (1/8)	0.085

Table 10: Observed counts of imaging features in dynamic T1w-FS phases of Gd-EOB-enhanced MRI in lesions of each subtype. APHE = arterial-phase hyperenhancement. PVP = portal venous phase. HBP = hepatobiliary phase. SD = standard deviation.

DYNAMIC PHASE ENHANCEMENT RATIOS	**Whole cohort (n=262)**	NOS-HCC (n=176)	FIB-HCC (n=5)	MTM-HCC (n=16)	CC-HCC (n=14)	ST-HCC (n=33)	SC-HCC (n=10)	CH-HCC (n=8)	**p-value**
Arterial, mean (SD)	6,23 (9,72) (n=181)	5,94 (8,21) (n=116)	17,61 (22,51) (n=3)	7,14 (6,67) (n=15)	4,71 (6,46) (n=12)	4,09 (4,72) (n=22)	18,15 (30,97) (n=7)	2,34 (0,92) (n=7)	0.072
Portal venous, mean (SD)	1,41 (0,99) (n=238)	1,39 (1,05) (n=159)	2,11 (1,04) (n=4)	1,62 (0,63) (n=16)	1,18 (0,39) (n=14)	1,28 (0,65) (n=28)	2,18 (1,78) (n=9)	1,21 (0,48) (n=8)	0.207
Venous, mean (SD)	1,16 (0,8) (n=233)	1,17 (0,87) (n=155)	1,23 (0,19) (n=5)	1,3 (0,44) (n=16)	0,92 (0,45) (n=14)	1,08 (0,74) (n=27)	1,52 (1,07) (n=8)	1,09 (0,5) (n=8)	0.266
Hepatobiliary, mean (SD)	0,7 (0,54) (n=226)	0,68 (0,53) (n=153)	0,44 (0,16) (n=5)	0,8 (0,79) (n=15)	0,87 (0,81) (n=10)	0,77 (0,47) (n=28)	0,68 (0,31) (n=8)	0,8 (0,15) (n=7)	0.501

Table 11: Mean ratio between lesion enhancement and liver enhancement in each phase of dynamic T1w-FS imaging with Gd-EOB-enhanced MRI. SD = standard deviation.

DYNAMIC PHASE SUBJECTIVE EVALUATION	Whole cohort (n=262)	NOS-HCC (n=176)	FIB-HCC (n=5)	MTM-HCC (n=16)	CC-HCC (n=14)	ST-HCC (n=33)	SC-HCC (n=10)	CH-HCC (n=8)	p-value
Arterial phase Signal intensity	0: 6% (15/247) 1: 14% (35/247) 2: 11% (28/247) 3: 33% (81/247) 4: 36% (88/247)	0: 5% (9/167) 1: 12% (20/167) 2: 10% (17/167) 3: 31% (52/167) 4: 41% (69/167)	0: 0% (0/4) 1: 0% (0/4) 2: 25% (1/4) 3: 50% (2/4) 4: 25% (1/4)	0: 13% (2/15) 1: 20% (3/15) 2: 7% (1/15) 3: 60% (9/15) 4: 0% (0/15)	0: 14% (2/14) 1: 14% (2/14) 2: 21% (3/14) 3: 14% (2/14) 4: 36% (5/14)	0: 7% (2/30) 1: 17% (5/30) 2: 10% (3/30) 3: 43% (13/30) 4: 23% (7/30)	0: 0% (0/9) 1: 0% (0/9) 2: 22% (2/9) 3: 22% (2/9) 4: 56% (5/9)	0: 0% (0/8) 1: 63% (5/8) 2: 13% (1/8) 3: 13% (1/8) 4: 13% (1/8)	0.018*
Portal venous phase Signal intensity	0: 16% (42/258) 1: 36% (93/258) 2: 17% (43/258) 3: 25% (65/258) 4: 6% (15/258)	0: 16% (27/173) 1: 37% (64/173) 2: 17% (30/173) 3: 25% (43/173) 4: 5% (9/173)	0: 0% (0/5) 1: 20% (1/5) 2: 0% (0/5) 3: 60% (3/5) 4: 20% (1/5)	0: 38% (6/16) 1: 44% (7/16) 2: 6% (1/16) 3: 13% (2/16) 4: 0% (0/16)	0: 14% (2/14) 1: 43% (6/14) 2: 14% (2/14) 3: 21% (3/14) 4: 7% (1/14)	0: 16% (5/32) 1: 31% (10/32) 2: 16% (5/32) 3: 31% (10/32) 4: 6% (2/32)	0: 0% (0/10) 1: 20% (2/10) 2: 30% (3/10) 3: 30% (3/10) 4: 20% (2/10)	0: 25% (2/8) 1: 38% (3/8) 2: 25% (2/8) 3: 13% (1/8) 4: 0% (0/8)	0.466
Venous phase Signal intensity	0: 32% (80/252) 1: 41% (104/252) 2: 18% (45/252) 3: 8% (21/252) 4: 1% (2/252)	0: 30% (50/168) 1: 45% (75/168) 2: 17% (28/168) 3: 8% (14/168) 4: 1% (1/168)	0: 40% (2/5) 1: 40% (2/5) 2: 20% (1/5) 3: 0% (0/5) 4: 0% (0/5)	0: 44% (7/16) 1: 44% (7/16) 2: 6% (1/16) 3: 6% (1/16) 4: 0% (0/16)	0: 29% (4/14) 1: 43% (6/14) 2: 21% (3/14) 3: 7% (1/14) 4: 0% (0/14)	0: 35% (11/31) 1: 29% (9/31) 2: 26% (8/31) 3: 6% (2/31) 4: 3% (1/31)	0: 10% (1/10) 1: 30% (3/10) 2: 40% (4/10) 3: 20% (2/10) 4: 0% (0/10)	0: 63% (5/8) 1: 25% (2/8) 2: 0% (0/8) 3: 13% (1/8) 4: 0% (0/8)	0.641
Hepatobiliary phase Signal intensity	0: 31% (80/257) 1: 62% (160/257) 2: 4% (10/257) 3: 1% (3/257) 4: 2% (4/257)	0: 31% (54/173) 1: 61% (105/173) 2: 5% (9/173) 3: 1% (2/173) 4: 2% (3/173)	0: 60% (3/5) 1: 40% (2/5) 2: 0% (0/5) 3: 0% (0/5) 4: 0% (0/5)	0: 44% (7/16) 1: 56% (9/16) 2: 0% (0/16) 3: 0% (0/16) 4: 0% (0/16)	0: 23% (3/13) 1: 69% (9/13) 2: 0% (0/13) 3: 0% (0/13) 4: 8% (1/13)	0: 24% (8/33) 1: 70% (23/33) 2: 3% (1/33) 3: 3% (1/33) 4: 0% (0/33)	0: 30% (3/10) 1: 70% (7/10) 2: 0% (0/10) 3: 0% (0/10) 4: 0% (0/10)	0: 29% (2/7) 1: 71% (5/7) 2: 0% (0/7) 3: 0% (0/7) 4: 0% (0/7)	0.910
Hepatobiliary phase Signal heterogeneity	0: 33% (85/257) 1: 42% (108/257) 2: 19% (49/257) 3: 6% (15/257) 4: 0% (0/257)	0: 34% (59/173) 1: 42% (72/173) 2: 18% (31/173) 3: 6% (11/173) 4: 0% (0/173)	0: 60% (3/5) 1: 40% (2/5) 2: 0% (0/5) 3: 0% (0/5) 4: 0% (0/5)	0: 60% (9/15) 1: 20% (3/15) 2: 20% (3/15) 3: 0% (0/15) 4: 0% (0/15)	0: 23% (3/13) 1: 38% (5/13) 2: 38% (5/13) 3: 0% (0/13) 4: 0% (0/13)	0: 21% (7/33) 1: 55% (18/33) 2: 18% (6/33) 3: 6% (2/33) 4: 0% (0/33)	0: 20% (2/10) 1: 50% (5/10) 2: 20% (2/10) 3: 10% (1/10) 4: 0% (0/10)	0: 25% (2/8) 1: 38% (3/8) 2: 25% (2/8) 3: 13% (1/8) 4: 0% (0/8)	0.515
Hepatobiliary phase Gd-EOB uptake area	0: 30% (78/258) 1: 42% (109/258) 2: 19% (49/258) 3: 5% (12/258) 4: 4% (10/258)	0: 31% (54/174) 1: 43% (75/174) 2: 17% (29/174) 3: 5% (8/174) 4: 5% (8/174)	0: 60% (3/5) 1: 40% (2/5) 2: 0% (0/5) 3: 0% (0/5) 4: 0% (0/5)	0: 44% (7/16) 1: 44% (7/16) 2: 13% (2/16) 3: 0% (0/16) 4: 0% (0/16)	0: 23% (3/13) 1: 38% (5/13) 2: 15% (2/13) 3: 15% (2/13) 4: 8% (1/13)	0: 21% (7/33) 1: 42% (14/33) 2: 27% (9/33) 3: 6% (2/33) 4: 3% (1/33)	0: 20% (2/10) 1: 40% (4/10) 2: 40% (4/10) 3: 0% (0/10) 4: 0% (0/10)	0: 29% (2/7) 1: 29% (2/7) 2: 43% (3/7) 3: 0% (0/7) 4: 0% (0/7)	0.726

Table 12: Subjective rating of enhancement patterns and signal intensities in multi-phase T1w-FS imaging in Gd-EOB-enhanced MRI. Legend: Signal intensity: 0: hypo, 1: iso to hypo, 2: iso, 3: iso to hyper, 4: hyperintense relative to liver parenchyma. Signal heterogeneity and Gd-EOB uptake area: 0: 0-5%, 1: 5-25%, 2: 25-50%, 3: 50-75%, 4: 75-100% of total lesion area.

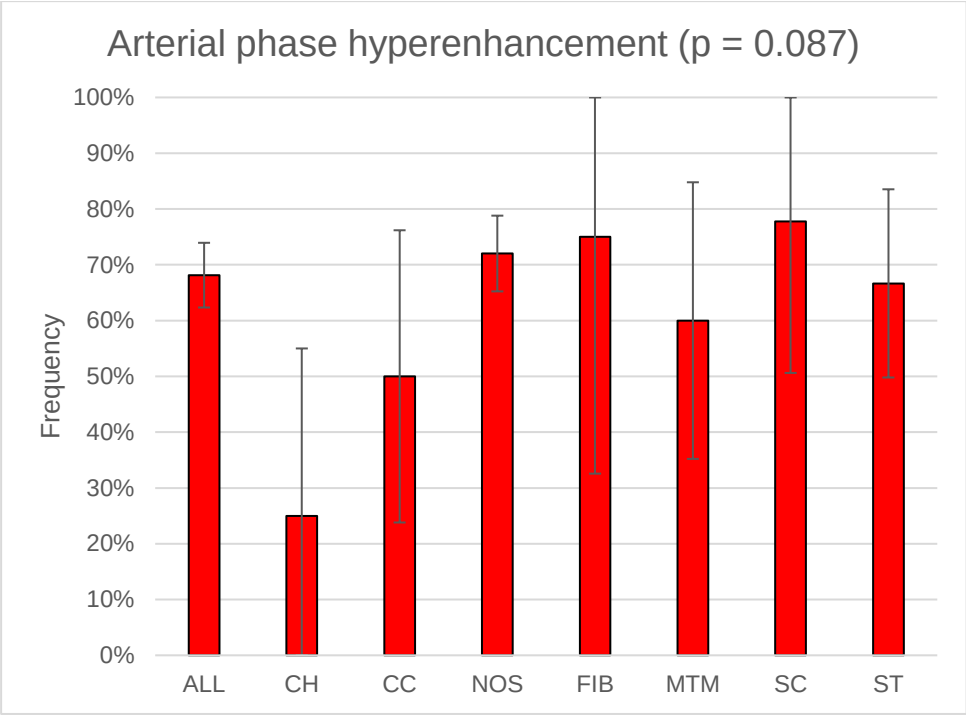

Figure 24: Arterial phase hyperenhancement, defined as a subjectively rated signal intensity of 3 (iso- to hyperintense) or 4 (hyperintense), by subtype. Error bars represent 95% confidence intervals.

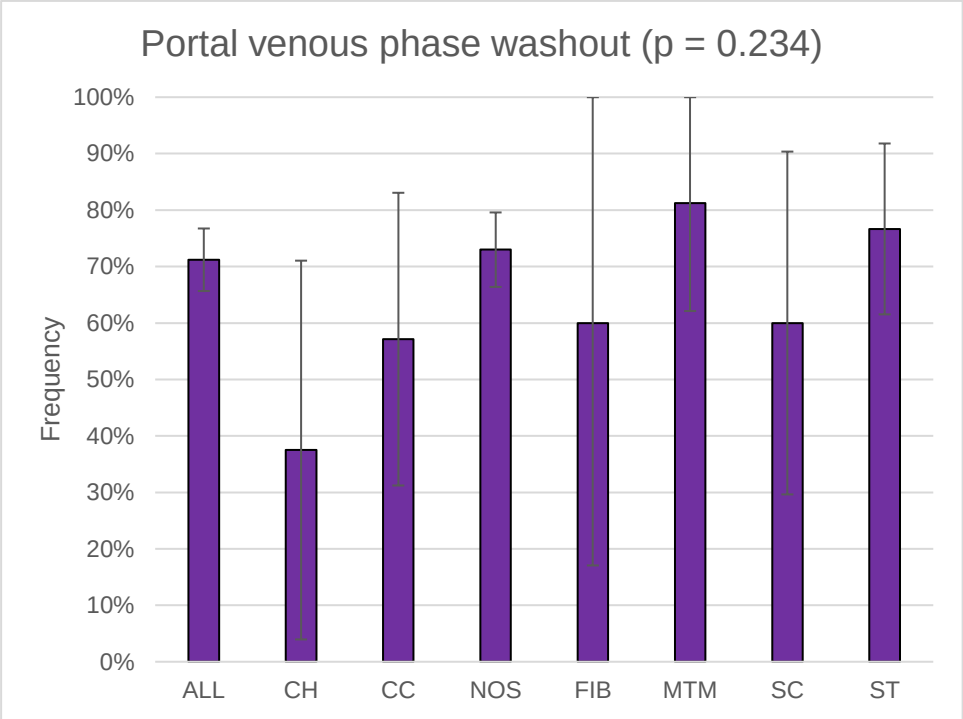

Figure 25: Portal venous washout appearance, defined as a drop in signal intensity in the portal venous phase compared to the arterial phase, by subtype. Error bars represent 95% confidence intervals.

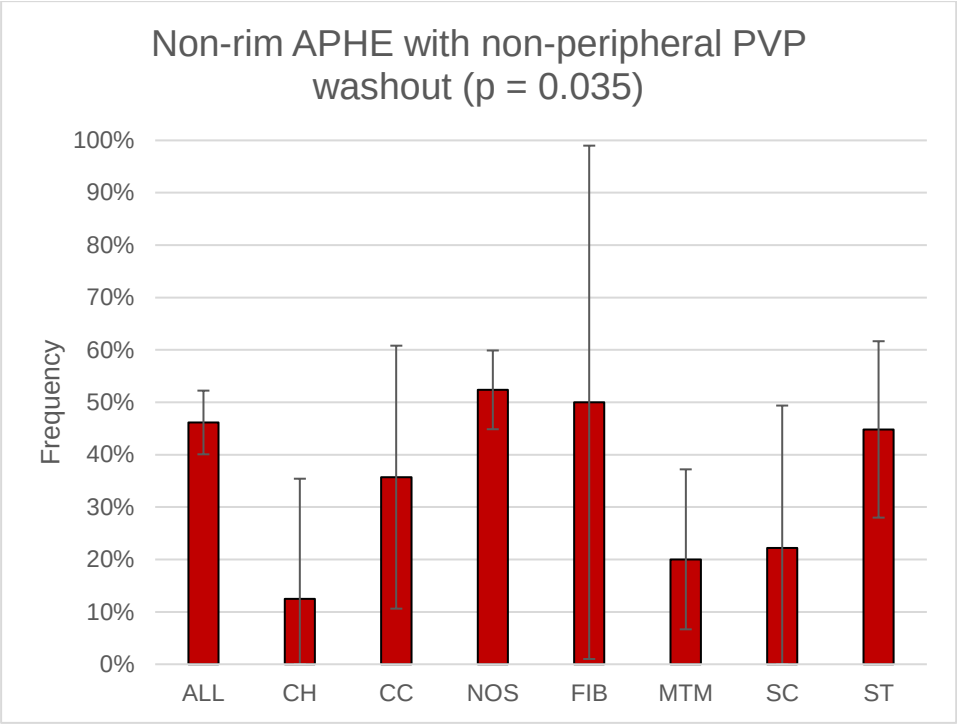

Figure 26: Frequency of non-rim APHE and non-peripheral PVP washout by subtype, representing a classical enhancement pattern for HCC. Error bars represent 95% confidence intervals.

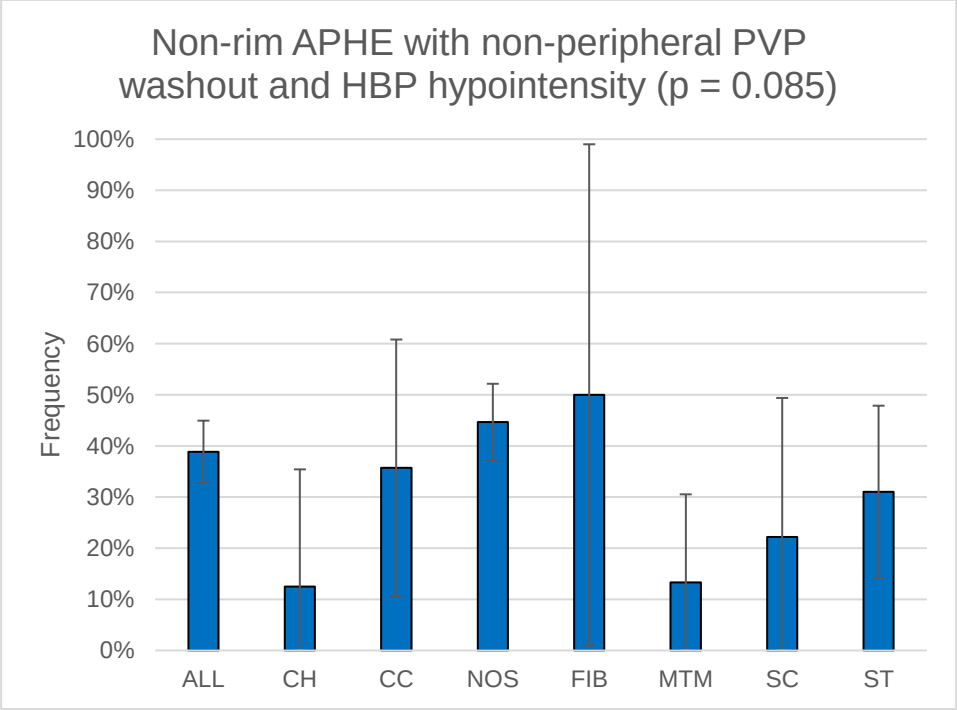

Figure 27: Frequency of non-rim APHE, non-peripheral PVP washout and HBP hypointensity (defined as subjectively rated HBP signal intensity of 0 (hypointense) or 1 (iso- to hypointense)) by subtype, representing a classical enhancement pattern for HCC. Error bars represent 95% confidence intervals.

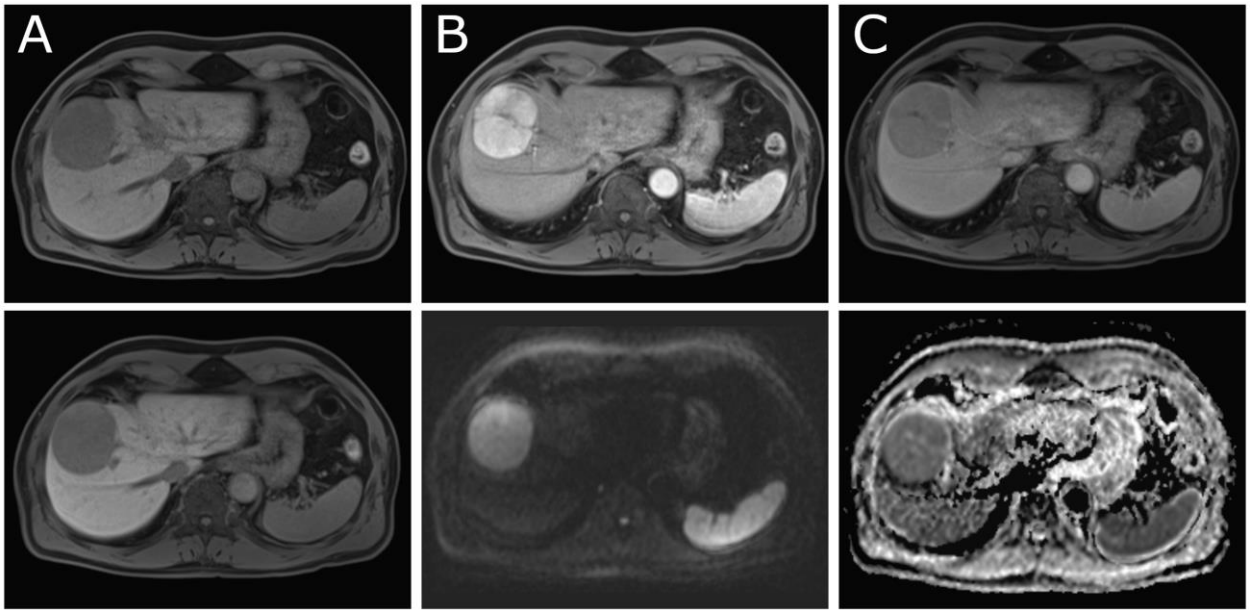

Figure 28: 74-year-old man with liver fibrosis and no known risk factors for HCC. Moderately differentiated NOS-HCC in segment VII with a typical enhancement pattern for HCC (A, B) due to marked non-rim APHE from pre-contrast to arterial phase T1w imaging, (C) non-peripheral washout in the portal venous phase and (D) HBP hypointensity. (E, F) Hyperintensity in DWI (B-value 800) and isointensity in the ADC map indicate diffusion restriction, further suggesting HCC.

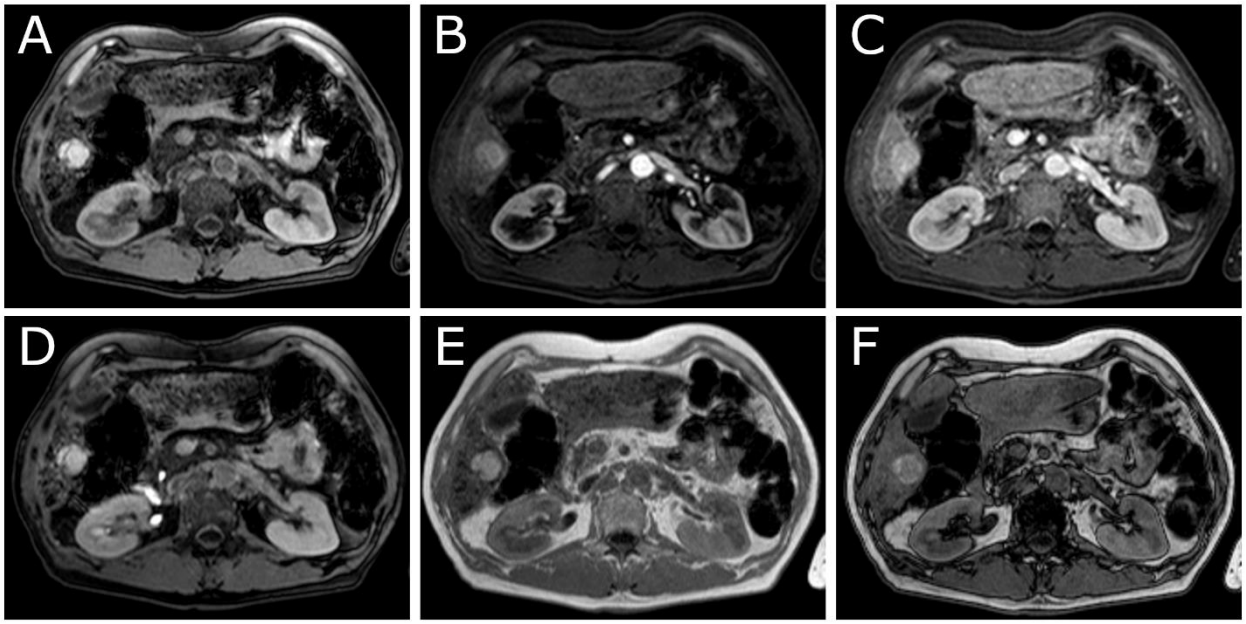

Figure 29: 61-year-old man with liver cirrhosis secondary to alcoholism and diabetes mellitus type II who later underwent liver transplantation. Moderately differentiated ST-HCC in segment VI (A) that is markedly hyperintense in pre-contrast T1w imaging, (B) and shows an atypical enhancement pattern as it drops in signal intensity during the arterial phase, (C) does not show washout in the portal venous phase and (D) remains markedly hyperintense in the HBP. (E, F) Intralesional signal drop from in-phase to opposed-phase T1w imaging indicates intralesional steatosis.

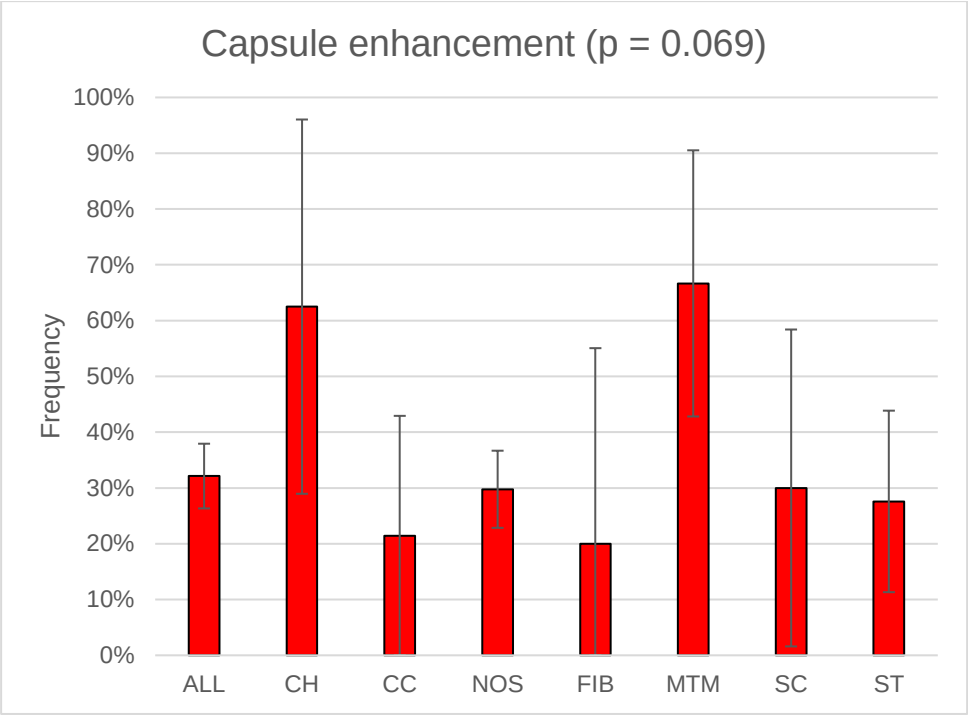

Figure 30: Frequency of capsule enhancement in the arterial phase, defined as a distinct thin band of increased signal intensity along the periphery of the lesion during the arterial phase, by subtype. Error bars represent 95% confidence intervals.

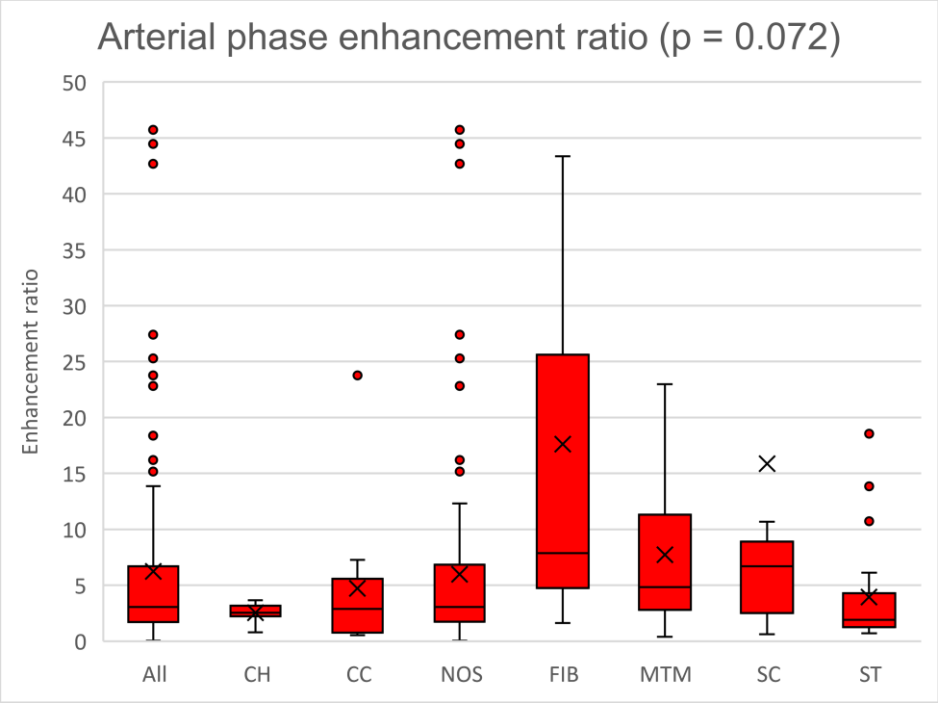

Figure 31: Box-and-whisker plots of the ratio between lesion and liver enhancement during the arterial phase of T1w-FS dynamic multiphase imaging in Gd-EOB-enhanced MRI. Circles represent outliers. Crosses represent the mean of each group.

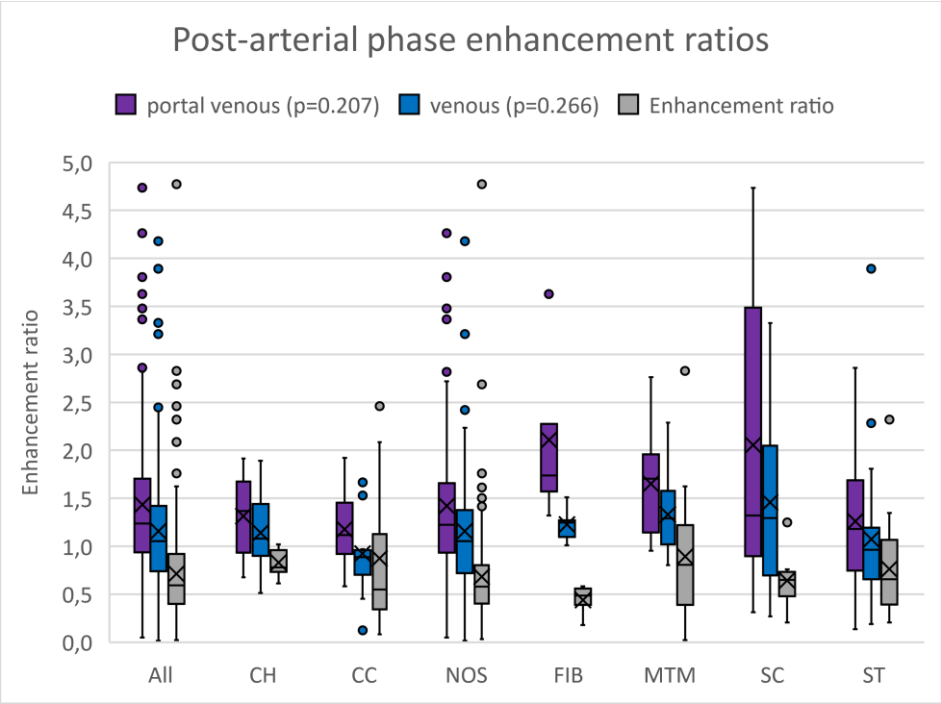

Figure 32: Box-and-whisker plots of the ratio between lesion and liver enhancement during the post-arterial phases of T1w-FS dynamic multiphase imaging in Gd-EOB-enhanced MRI. Circles represent outliers. Crosses represent the mean of each group during the respective phase.

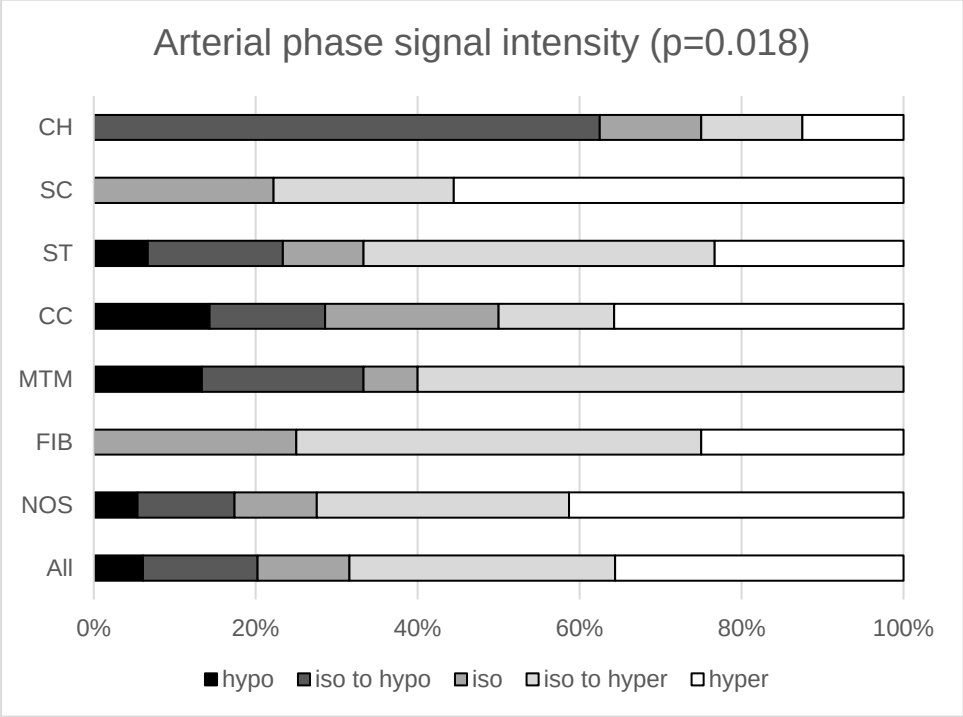

Figure 33: Distribution of subjectively rated predominant signal intensities of HCC lesions relative to liver parenchyma in the arterial phase by subtype.

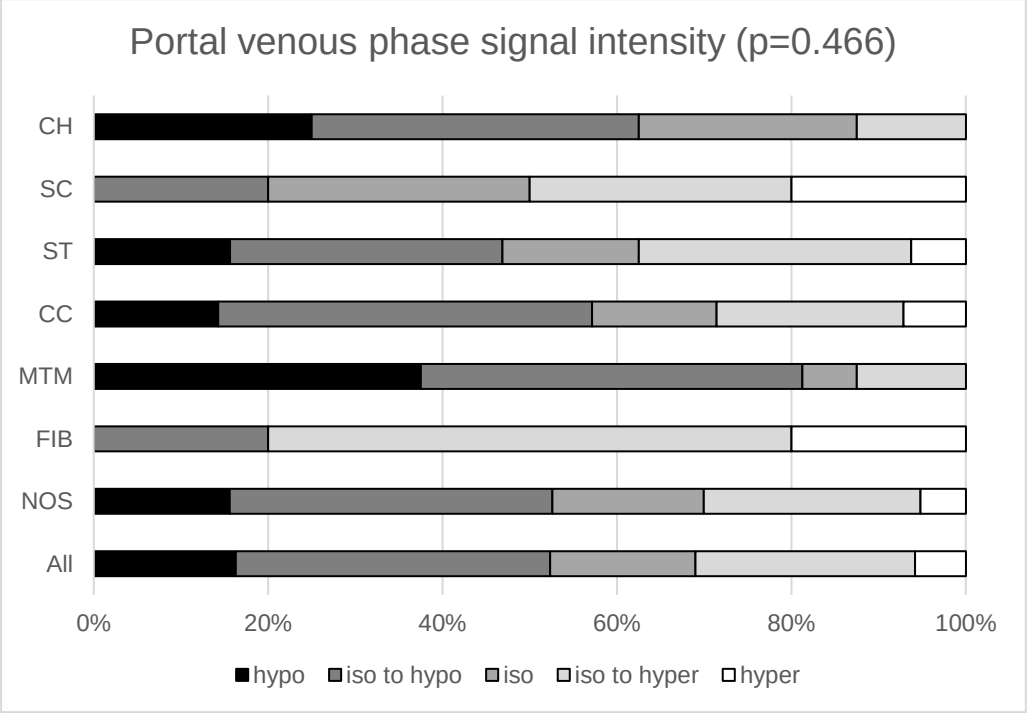

Figure 34: Distribution of subjectively rated predominant signal intensities on a 5-point scale of HCC lesions relative to liver parenchyma in the portal venous phase by subtype.

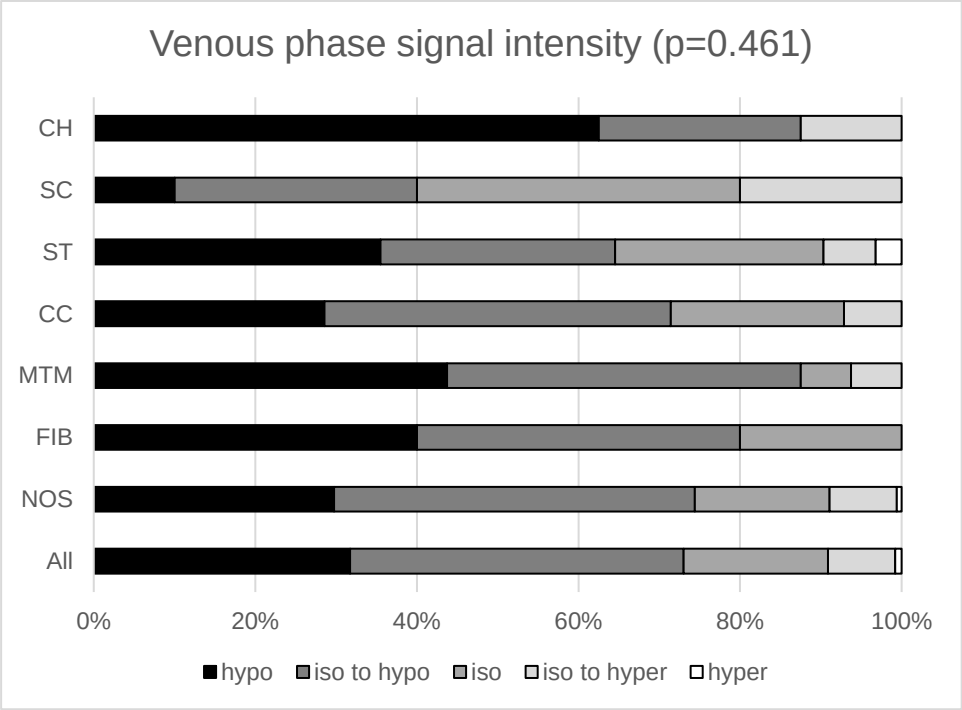

Figure 35: Distribution of subjectively rated predominant signal intensities on a 5-point scale of HCC lesions relative to liver parenchyma in the venous phase by subtype.

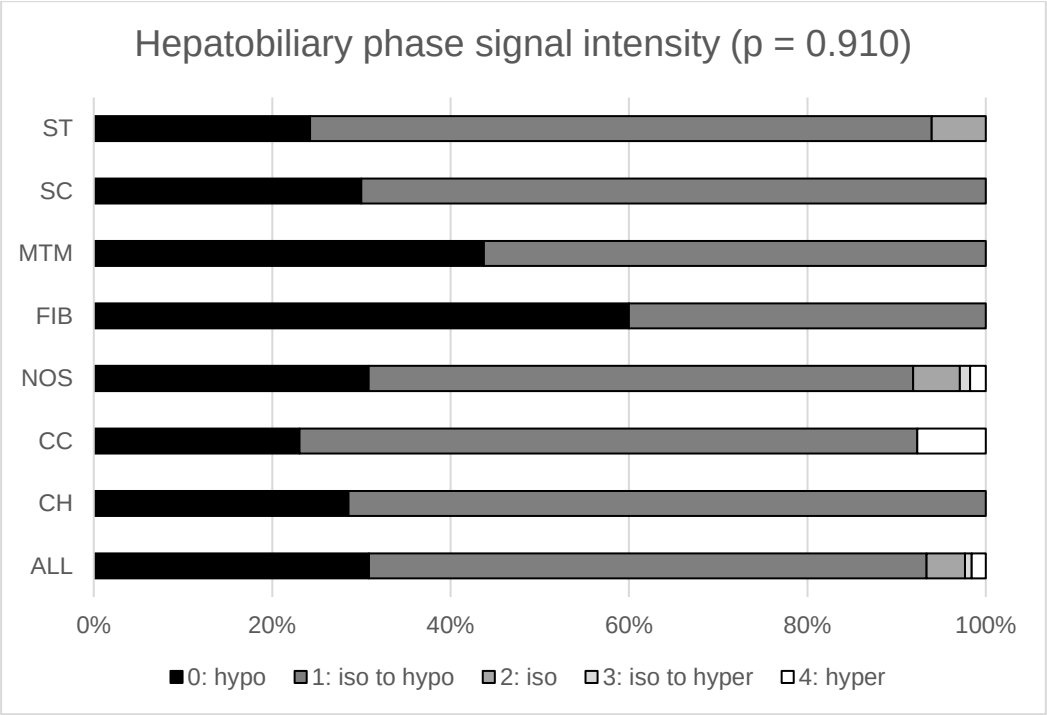

Figure 36: Distribution of subjectively rated predominant signal intensities on a 5-point scale of HCC lesions relative to liver parenchyma in the hepatobiliary phase by subtype.

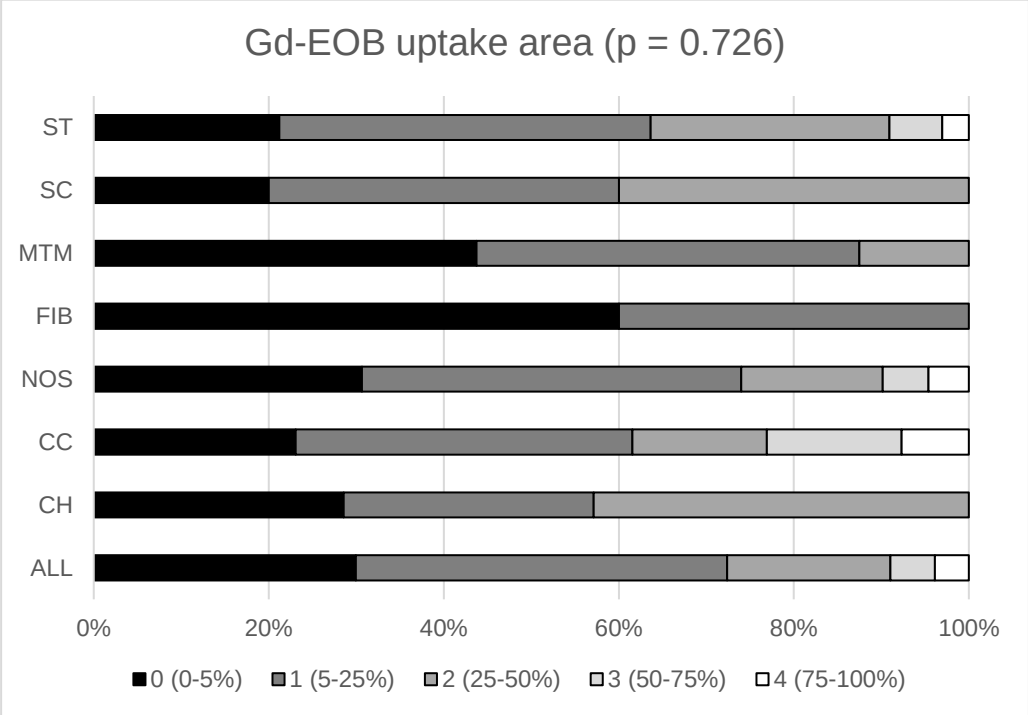

Figure 37: Subjectively rated Gd-EOB uptake area on a 5-point scale, as the proportion of the total lesion area with a signal intensity that is iso- or hyperintense to surrounding parenchyma.

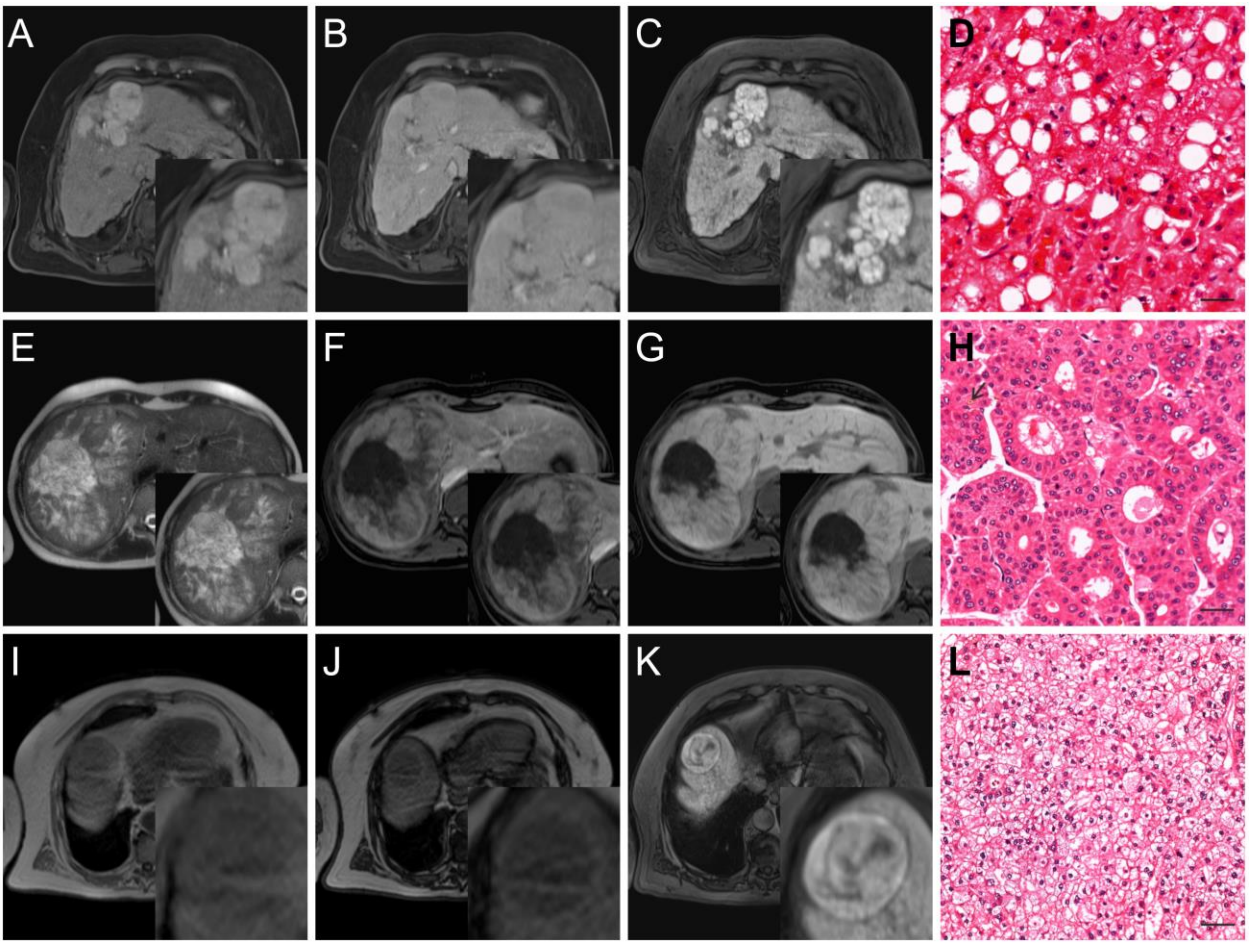

Figure 38: Examples of lesions showing high enhancement in more than 50% of their area in HBP, one per row. The right column represents H&E-stained histopathological slides of each lesion at high magnification. The bar is to scale 50 µm. Quoted histopathological descriptions originate from Auer et al. (2023)[189]

Top row: Man aged 69 years with the following risk factors: liver cirrhosis, diabetes, and alcoholism. Polycyclic NOS-HCC primarily in segment IV with an initially typical enhancement pattern of (A) APHE and (B) portal venous washout, but followed by (C) hyperintensity with prominent septae in the HBP. (D) "The tumor predominantly shows a pseudoglandular growth pattern that might be a correlate for hyperintensity. Tumor cells show mild nuclear atypia. Focally, bile production is visible."
Middle row: Woman aged 23 years with liver steatosis, otherwise no known risk factors. Very large ST-HCC occupying much of the right liver lobe with (E) central T2-hyperintensity representing necrosis, (F) heterogeneous arterial phase enhancement in non-necrotic areas (G) which progressively fill in until the HBP, becoming predominantly isointense to liver parenchyma. (H) "This borderline neoplasia shows predominantly mild nuclear atypia and is mostly encapsulated. Tumor cells contain fat vacuoles and are ballooned. Also, few intratumoral lymphocytes are present. However, there are invasive areas with destroyed reticulin fibers and moderate cellular and nuclear atypia, which promoted the diagnosis of HCC. In the surrounding liver tissue severe steatosis is present."
Bottom row: Man aged 82 years with the following risk factors: liver cirrhosis and diabetes type II. CC-HCC in segment VIII, showing a steatotic phenotype due to signal drop between (I) in-phase and (J) opposed-phase chemical shift imaging. (K) The lesion becomes hyperintense with a prominent capsule in the HBP. (L) "Tumor cells show clear cytoplasm and bland nuclei."

8.3 Predictors for NOS and subtypes of HCC

Finally, on the basis of an evaluation of all available results, potential non-invasive predictors were selected for NOS-HCC (Table 13), FIB-HCC (*Table 14*), ST-HCC (Table 15), MTM-HCC (Table 16), CH-HCC (Table 17), SC-HCC (Table 18) and CC-HCC (Table 19). Predictors were selected according to the following criteria, with preference given to predictors that fulfil multiple criteria:

- Variables whose distribution differed significantly – or close to the significance threshold of p=0.05 – across all subtypes or between NOS and non-NOS.
- Variables that have previously been associated with specific subtypes in the literature.
- Variables whose estimate for mean or median deviated considerably from that of the whole cohort.
- Continuous variables whose AUC according to ROC curve analysis is greater than 0.6 for predicting a specific subtype.

Each chosen predictor was based on these specific criteria and a rationale was provided for their selection. ROC curve analysis with a step-wise function was utilized to determine the optimal threshold, with sensitivity and specificity equally considered. These predictors were then combined to generate potential tests for each HCC subtype. Sensitivity (SEN), specificity (SPE), positive predictive value (PPV), negative predictive value (NPV), positive likelihood ratio (PLR), and negative likelihood ratio (NLR) were reported for each test. To facilitate an improved understanding, color coding was implemented to indicate poor values (deep red) and good values (deep green) for diagnostic accuracy indicators.

Diagnostic accuracy of predictors for NOS-HCC	SEN	SPE	PPV	NPV	PLR	NLR
(1) Typical enhancement pattern	52%	67%	77%	40%	1.58	0.72
(2) Typical enhancement pattern with HBP hypointensity	45%	73%	78%	38%	1.67	0.75

Rationale for the choice of predictors

Classical enhancement pattern: the combination of non-rim APHE and non-peripheral portal venous washout is considered a "classic" enhancement pattern of HCC is commonly evaluated in diagnostic imaging studies of HCC. It has been posited that certain subtypes of HCC may be less likely to exhibit this typical enhancement pattern compared to the more common non-specific (NOS) HCC subtype. In our study cohort, we observed a lower prevalence of this typical enhancement pattern in non-NOS subtypes (33%) compared to NOS-HCC (52%) (p=0.035 across all subtypes and p=0.001 for NOS vs. non-NOS).

HBP hypointensity: another hallmark of HCC is hypointensity in the HBP of Gd-EOB-enhanced MRI, due to a reduced expression of transporters such as OATP1B3 during dedifferentiation. However, this combination remained highly significant for differentiating the NOS subtype from non-NOS subtypes. Specifically, the combination of non-rim APHE, non-peripheral washout, and HBP hypointensity was present in 45% of NOS-HCC cases compared to 27% of non-NOS HCC cases (p=0.008).

Table 13: Diagnostic accuracy of predictors for NOS-HCC among histopathologically confirmed HCC.

Diagnostic accuracy of predictors for FIB-HCC	SEN	SPE	PPV	NPV	PLR	NLR
(1) No pathology and no risk factors	100%	99%	71%	100%	100.0	0.00
(2) No pathology, no risk factors and age <= 60	80%	100%	100%	100%		0.20
(3) No pathology, no risk factors, age <= 60 and female gender	60%	100%	100%	99%		0.40

Rationale for the choice of predictors

Absence of liver pathology and risk factors: FIB-HCC is recognized to occur most often in the absence of any liver pathology or risk factors predisposing to HCC. In our cohort, all FIB-HCCs occurred in the absence of any liver pathology ($p<0.001$) and known risk factors ($p=0.002$).

Female gender: FIB-HCC is reported to have no gender bias, while NOS-HCC is more common in men. In our cohort, 80% of FIB-HCC lesions occurred in women compared to 28% for the cohort as a whole ($p=0.023$).

Age: FIB-HCC occurs more frequently in younger patients, with the median (IQR) in our cohort at 44 (19-66) years compared to 66 (59-72) for the cohort as a whole ($p<0.001$).

*Table 14: Diagnostic accuracy of predictors for FIB-HCC among histopathologically confirmed HCC. *PLR could not be computed as the false positive rate was 0 for tests 2 and 3.*

Diagnostic accuracy of predictors for ST-HCC	SEN	SPE	PPV	NPV	PLR	NLR
(1) Intralesional steatosis	88%	81%	41%	98%	4.63	0.15
(2) Intralesional steatosis and diabetes	53%	96%	65%	93%	13.25	0.49
(3) Diabetes, intralesional steatosis and AFP <= 43 µg/l	54%	96%	67%	93%	13.50	0.48
(4) Diabetes, intralesional steatosis and arterial ER <= 1.725	14%	99%	60%	89%	14.00	0.87
(5) Diabetes, intralesional steatosis, AFP <= 43 µg/l and arterial ER <= 1.725	12%	99%	67%	88%	12.00	0.89

Rationale for the choice of predictors

Intralesional steatosis and diabetes type II: both varied significantly among subtypes, with in particular intralesional steatosis being much higher in ST-HCC (88%) than the cohort average (27%) ($p<0.0001$). Diabetes type II ($p=0.027$) is known to be a recognized risk factor for FLD which is associated with hepatocyte steatosis, similar to the intracellular steatosis observed in ST-HCC.

AFP: the distribution of log AFP varied significantly among subtypes ($p=0.001$), with ST-HCC displaying a lower upper quartile, maximum and IQR than the cohort in its entirety. ROC analysis determined the AUC of AFP to be 0.622 for identifying ST-HCC, with the optimal threshold at 43.6 µg/l with 96.3% sensitivity and 33.3% specificity.

Arterial phase enhancement ratio: the distribution for this variable was close to significant ($p=0.072$), with ST-HCC showing a lower median and upper quartile than most other subtypes. According to ROC analysis, the AUC of the arterial phase enhancement ratio for ST-HCC is 0.615, with the optimal threshold at 1.725 with 50.0% sensitivity and 76.7% specificity.

Table 15: Diagnostic accuracy of predictors for steatohepatitic HCC among histopathologically confirmed HCC.

Diagnostic accuracy of predictors for MTM-HCC	SEN	SPE	PPV	NPV	PLR	NLR
(1) AFP >= 48 µg/l	92%	76%	22%	99%	3.83	0.11
(2) Macrovascular invasion	31%	93%	24%	95%	4.43	0.74
(3) AFP >= 48 µg/l and macrovascular invasion	31%	97%	44%	95%	10.33	0.71
(4) AFP >= 48 µg/l, macrovascular invasion and atypical enhancement	25%	99%	75%	95%	25.00	0.76
(5) AFP >= 48 µg/l, macrovascular invasion and atypical enhancement with no HBP hypointensity	25%	99%	75%	95%	25.00	0.76

Rationale for the choice of predictors

AFP: the association of MTM-HCC with high AFP is recognized, and the value of log AFP varied significantly among subtypes (p=0.001) with MTM-HCC exhibiting the highest median and quartile values. ROC analysis determined the AUC of AFP for identifying MTM-HCC to be 0.824, with the optimal threshold at 48 µg/l with 92.3% sensitivity and 76.4% specificity.

Macrovascular invasion: the literature recognizes the association of MTM-HCC with macrovascular invasion, indicating aggressive growth that is common for this subtype. Macrovascular invasion was significantly more common in MTM-HCC (31%) than in the cohort as a whole (8%) (p=0.033).

Atypical enhancement and no HBP hypointensity: different subtypes of HCC may exhibit a lower likelihood of displaying an atypical enhancement pattern and HBP hypointensity, which helps account for the diverse imaging morphology of HCC. Particularly, MTM-HCC demonstrated notably lower rates of the classic enhancement pattern of non-rim APHE and non-peripheral washout (20% vs. 46% for the entire cohort, p = 0.035 across all subtypes), including in combination with no HBP hypointensity (13% vs. 39% for the entire cohort, p = 0.085 across all subtypes).

Table 16: Diagnostic accuracy of predictors for macrotrabecular massive HCC among histopathologically confirmed HCC.

Diagnostic accuracy of predictors for CH-HCC	SEN	SPE	PPV	NPV	PLR	NLR
(1) Atypical enhancement pattern and arterial ER <= 3.66	86%	66%	9%	99%	2.97	0.20
(2) Atypical enhancement pattern including HBP hypointensity and arterial ER <= 3.66	86%	66%	9%	99%	2.53	0.21
Rationale for the choice of predictors						
Atypical enhancement pattern: the absence of the classical combination of non-rim APHE and non-peripheral washout, with or without HBP hypointensity, may suggest a non-NOS subtype of HCC. Both of these combinations were significantly or close to significantly less common in CH-HCC than our cohort as a whole, at 13% vs. 46% (p = 0.035) and 13% vs. 39% (p = 0.085). **Arterial phase enhancement ratio:** this variable was close to significance (p=0.072) and lower in CH-HCC than in most other subtypes of HCC with very little spread. ROC analysis showed the AUC of the arterial phase enhancement ratio for CH-HCC to be 0.601 with an optimal threshold of 3.66 with 100% sensitivity and 44.3% specificity.						

Table 17: Diagnostic accuracy of predictors for chromophobe HCC among histopathologically confirmed HCC.

Diagnostic accuracy of predictors for scirrhous HCC	SEN	SPE	PPV	NPV	PLR	NLR
(1) Atypical enhancement pattern and no intralesional steatosis	63%	61%	5%	98%	1.62	0.61
(2) Atypical enhancement pattern with no HBP hypointensity and no intralesional steatosis	63%	54%	5%	98%	1.37	0.69
Rationale for the choice of predictors						
Atypical enhancement pattern with no HBP hypointensity: absence of non-rim APHE and non-peripheral washout, with or without HBP hypointensity, may serve as identifiers for non-NOS-HCC. Both of these combinations were less frequent in scirrhous HCC compared to the entire cohort, with rates of 22% vs. 46% (p=0.035) and 22% vs. 39% (p=0.085), respectively. **Intralesional steatosis:** the distribution of this variable differed significantly (p<0.0001) and was less common in scirrhous HCC than in the cohort as a whole at 11% vs. 27%.						

Table 18: Diagnostic accuracy of predictors for scirrhous HCC among histopathologically confirmed HCC.

Diagnostic accuracy of predictors for CC-HCC	SEN	SPE	PPV	NPV	PLR	NLR
(1) AFP <= 5.8 µg/l and Gd-EOB uptake area >50%	8%	97%	17%	94%	2.67	0.95
(2) AFP <= 5.8 µg/l, Gd-EOB uptake area >50% and no capsule enhancement	8%	98%	25%	94%	4.00	0.94
(3) AFP <= 5.8 µg/l, Gd-EOB uptake area >50%, no diabetes and no intralesional steatosis	8%	99%	50%	94%	8.00	0.93
(4) AFP <= 5.8 µg/l, Gd-EOB uptake area >50%, no capsule enhancement, no diabetes and no intralesional steatosis	8%	99%	50%	94%	8.00	0.93

Rationale for the choice of predictors

AFP: the distribution of log AFP varied significantly among subtypes (p=0.001), with CC-HCC showing consistently low AFP values. ROC analysis revealed the AUC of AFP for identifying CC-HCC to be 0.679, with the optimal threshold at 5.8 µg/l with 83.3% sensitivity and 61.7% specificity.

Gd-EOB uptake area: while this variable did not vary significantly among subtypes (p=0.726), an uptake area over 50% was found to be exclusive to NOS-HCC, ST-HCC and CC-HCC (p=0.042).

No diabetes and no intralesional steatosis: an important differential diagnosis for CC-HCC in lesions with Gd-EOB uptake area > 50% is ST-HCC. The presence of intralesional steatosis and diabetes was observed to be highly predictive of ST-HCC, implying that their absence could potentially suggest CC-HCC. It is important to note that while intralesional steatosis has also been associated with CC-HCC, this subtype may alternatively exhibit a glycogen-rich phenotype.

No capsule enhancement: the distribution of this variable was close to significance (p=0.069) and was relatively uncommon in CC-HCC (22% vs. 33% for the whole cohort).

Table 19: Diagnostic accuracy of predictors for clear cell HCC among histopathologically confirmed HCC.

9 Discussion

The heterogeneity of HCC presents significant challenges in its management and leads to poor prognoses. While contrast-enhanced imaging techniques have allowed for a confident non-invasive diagnosis of HCC with typical features like APHE and portal venous phase enhancement, up to 40% of HCC cases suitable for curative therapy do not exhibit these classical patterns. This discrepancy can be attributed to variations in differentiation levels and histopathological variants expressing atypical tumor phenotypes. Current staging systems such as BCLC stratify patients and guide treatment decisions based on estimates of their prognosis and risk of recurrence. While anatomical spread of the tumor and clinical features are considered, the histological and molecular features of the tumor are not, despite their profound impact on prognosis. This results in considerable heterogeneity within each staging group.

The 5th edition of the WHO Classification of Digestive System Tumors now defines 8 subtypes of HCC based on histopathological, immunohistochemical and clinical properties. This may provide a finely granular system to distinguish patients with varying tumor-specific prognoses and identify those who may benefit from specific therapies, including targeted therapy against molecular targets. However, the adoption of this classification into clinical practice is hindered by the need for invasive biopsies, which carry inherent risks and only investigate a portion of the tumor.

Modern imaging techniques may be a powerful tool for non-invasively diagnosing not only typical forms of HCC, but also its variants. MRI enhanced with hepatocyte-specific contrast agents is particularly promising due to its excellent soft-tissue contrast, high sensitivity for detecting even small HCC, and its ability to visualize both vascularity and hepatocyte function.

Our study aimed to explore the potential of Gd-EOB-enhanced MRI, combined with clinical features, for non-invasively differentiating HCC subtypes. This discussion summarizes our findings, considers their clinical implications, and compares them with previous research by other groups. Finally, we analyze the strengths and limitations of our methodology. By harnessing the power of imaging techniques, we hope to contribute to improved management and treatment strategies for HCC patients based on their specific subtypes.

9.1 Brief summary of results

We retrospectively investigated the distribution of clinical and imaging features in preoperative Gd-EOB-enhanced MRI among 262 histopathologically confirmed HCC lesions after hepatectomy or liver transplantation. Between 5 and 33 lesions were found for each subtype except for the very rare LR-HCC and GR-HCC. We compared clinical characteristics, laboratory values, and quantitative and qualitative imaging features in preoperative Gd-EOB-enhanced MRI between the different groups.

NOS-HCC was more likely to show a typical enhancement pattern for HCC, characterized by non-rim APHE and non-peripheral washout, with or without HBP hypointensity. This pattern was particularly uncommon in MTM-HCC, CH-HCC and SC-HCC. FIB-HCC was linked to younger age, female gender and the absence of liver pathology and other risk factors for HCC. MTM-HCC was associated with high AFP and macrovascular invasion. ST-HCC was strongly associated with diabetes mellitus type II and intralesional steatosis. AFP levels were moderately elevated in CH-HCC and slightly elevated in FIB-HCC. A high Gd-EOB uptake area (score of 3 or 4) was unique to NOS-HCC, CC-HCC, and ST-HCC, although not significantly different across all subtypes.

Diagnostic tests were developed for NOS-HCC, FIB-HCC, ST-HCC, MTM-HCC, CH-HCC and CC-HCC, which combined imaging and clinical features to provide a binary test result indicating the presence or absence of a specific subtype. These tests generally exhibited high specificity and NPV of over 90% for MTM-HCC, ST-HCC, FIB-HCC, and CC-HCC. Additionally, some tests also showed high PLR and NLR for these subtypes. However, high sensitivity and PPV were only observed for FIB-HCC.

9.2 Interpretation of results

9.2.1 Study cohort

This study represents an investigation into the clinical and imaging features of a large cohort of HCC lesions in a Western population. The relative frequencies of subtypes in our cohort approximately matched those defined by the WHO. We were also able to reproduce commonly reported clinical and imaging features for some subtypes, such as macrovascular invasion by MTM-HCC and an association with diabetes type II and intralesional steatosis with ST-HCC. This suggests that our study cohort is comparable to the population that

formed the basis for the WHO Classification. However, some notable differences were observed for certain subtypes which will be subsequently described.

9.2.2 Evaluation of the diagnostic accuracy of our tests

The diagnostic tests developed for certain subtypes of HCC are a significant research outcome. When assessing their diagnostic efficacy, it is crucial to consider how their accuracy parameters will be useful in the intended clinical context. We believe Gd-EOB-enhanced MRI has the potential to either provide a non-invasive diagnosis of certain subtypes, or to screen for patients who may benefit from biopsy due to an elevated likelihood of a specific subtype.

9.2.2.1 Sensitivity and specificity

Our diagnostic tests showed high specificity (over 90%), but sensitivity was lower. These parameters represent the extent to which the presence or absence of a condition, such as a subtype of HCC, predicts the result of a test with a dichotomous outcome, relative to the reference standard. The utility of these metrics is limited in a screening context, as they provide no information about the proportion of individuals with a certain subtype among individuals with a positive or negative test result. Diagnostic tests with a high specificity may, however, allow to rule in the presence of a subtype among those who have a positive test result[190]. Furthermore, high specificity minimizes screening-related harms due to a low rate of false-positives[191].

The sensitivity levels were generally low. For instance, four out of the five tests for MTM-HCC had sensitivities ranging from 25% to 31%. This indicates the proportion of subtypes that meet the criteria of the respective test. In cases where the other parameters of diagnostic accuracy are sufficiently high to ensure a confident diagnosis, a biopsy may become unnecessary for these patients. Hence, even tests with low sensitivity can hold clinical significance as they can lead to a corresponding reduction in the number of biopsies performed.

9.2.2.2 Predictive values

High predictive values can form the basis for clinical decisions because they reflect the post-test-probability for a subtype[190]. Certain diagnostic tests showed high NPV for MTM-HCC,

ST-HCC, and FIB-HCC. Consequently, these subtypes can be confidently excluded if the test yields a negative result. This exclusion is particularly relevant when determining whether a lesion requires additional, subtype-specific therapy targeted at molecular targets, as seen in MTM-HCC and FIB-HCC. Another potential application is ruling out subtypes that have a high risk of recurrence to specific therapies, such as MTM-HCC.

Given the relative infrequency of most subtypes and the dependence of predictive values on prevalence, high NPV is an expected finding. Nevertheless, our tests offer an added benefit because they reduced the post-test-probability to a significant extent. Most notably, only 1.0% of lesions with AFP < 48 µg/l were MTM-HCC (test 1 for MTM-HCC), compared to a pre-test probability of 6.1% for this subtype. Among lesions without intrahepatic steatosis (test 1 for ST-HCC), 2.2% were found to be ST-HCC, in contrast to 12.6% in the entire cohort. A similar reduction was observed for CH-HCC in lesions with typical enhancement pattern and an arterial phase ER over 3.66 (test 1 for CH-HCC), but this may not be significant as only few lesions of this subtype were observed.

PPV was generally lower than NPV, with the best values achieved for MTM-HCC at 75%, NOS-HCC at 78% and FIB-HCC at 100%. Notably, the study cohort included no non-HCC lesions, so that PPV would be further reduced in a clinical setting where other malign or benign focal liver lesions occur. As a false-positive diagnosis can incur significant costs and harm, these PPVs may not be sufficiently high to form the basis for treatment decisions, with the exception of FIB-HCC.

A drawback of both NPV and PPV is that they may not be generalizable to other cohorts if the prevalence of certain subtypes is considerably different. This limitation may be overcome by likelihood ratios, explained below.

9.2.2.3 Likelihood ratios

Likelihood ratios are ratios between the pre-test and post-test odds of a subtype. These ratios can be utilized to inform clinical decisions when the pre-test odds are known. Unlike predictive values, likelihood ratios are independent of prevalence and can be more easily generalized beyond the specific study population[192].

Values for PLR over 10 and NLR under 0.1 are commonly cited in the literature as a large change in odds[193, 194]. However, some subtypes are relatively rare, so that an even higher PLR may be needed to achieve sufficiently high post-test odds to make a treatment decision. Our tests achieved a PLR of up to 14 for ST-HCC and 25 for MTM-HCC, which elevated the post-test-probability to 60% and 75%, respectively, in our study cohort. This may not be sufficiently high to diagnose these subtypes, but could indicate a benefit from performing biopsy in these patients.

An NLR below 0.10 was observed only for FIB-HCC (0.00), but it came close for ST-HCC (0.15) and MTM-HCC (0.11). This indicates that these tests significantly reduce the post-test odds of these subtypes.

Certain tests had relatively high PLR, but poor NLR, like tests 3 and 4 for CC-HCC, both with a PLR of 8.00 and an NLR of 0.93. This demonstrates that a test can provide asymmetric information, where a positive result may strongly suggest CC-HCC, but a negative result may have little clinical impact.

9.2.2.4 Overfitting

Importantly, when more predictors are added the test becomes more specific to our cohort and its performance is overestimated. This phenomenon is known as overfitting and denotes a common predicament in developing predictive models[195]. Preference should, therefore, be given to tests with fewer predictors, even if this results in an ostensibly lower diagnostic performance. Internal and external validation should also be performed, which will be discussed under limitations of this study.

9.2.3 Subtype-specific interpretation of results

After analyzing the overall diagnostic accuracy and utility of the tests generated by this study, each subtype will be discussed individually in this section.

9.2.3.1 Macrotrabecular massive HCC

MTM-HCC is a subtype of HCC associated with a notably unfavorable prognosis, displaying rapid growth, vascular invasion, early metastasis, and high recurrence rates with therapies like RFA. These characteristics have been linked to the activation of neoangiogenesis[149],

indicating that patients with MTM-HCC could potentially benefit from targeted therapy using neo-angiogenesis inhibitors. These are important reasons to be able to rule out or to diagnose this aggressive subtype with high confidence.

We found strong associations of MTM-HCC with high AFP and macrovascular invasion, reproducing previous findings in the literature. AFP over 48 µg/ml (test 1 for MTM-HCC) demonstrated excellent sensitivity, NPV, NLR and AUC in our cohort, at 92%, 99%, 0.11 and 0.824, respectively, indicating a strong potential in screening for patients who may have MTM-HCC and for excluding this subtype. The combination of AFP with macrovascular invasion (test 3) attained high specificity, NPV and PLR of 97%, 95% and 10.33 respectively, indicating its potential for effectively diagnosing or excluding this subtype. However, its sensitivity was 31% as only one-third of MTM-HCC cases in our cohort exhibited macrovascular invasion. Consequently, the post-test probability for test 3 in our cohort was only 44%, which might not be sufficient to initiate subtype-specific therapy for patients with a positive result. To enhance diagnostic accuracy, the addition of atypical enhancement (test 4) improved PPV to 75%, PLR to 25.00, and specificity to 99%, with only a slight reduction in sensitivity to 25%.

While we believe tests 1 and 4 to have good potential for screening, diagnosing or ruling out MTM-HCC, it is crucial to emphasize the significance of external validation. Our reported relative frequency of MTM-HCC was 6.1%, consistent with the WHO Classification's value of 5%. However, it is worth noting that other researchers have observed higher frequencies for MTM-HCC in their studies. In North American and European cohorts, relative frequencies of 7.8%[144] and 15%[143] have been reported, while figures as high as 40%[196] and 42%[197] have been reported in two Asian cohorts. These discrepancies could be attributable to differences in institutional practice, since these are all surgical cohorts and some centers may be less likely to offer surgery to patients with MTM-HCC due to its early metastasis and rapid growth. Furthermore, MTM-HCC is associated with HBV infection[78, 198], a risk factor that is more prevalent in Asian countries. In cohorts with higher prevalence of MTM-HCC, our tests would perform better at diagnosing MTM-HCC, but worse at excluding it.

Additionally, in our cohort, MTM-HCC lesions were relatively small, with a median size of 31 mm compared to the overall cohort's median size of 33 mm. Other research groups have reported a size over 5 cm at the time of diagnosis to be a significant predictor of MTM-HCC,

which is explained by its activation of neo-angiogenesis, facilitating rapid growth. One possible explanation is that surveillance programs in our western European country may be more effective in detecting HCC at an earlier and smaller stage. However, it is important to note that our HCC lesions were not consistently smaller than those observed in other cohorts. For instance, Mulé reported a median size of 28 mm for NOS-HCC, which is comparable to our findings, but a median size of 74 mm for MTM-HCC. This suggests that the discrepancy between our results and the literature regarding lesion size may be attributed to institutional practices. Nevertheless, our study offers an added benefit by providing a better characterization of earlier stages of MTM-HCC, contributing valuable insights to the existing literature.

Thirdly, while AFP alone showed excellent diagnostic performance for MTM-HCC in our cohort, its performance may be lower in other populations. To illustrate, 25% of patients with MTM-HCC did not have elevated AFP above 20 ng/ml in one Asian cohort[196]. This highlights the importance of external validation of these predictors.

9.2.3.2 Steatohepatitic HCC

ST-HCC is a common subtype of HCC with a histological phenotype and molecular profile similar to inflamed liver tissue in NASH[140]. Due to its common occurrence and association with improved prognosis, identifying this subtype non-invasively could be a valuable contribution towards selecting patients who would benefit from curative therapies. The combination of intralesional steatosis, found in 88% of ST-HCC lesions in our cohort, along with diabetes mellitus type II (test 2 for ST-HCC), has demonstrated relatively good diagnostic performance for this purpose, with a PLR of 13.25, a PPV of 65% and a specificity of 96%.

However, it is noteworthy that intralesional steatosis is also a common feature of premalignant lesions, well-differentiated HCC and HCA[186]. The classical HCC enhancement pattern or biopsy may be helpful in ruling out these alternative diagnoses. Other HCC subtypes may also show intralesional steatosis, which we observed in CC-HCC (4/13, 31%) and MTM-HCC (4/15, 27%) compared to NOS (29/168, 17%). CC-HCC may express either a glycogen-rich or steatoic phenotype[157] and therefore represents an important differential diagnosis. While the diagnosis of CC-HCC in a lesion with intralesional steatosis could be suggested if diabetes and NASH are absent and the tumor has a large size, we only

observed significant differences for diabetes type II. Meanwhile, AFP could be included to rule out MTM-HCC (test 3).

ST-HCC was one of the 3 subtypes that showed high HBP-enhancement in our cohort, present in 3/32 cases (9.4%). This is an interesting finding because Wnt/β-catenin pathway activation, a possible mechanism for high HBP-enhancement, has been reported to be rare in this subtype[199]. An explanation for this feature could be that, as ST-HCC retains similarity to non-tumor liver tissue, it may be more likely to show preserved hepatocyte function. This is consistent with our observation that all 3 lesions were iso-, but not hyperintense to liver parenchyma. As this feature is uncommon, the previously mentioned predictors may be more valuable for identifying ST-HCC.

9.2.3.3 Clear cell HCC

CC-HCC is characterized by aberrant insulin signaling and excessive glycogen storage, giving it its characteristic clear histological appearance and energy stores that allow for rapid growth[156]. In a large focal liver lesion, CC-HCC can therefore represent an important differential diagnosis to MTM-HCC. This distinction is clinically important because CC-HCC has been associated with a better prognosis and longer time to recurrence compared to NOS-HCC and especially MTM-HCC[158]. In our cohort AFP was exceptionally useful for making this distinction, as CC-HCC had the lowest median AFP of all subtypes.

CC-HCC has been reported to appear similarly to NOS-HCC on imaging[162, 164]. Accordingly, we did not find powerful predictors for CC-HCC. CC-HCC tended to be larger than NOS-HCC, but this did not reach statistical significance. We also found an elevated likelihood of intralesional steatosis, indicating CC-HCC that expresses a steatotic phenotype[156]. However, the PPV of this feature was low because it occurred very commonly in ST-HCC.

Notably, CC-HCC was among the three subtypes showing high HBP-enhancement, the others being NOS-HCC and ST-HCC. Hence, all our tests for this subtype focused on investigating this particular imaging feature. However, sensitivity was very low at 8%. Nevertheless, a high PLR of 8.00 could be achieved by incorporating the absence of diabetes and intralesional steatosis to exclude ST-HCC, and by considering atypical enhancement to reduce the likelihood of NOS-HCC (tests 3 and 4). Nevertheless, there is a

concern regarding overfitting since these tests involve 4 to 5 predictors. Further research is necessary to enable a non-invasive diagnosis of this subtype.

9.2.3.4 Scirrhous HCC

SC-HCC is characterized by dense intratumoral fibrosis and is therefore a mimic of non-HCC lesions on imaging, including CCA, FIB-HCC and liver metastases[170]. In fact, SC-HCC has been hypothesized to represent an intermediate stage on a continuous spectrum between HCC and CCA[200]. Differentiation from these other entities is further complicated by SC-HCC commonly occurring in non-cirrhotic livers[167] and the high prevalence of liver metastases.

Making the correct diagnosis is crucial as the therapy of HCC, CCA and liver metastases differs considerably. For CCA, only radical surgery is considered curative, resectability is often low due to early metastasis and vascular invasion, and the survival benefit from liver transplantation is equivocal[201]. Liver metastases require an interdisciplinary therapeutic approach tailored to tumor burden, biology and origin[202]. However, as our study included only HCC lesions, we could only investigate predictors for SC-HCC among HCC lesions. These included atypical enhancement and lack of intralesional steatosis, but their diagnostic performance was poor with sensitivity and specificity of approx. 60%.

Nevertheless, some interesting observations could be made. The majority of SC-HCCs in our cohort occurred in cirrhotic or fibrotic livers, at similar rates as NOS-HCC, which is at odds with the literature[167]. In addition, the presence of a fibrous stroma is a possible mechanism for higher HBP signal intensity due to retention of contrast agent. However, no SC-HCCs showed high HBP enhancement in our cohort. SC-HCC did show higher rates of rim APHE (44%, 4/9) compared to NOS-HCC (13%, 22/168), which is consistent with the literature[168], but not significant with only 10 SC-HCC lesions. This highlights the need for further research on this subtype, including comparison with common non-HCC mimics of SC-HCC.

9.2.3.5 Fibrolamellar HCC

FIB-HCC is a rare subtype that stands out for occurring in the absence of liver pathology, in younger patients aged 10 to 30 years and in both genders equally[175]. Accordingly, these variables served as excellent predictors for FIB-HCC in our cohort of HCC lesions. Identifying this subtype is clinically valuable because FIB-HCC has been reported to be less

responsive to chemotherapy[175], and its DNAJB1-PRKACA fusion gene product may be a target for immunotherapy[77].

The primary challenge in effectively managing FIB-HCC lies in the difficulty of identifying a suitable screening population of high-risk individuals, as its underlying causes and risk factors are not well understood. As a result, FIB-HCC is often detected at an advanced stage, where the tumor mass causes clinically evident disease. However, unlike other subtypes, surgery may still be a curative option at these more advanced stages due to the absence of significant comorbidities[203].

A further important consideration is that FIB-HCC is reported to have a second age peak at 70-79 years, which overlaps with that of other subtypes[175]. In these older patients, imaging morphology may play a larger role compared to clinical features. Our cohort only included few observations of this rare subtype, so no imaging features were significantly different for FIB-HCC. This suggests a need for large multi-center studies that pool their observations. Furthermore, these studies should also include non-HCC liver lesions with dense fibrosis, primarily CCA and some liver metastases, to permit a confident exclusion of these differential diagnoses[170].

9.2.3.6 Chromophobe HCC

There is only scarce literature available for the imaging features of CH-HCC, which likely stems from its relative rarity and that it is a new subtype in the 5th edition of the WHO Classification. Our analysis of 8 lesions therefore represents a significant contribution towards characterizing this subtype.

In our cohort, CH-HCC stood out for hypovascular appearance, as only 2 lesions (25%) showed APHE and arterial phase ER was the lowest of all subtypes. However, diagnostic tests with these predictors were unspecific (66%) and had low PPV (9%) and PLR (2.53-2.97). These observations are also at odds with the findings of Wood et al., who reported 5 out of 6 CH-HCC to have a typical enhancement pattern in MRI[165]. This discrepancy could be explained by the fact that a higher proportion of CH-HCCs (63%) occurred in non-cirrhotic livers, where rapid parenchymal enhancement may mask APHE. This is one of the potential pitfalls in interpreting Gd-EOB-enhanced MRI[204]. We were able to reproduce Wood et al.'s finding of elevated AFP and no gender bias in CH-HCC, thus suggesting that our samples

may be comparable. More investigation will be needed to clarify these heterogeneous results.

9.2.3.7 Lymphocyte-rich and granulocyte-rich HCC

Consistent with the rarity of these subtypes, no GR-HCC and only a single LR-HCC lesion was present in our cohort. The LR-HCC lesion showed the typical enhancement pattern for HCC, with APHE, washout and HBP hypointensity, consistent with previous case reports. Notable findings were a very high AFP of 4027 µg/l and female gender of the patient, but the singular lesion precluded statistical analysis. These subtypes may be too rare to be investigated adequately even with large, multi-centric cohort studies. A more effective approach may be to obtain original imaging data from authors of case reports to conduct a secondary analysis and pool the results.

9.2.3.8 NOS-HCC

NOS-HCC is sometimes referred to as “conventional HCC”, which suggests uniform expression of typical features of HCC. Our results only partially support this. Although the typical enhancement pattern was significantly more common in NOS-HCC (52.4%) compared to other HCC subtypes (32.9%), it was still absent in nearly half of NOS-HCC cases. This suggests that NOS-HCC should be seen as a diverse group that encompasses lesions for which robust subtype criteria have not yet been established. . Several other potential subtype candidates were considered for inclusion in the 5th edition of the WHO Classification, but were excluded due to insufficient evidence to meet all the criteria required to define a distinct subtype[5]. There is likely significant potential to identify further clinical, histopathological and radiological patterns within the NOS-HCC group.

The clinical utility of identifying NOS-HCC or ruling out atypical HCC warrants discussion. Presently, clinical guidelines primarily rely on the presence or absence of the classic HCC enhancement pattern to determine whether follow-up examinations, such as biopsy, are necessary for diagnosing HCC. However, in our cohort, the classic enhancement pattern was a weak predictor for NOS-HCC in our cohort, with a PLR of 1.58-1.67 and NLR of 0.72-0.75 (tests 1 and 2 for NOS-HCC). A more effective approach could involve integrating multiple imaging features to identify atypical HCC, as exemplified in the LR-M category of LI-RADS v2018 CT/MRI[135]. However, even this approach is not impervious to limitations, as existing literature suggests that the distribution of most LI-RADS features and categories

may not differ significantly among common subtypes[144]. New subtype-specific imaging features are needed to guide the diagnostics and management of atypical HCC.

9.2.4 Intra-tumor heterogeneity

In the histopathological analysis, 32% of lesions exhibited distinct regions, each representing a different subtype from the one assigned to the entire lesion. For lesions classified as NOS-HCC, this was often because the region's size did not meet the WHO's threshold for diagnosing a specific subtype. Interestingly, no FIB-HCC, CH-HCC and LR-HCC lesions demonstrated such mixed phenotypes, while 25-39% of all other subtypes displayed intra-tumor heterogeneity (ITH). This ITH has significant implications. Lesions with subtype-specific regions may possess different clinicopathological and radiological features than more homogenous lesions of the same subtype, which can confound our analysis. In clinical practice, high ITH serves as an independent predictor of poor prognosis in solid tumors since targeted therapies might only be effective against certain portions of the tumor[69]. Additionally, the exact thresholds of lesion area and certain other criteria for diagnosing subtypes are subject to ongoing debate, thereby compromising the comparability of research outcomes[184].

Here an analogy could be drawn to cHCC-CCA, which expresses both an HCC and a CCA phenotype. According to the literature, the imaging morphology of cHCC-CCA is determined by its predominant histopathological component, closely mimicking HCC or CCA[205]. If there is a clearly demarcated transition zone, imaging of cHCC-CCA may reveal distinct regions, each showing unique imaging features. From a clinical perspective, the presence of both tumor phenotypes results in an intermediate prognosis of cHCC-CCA between HCC and CCA[205]. It is an important question whether similar findings can be observed in mixed-subtype HCC, which warrants further investigation. Additionally, in the 5th edition of the WHO Classification, thresholds for cHCC-CCA are no longer defined, simply requiring the unequivocal presence of both cancer phenotypes within a lesion. This raises the possibility that HCC, too, could be recognized as a cancer entity capable of expressing multiple subtypes, potentially increasing precision in statistical analysis and therapeutic stratification.

9.2.5 Added value of Gd-EOB-enhanced MRI?

One of the premises of this study was that the ability of Gd-EOB-enhanced MRI to visualize both vascularity and hepatocyte function provides an additional dimension of information

compared to ECA to aid in differentiating between subtypes. Various qualitative and quantitative imaging features in the HBP were assessed, including subjective assessment of signal intensity, Gd-EOB uptake area, and lesion-to-liver ER. However, the distribution of these variables did not show significant differences among all subtypes. It is important to note that there were relatively few lesions per subtype and a high number of degrees of freedom, particularly for multi-level variables, which should be considered in interpreting the results. Other groups have overcome this issue by summarizing infrequent types of HCC, but at the expense of providing less detailed information for each subtype[143].

Although this study did not involve ECA-enhanced MRI, which prevents a direct comparison, it successfully reproduced imaging features in Gd-EOB-enhanced MRI that have been previously reported for certain HCC subtypes on ECA-enhanced MRI and CT. Particularly noteworthy is the identification of macrovascular invasion for MTM-HCC, which is a significant finding considering that Gd-EOB-enhanced MRI has been known to exhibit lower vascular contrast in the arterial and venous phases[133]. This observation suggests that Gd-EOB-enhanced MRI can still provide valuable information about macrovascular invasion, even with potential limitations in vascular contrast, which could potentially hinder its ability to identify vascular invasion by an enhancing mass. Another significant aspect is the relatively high rate of transient respiratory motion artifacts associated with Gd-EOB-MRI, especially in the arterial phase. Despite this, 95% (248/262) of arterial phase sequences were considered to be of sufficient diagnostic quality for assessing APHE.

The incorporation of HBP hypointensity into diagnostic tests led to slightly reduced sensitivity and slightly higher specificity for NOS-HCC. It had minimal impact on the prediction of CH-HCC or MTM-HCC, and a slight reduction of specificity for SC-HCC.

However, an important finding was that Gd-EOB uptake area over 50% was only found in NOS-HCC, CC-HCC and ST-HCC, with post-hoc analysis indicating statistical significance at a p-value of 0.031. While this finding only occurred in 8% of all lesions, it allowed the creation of diagnostic tests for CC-HCC with low sensitivity but moderate PLR of 8.00. For ST-HCC and NOS-HCC, better performance was found using features such as diabetes, intralesional steatosis and typical enhancement pattern.

Mechanistically, this finding is consistent with the literature, which reports that 10-15% of HCCs may appear iso- to hyperintense on imaging[106] and that this feature is associated with longer time to recurrence as well as lower rates of vascular invasion[121, 122]. Accordingly, CC-HCC and ST-HCC are both reported to have better prognosis than NOS-HCC[5]. Furthermore, CC-HCC and NOS-HCC are reported to appear similarly on imaging[162, 164], which could explain why both forms of HCC share this imaging feature. More research would be merited to investigate the distribution of HBP iso- to hyperintensity among subtypes of HCC.

9.2.6 Abbreviated MRI protocols for subtype differentiation

Current AMRI protocols for HCC screening may consist of DWI, T2-weighted and/or T1-weighted imaging with or without HCSA[139]. In our cohort, imaging features in DWI, non-contrast T1-weighted imaging and T2-weighted imaging did not show significant differences between subtypes and were not included in our diagnostic tests. High HBP enhancement, while potentially indicative of NOS-HCC, CC-HCC or ST-HCC, was infrequent. As a result, current AMRI protocols may not offer substantial value for non-invasive differentiation between HCC subtypes. However, the inclusion of chemical shift imaging for visualizing intralesional steatosis may be beneficial in identifying ST-HCC and CC-HCC.

9.3 Strengths of the study

9.3.1 Choice of reference standard

The strengths of this study begin with the decision to use surgical resection as the reference standard. This allowed for the examination of the entire tumor volume, meeting the threshold criteria established by the WHO for specific subtypes. Additionally, interobserver agreement between the pathologists was deemed almost perfect, indicating a high level of confidence in the accuracy of our subtype assignments.

9.3.2 Choice of imaging features

Many imaging features analyzed in this study were derived from guidelines for HCC including LI-RADS, which state typical and ancillary imaging features for HCC. This indeed represents a strength as these features are well defined and studied in the setting of HCC, facilitating comparison of our results with those of other research groups. Beyond this, we

also developed our own imaging features such as Gd-EOB uptake area, giving the potential to establish previously undescribed imaging features.

9.3.3 Size and geography of the cohort

We had the opportunity to analyze a substantial cohort of 240 patients at a tertiary care center, a comparatively large sample size for a western study center. As mentioned earlier, the etiologies of HCC exhibit considerable geographic variation, consequently influencing phenotypic tumor output. Therefore, it is crucial to conduct research in both Western and Eastern populations to ensure that research outcomes can be reliably applied across different regions.

9.3.4 Granularity of results

We provide detailed results for almost all subtypes regardless of rarity, in contrast to other groups that have combined uncommon subtypes into a single group[143, 144]. This represents a strength as there is only scarce literature on the imaging features of certain uncommon subtypes, in particular those that were not already part of the 4th edition of the WHO Classification. We also provide multiple levels or categories for variables such as signal intensity or enhancement pattern. This offers detailed insights into their behavior and distribution among subtypes. However, such an approach requires a high number of observations in order to reliably identify statistically significant relationships, which, in turn, may only be achievable with a large multi-center investigation.

9.4 Limitations of the study

9.4.1 Surgical cohort

An important limitation of this study is its reliance on a surgical cohort, which represents a selected subset of patients with HCC. This selection bias occurs because patients are typically assigned to surgical therapy when they are in the early stages of the disease, with small, solitary nodules. For patients who are not suitable candidates for resection, liver transplantation may be considered, but only if they still meet the Milan Criteria[206]. This suggests that the cohort might consist primarily of early-stage HCC, thus raising questions about the transferability of our results to a clinical setting. This is attributed to the fact that the majority of HCCs are still detected at an inoperable stage[207], where their imaging morphology may have evolved.

This concern is somewhat alleviated by the fact that our institution has provided surgery or liver transplantation to patients with more advanced HCC. Among all resected lesions, 26% (73/261) were over 5 cm, and 24% (14/59) of liver transplantations were performed in patients outside of the Milan Criteria. This enabled us to examine the imaging features of these more advanced lesions, even though it introduced some heterogeneity into the study.

Finally, it is worth noting that finding a comparable alternative reference standard may be challenging. HCC displays significant intralesional heterogeneity, and tissue biopsy, which only analyzes a small volume, may not fully represent the entire tumor. While standardized sampling techniques are available, their implementation in clinical routines is hindered by their cost and complexity[81]. This underscores the significace of overcoming the limitations of a surgical cohort to establish non-invasive imaging markers.

9.4.2 Observations per subtype

While the studied cohort is comparatively large, only 33% (87/262) of analyzed lesions could be assigned to a subtype, which is why relatively few lesions were available per subtype. This indicates a need for a larger cohort, which may be achieved via multi-center cooperation. The Radiological Cooperative Network (RACOON) may be particularly well suited for this as a research infrastructure that connects the radiological departments of all university clinics in Germany and provides a common framework for sharing and reporting on imaging. Given the relative abundance of NOS-HCC compared to subtypes, statistical analysis could be further facilitated by matching NOS-HCC with subtypes of HCC based on propensity scores.

9.4.3 Absence of non-HCC lesions

Another limitation of this study is that it only included histopathologically confirmed resected HCC lesions. This pre-selection process does not reflect the real-world diagnostic workup of a focal liver lesion, where various benign and malignant non-HCC entities are encountered. Some of these entities may share imaging features with subtypes of HCC, making it challenging to accurately differentiate between them. For example, CCA, similar to SC-HCC and FIB-HCC, can contain fibrotic areas with characteristic slow enhancement, and it may develop satellite nodules, similar to MTM-HCC. Future studies should therefore also include non-HCC tumor entities to ensure the diagnostic efficacy of imaging biomarkers in

differentiating between both subtypes and HCC/non-HCC lesions. This would also permit to compute more accurate predictive values as the prevalence of each subtype in the target population would be known, which plays an important role in the integration of diagnostic tests into guidelines.

9.4.4 Lack of molecular analysis in subtype determination

In this study, subtype identification relied solely on histopathological morphology as the reference standard. However, the WHO Classification also defines immunohistochemical criteria for each subtype, such as DNAJB1-PRKACA for FIB-HCC. Conducting molecular analyses can be expensive and is primarily performed at our center when histopathology alone does not provide a definitive diagnosis of HCC. Unfortunately, retrospective analyses for the molecules specified by the WHO Classification were not available, potentially limiting the accuracy of our subtype assignments. Subtypes that share histopathological features, such as steatosis in CC-HCC and ST-HCC, may be particularly impacted by this limitation. However, similar imaging studies of HCC subtypes similarly did not perform molecular analysis as part of their reference standard[143, 144]. This ensures comparability of research outcomes. Furthermore, there are strong associations between molecular markers and histopathologic phenotypes for HCC[78], ameliorating this limitation.

9.4.5 Internal validation of predictors

There remains untapped potential for internally validating our predictors, which is crucial because the diagnostic performance of predictors can be overestimated in the cohorts where they were initially developed. Several methods are available for internal validation, such as data-splitting and cross-validation, which involve dividing the cohort into a training and test sample to assess the performance of the predictors on independent datasets[195] However, we believe that further subdivision of the cohort would disproportionally elevate the risk of a type II error due to the low number of observations of some subtypes, which is not desirable in an exploratory study design.

9.4.6 Selection of predictors and the need for external validation

The predictors that form the basis for our diagnostic tests were chosen according to both subjective and objective criteria laid out in “*8.3 Predictors for NOS and subtypes of HCC*”. As the reporting of results of exploratory analyses should not be determined solely by the

statistical significance due to limitations of the p-value[208], we also included variables that were not significant, but close to the significance threshold or for which associations with specific subtypes had previously been reported in the literature. We also set a relatively low threshold of 0.6 AUC in ROC curve analysis for inclusion of continuous variables such as arterial-phase ER.

The chosen approach aimed to maximize the sensitivity of this study in identifying predictors for subtypes. However, this also raised the risk of type I errors, where the null hypothesis is falsely rejected due to sampling error. Therefore, external validation of our current results in future studies becomes crucial. These studies should follow a confirmatory study design, optimized for confirming or refuting our findings.

Moreover, an automatic method of variable selection could have been employed to mitigate investigator bias and control for confounders in the selection of predictors. However, in this case, the low number of observations per subtype relative to the number of investigated variables would hinder the application of such a model. Additionally, it remains challenging to develop models that consistently select genuine predictors without excessive bias towards statistically significant variables[209].

9.4.7 Impact of multiple comparisons

In this study, numerous variables have been individually examined for statistically significant associations with subtypes. The use of multiple comparisons raises concerns about the possibility of false statistical inferences, particularly type I errors. With approximately 44 p-values presented in our results tables, the probability of mistakenly rejecting at least one true null hypothesis is approximately 90% at a significance threshold of $p = 0.05$. In comparison, when testing only a single hypothesis, the probability of such an error is 5%[210].

Several methods for adjusting for multiple comparisons are available to reduce the probability of a type I error. One conservative approach is the Bonferroni method, which adjusts the significance threshold in proportion to the number of hypotheses tested. Alternatively, other methods may utilize step-wise functions to assess p-values in order of their magnitude until the significance threshold is reached[210]. However, as our aim is to identify potential predictors for further investigation and confirmatory analysis, we believe it should be more important to minimize Type II error than to control Type I error.

It is encouraging to observe that 10 of the tested variables in this study yielded statistically significant results. On average, if the null-hypothesis were true for all 44 variables, only 2.2 would be expected to be significant. Additionally, the significant variables align with the findings from previous studies, supporting the association of macrovascular invasion with MTM-HCC, diabetes type II and intralesional steatosis with ST-HCC, and the absence of liver pathology with FIB-HCC. Based on this consistency and concurrence with prior investigations, we are confident that the majority of our significant findings are not merely type I errors.

9.4.8 Detection bias

Readers were aware of the study design, which could introduce detection bias.

9.5 Outlook

9.5.1 Implications for clinical practice: a new diagnostic strategy

The research conducted by our team and other groups has revealed that specific HCC subtypes, notably MTM-HCC, ST-HCC, and FIB-HCC, can be suggested or ruled out by a combination of imaging features and clinical parameters. This finding holds significant implications as our growing knowledge of the causes, tumor microenvironment, and molecular changes has facilitated progress towards precision oncology. However, compared to other types of cancer, HCC has made relatively limited advancements in this area due to the absence of robust biomarkers that predict response to targeted therapies[211]. The WHO Classification as an international standard for subtypes of HCC, each with clear clinical, pathological, molecular and radiological correlates, may be a powerful tool for the establishment of precision oncology in HCC. This is especially the case if subtypes may be determined without invasive diagnostics.

While non-invasive diagnostics are valuable, they may not always provide enough information due to the lack of imaging correlates for certain subtypes. Additionally, as subtypes account for only 35% of all HCC cases, the current suggested biomarkers' predictive values may not be sufficient to confidently diagnose individual subtypes. Moreover, not all lesions may exhibit the typical molecular profile of their subtype. To achieve the best outcomes, a new diagnostic algorithm could integrate non-invasive

diagnostics more closely with biopsy. In this approach, imaging could help identify patients who are most likely to benefit from biopsy. For instance, it could be useful in identifying individuals with a high probability of having an aggressive subtype, which should be confirmed or ruled out before initiating precision therapy.

Such an integrated diagnostic strategy brings several potential benefits. Firstly, it would enable the identification of a larger proportion of patients who could benefit from subtype-specific targeted therapy, potentially leading to a substantial improvement in prognosis, similar to the achievements in other solid cancers. Secondly, the risks associated with tissue biopsy would be minimized, as its use would be guided by prior non-invasive diagnostic assessments. Thirdly, it would enhance the availability of HCC tissue for research purposes, which is particularly significant for advanced stages of HCC, where a precise understanding of the interactions between the cancer and targeted therapies is crucial[211].

This approach has its limitations. Firstly, as previously mentioned, tissue biopsy is an invasive procedure that poses tangible risks to the patient, is not easily repeatable, and may not be feasible for all lesions. Secondly, tissue biopsy cannot capture spatial heterogeneity within the tumor. However, there is evidence suggesting that the primary driver genes of HCC, such as CTNNB1, TP53, and TERT, are clonal trunk mutations present throughout much of the lesion, indicating that biopsy can reliably identify druggable targets[186]. Thirdly, still more research will be needed to further develop and validate these non-invasive biomarkers across populations, and to investigate the diagnostic performance and clinical impact of such an integrated strategy.

Another crucial limitation of subtype prediction is that it is based on associations between clusters of molecular alterations and their histopathological or radiological phenotypes, which are not definitive. In certain instances, it may be more precise to directly predict specific molecular alterations instead. For instance, β-catenin activation has been reported to promote resistance to anti-PD-1 therapy[212], a mutation that is likely to manifest as HBP hyperintensity in Gd-EOB-enhanced MRI[114]. DWI, on the other hand, has proven valuable for prediction of expression of endothelial growth factors and response to anti-angiogenic therapies[213]. Indeed, this indicates the potential advantage of classifications that take into account not only histopathologically distinct subtypes but also morphological features associated with specific molecular alterations. For instance, Calderaro et al. (2019)

introduced the concept of progenitor HCC, characterized by the presence of more than 5% neoplastic cells expressing CK19. This characteristic may be observed in various morphological subtypes, with a notable association in MTM-HCC and SC-HCC[214].

9.5.2 Future research: potential role of liquid biopsy

In the future, Gd-EOB-enhanced MRI could potentially be complemented by liquid biopsy, a non-invasive method for obtaining tumor material from bodily fluids like blood. This material may consist of circulating tumor DNA or cells, mRNA, microRNA, and exosomes, which are released during processes like necrosis, apoptosis, or active secretion by tumor cells[215, 216]. It bypasses important limitations of tissue biopsy by capturing the temporal and spatial heterogeneity of solid cancers in an easily repeatable fashion[216] and represents a powerful potential tool in the non-invasive armamentarium for subtype differentiation. The implementation of liquid biopsy into clinical routines still faces significant technical hurdles, especially concerning the sensitive detection of early-stage cancer. This challenge arises from the correlation between the quantity of circulating material and the tumor burden[215]. In this light, liquid biopsy could be most valuable for detecting aggressive subtypes such as MTM-HCC, which is characterized by rapid growth and necrosis. However, liquid biopsy may not be a full replacement for tissue biopsy due to its inability to analyze histopathological patterns.

10 Conclusion

Our findings suggest that Gd-EOB-enhanced MRI, combined with clinical features, can be a valuable tool for suggesting or ruling out certain subtypes, particularly MTM-HCC and ST-HCC. Imaging features previously identified in CT and MRI enhanced with extracellular contrast agents could be reproduced with Gd-EOB MRI. The HBP provides unique, but uncommon imaging features that could add value in diagnosing NOS-HCC, ST-HCC and CC-HCC. We believe that Gd-EOB-enhanced MRI has significant potential to guide the use of biopsy to confirm the diagnosis of a subtype, indicate the presence of molecular targets, and predict treatment response. This advancement is crucial in enabling patients with HCC to benefit from the progress made in precision oncology. Further research is required to better characterize NOS-HCC, identify additional predictors for uncommon HCC subtypes, and assess the clinical impact of diagnostic and therapeutic strategies based on the WHO subtypes of HCC.

11 References

1. Ferlay J, Colombet M, Soerjomataram I, Parkin DM, Piñeros M, Znaor A, Bray F. Cancer statistics for the year 2020: An overview. Int J Cancer. 2021.
2. Valery PC, Laversanne M, Clark PJ, Petrick JL, McGlynn KA, Bray F. Projections of primary liver cancer to 2030 in 30 countries worldwide. Hepatology. 2018;67(2):600-11.
3. Liu Z, Xu K, Jiang Y, Cai N, Fan J, Mao X, Suo C, Jin L, Zhang T, Chen X. Global trend of aetiology-based primary liver cancer incidence from 1990 to 2030: a modelling study. Int J Epidemiol. 2021;50(1):128-42.
4. Siegel RL, Miller KD, Fuchs HE, Jemal A. Cancer statistics, 2022. CA Cancer J Clin. 2022;72(1):7-33.
5. Nagtegaal ID, Odze RD, Klimstra D, Paradis V, Rugge M, Schirmacher P, Washington KM, Carneiro F, Cree IA. The 2019 WHO classification of tumours of the digestive system. Histopathology. 2020;76(2):182-8.
6. Sung H, Ferlay J, Siegel RL, Laversanne M, Soerjomataram I, Jemal A, Bray F. Global Cancer Statistics 2020: GLOBOCAN Estimates of Incidence and Mortality Worldwide for 36 Cancers in 185 Countries. CA Cancer J Clin. 2021;71(3):209-49.
7. Petrick JL, Florio AA, Znaor A, Ruggieri D, Laversanne M, Alvarez CS, Ferlay J, Valery PC, Bray F, McGlynn KA. International trends in hepatocellular carcinoma incidence, 1978-2012. Int J Cancer. 2020;147(2):317-30.
8. Llovet JM, Kelley RK, Villanueva A, Singal AG, Pikarsky E, Roayaie S, Lencioni R, Koike K, Zucman-Rossi J, Finn RS. Hepatocellular carcinoma. Nat Rev Dis Primers. 2021;7(1):6.
9. Li S, Saviano A, Erstad DJ, Hoshida Y, Fuchs BC, Baumert T, Tanabe KK. Risk Factors, Pathogenesis, and Strategies for Hepatocellular Carcinoma Prevention: Emphasis on Secondary Prevention and Its Translational Challenges. J Clin Med. 2020;9(12).
10. Kanwal F, Khaderi S, Singal AG, Marrero JA, Loo N, Asrani SK, Amos CI, Thrift AP, Gu X, Luster M, Al-Sarraj A, Ning J, El-Serag HB. Risk factors for HCC in contemporary cohorts of patients with cirrhosis. Hepatology. 2023;77(3):997-1005.
11. Ganne-Carrié N, Nahon P. Hepatocellular carcinoma in the setting of alcohol-related liver disease. J Hepatol. 2019;70(2):284-93.
12. Niemelä O, Parkkila S, Pasanen M, Iimuro Y, Bradford B, Thurman RG. Early alcoholic liver injury: formation of protein adducts with acetaldehyde and lipid peroxidation products, and expression of CYP2E1 and CYP3A. Alcohol Clin Exp Res. 1998;22(9):2118-24.
13. Seitz HK, Bataller R, Cortez-Pinto H, Gao B, Gual A, Lackner C, Mathurin P, Mueller S, Szabo G, Tsukamoto H. Alcoholic liver disease. Nat Rev Dis Primers. 2018;4(1):16.
14. Ganne-Carrié N, Chaffaut C, Bourcier V, Archambeaud I, Perarnau JM, Oberti F, Roulot D, Moreno C, Louvet A, Dao T, Moirand R, Goria O, Nguyen-Khac E, Carbonell N, Antonini T, Pol S, de Ledinghen V, Ozenne V, Henrion J, Péron JM, Tran A, Perlemuter G, Amiot X, Zarski JP, Beaugrand M, Chevret S. Estimate of hepatocellular carcinoma incidence in patients with alcoholic cirrhosis. J Hepatol. 2018;69(6):1274-83.
15. Liaw YF, Chu CM. Hepatitis B virus infection. Lancet. 2009;373(9663):582-92.
16. Burns GS, Thompson AJ. Viral hepatitis B: clinical and epidemiological characteristics. Cold Spring Harb Perspect Med. 2014;4(12):a024935.
17. Organization WH. Hepatitis B. Available online: https://www.who.int/news-room/fact-sheets/detail/hepatitis-b. Accessed 12 December 2022.
18. Organization WH. Preventing perinatal hepatitis B virus transmission: a guide for introducing and strengthening hepatitis B birth dose vaccination. Available online: http://apps.who.int/iris/bitstream/10665/208278/1/. Accessed 12 December 2022.
19. Lavanchy D. Hepatitis B virus epidemiology, disease burden, treatment, and current and emerging prevention and control measures. J Viral Hepat. 2004;11(2):97-107.
20. Tseng TC, Liu CJ, Yang HC, Su TH, Wang CC, Chen CL, Kuo SF, Liu CH, Chen PJ, Chen DS, Kao JH. High levels of hepatitis B surface antigen increase risk of hepatocellular carcinoma in patients with low HBV load. Gastroenterology. 2012;142(5):1140-9.e3; quiz e13-4.
21. Chen CJ, Yang HI, Su J, Jen CL, You SL, Lu SN, Huang GT, Iloeje UH. Risk of hepatocellular carcinoma across a biological gradient of serum hepatitis B virus DNA level. Jama. 2006;295(1):65-73.

22. Nguyen VT, Law MG, Dore GJ. Hepatitis B-related hepatocellular carcinoma: epidemiological characteristics and disease burden. J Viral Hepat. 2009;16(7):453-63.
23. Farci P, Niro GA, Zamboni F, Diaz G. Hepatitis D Virus and Hepatocellular Carcinoma. Viruses. 2021;13(5).
24. Stanaway JD, Flaxman AD, Naghavi M, Fitzmaurice C, Vos T, Abubakar I, Abu-Raddad LJ, Assadi R, Bhala N, Cowie B, Forouzanfour MH, Groeger J, Hanafiah KM, Jacobsen KH, James SL, MacLachlan J, Malekzadeh R, Martin NK, Mokdad AA, Mokdad AH, Murray CJL, Plass D, Rana S, Rein DB, Richardus JH, Sanabria J, Saylan M, Shahraz S, So S, Vlassov VV, Weiderpass E, Wiersma ST, Younis M, Yu C, El Sayed Zaki M, Cooke GS. The global burden of viral hepatitis from 1990 to 2013: findings from the Global Burden of Disease Study 2013. Lancet. 2016;388(10049):1081-8.
25. Manns MP, Buti M, Gane E, Pawlotsky JM, Razavi H, Terrault N, Younossi Z. Hepatitis C virus infection. Nat Rev Dis Primers. 2017;3:17006.
26. Bowen DG, Walker CM. Mutational escape from CD8+ T cell immunity: HCV evolution, from chimpanzees to man. J Exp Med. 2005;201(11):1709-14.
27. Gower E, Estes C, Blach S, Razavi-Shearer K, Razavi H. Global epidemiology and genotype distribution of the hepatitis C virus infection. J Hepatol. 2014;61(1 Suppl):S45-57.
28. Kobayashi M, Suzuki F, Fujiyama S, Kawamura Y, Sezaki H, Hosaka T, Akuta N, Suzuki Y, Saitoh S, Arase Y, Ikeda K, Kumada H. Sustained virologic response by direct antiviral agents reduces the incidence of hepatocellular carcinoma in patients with HCV infection. J Med Virol. 2017;89(3):476-83.
29. Pickova D, Ostry V, Malir F. A Recent Overview of Producers and Important Dietary Sources of Aflatoxins. Toxins (Basel). 2021;13(3).
30. Marroquín-Cardona AG, Johnson NM, Phillips TD, Hayes AW. Mycotoxins in a changing global environment--a review. Food Chem Toxicol. 2014;69:220-30.
31. Wild CP, Gong YY. Mycotoxins and human disease: a largely ignored global health issue. Carcinogenesis. 2010;31(1):71-82.
32. Chemical agents and related occupations. IARC Monogr Eval Carcinog Risks Hum. 2012;100(Pt F):9-562.
33. Ostry V, Malir F, Toman J, Grosse Y. Mycotoxins as human carcinogens-the IARC Monographs classification. Mycotoxin Res. 2017;33(1):65-73.
34. EASL-EASD-EASO Clinical Practice Guidelines for the management of non-alcoholic fatty liver disease. J Hepatol. 2016;64(6):1388-402.
35. Younossi ZM, Koenig AB, Abdelatif D, Fazel Y, Henry L, Wymer M. Global epidemiology of nonalcoholic fatty liver disease-Meta-analytic assessment of prevalence, incidence, and outcomes. Hepatology. 2016;64(1):73-84.
36. Bessone F, Razori MV, Roma MG. Molecular pathways of nonalcoholic fatty liver disease development and progression. Cell Mol Life Sci. 2019;76(1):99-128.
37. Huang DQ, El-Serag HB, Loomba R. Global epidemiology of NAFLD-related HCC: trends, predictions, risk factors and prevention. Nat Rev Gastroenterol Hepatol. 2021;18(4):223-38.
38. Chalasani N, Younossi Z, Lavine JE, Charlton M, Cusi K, Rinella M, Harrison SA, Brunt EM, Sanyal AJ. The diagnosis and management of nonalcoholic fatty liver disease: Practice guidance from the American Association for the Study of Liver Diseases. Hepatology. 2018;67(1):328-57.
39. Lee DH, Lee JM. Primary malignant tumours in the non-cirrhotic liver. Eur J Radiol. 2017;95:349-61.
40. Sanyal AJ, Yoon SK, Lencioni R. The etiology of hepatocellular carcinoma and consequences for treatment. Oncologist. 2010;15 Suppl 4:14-22.
41. Farges O, Ferreira N, Dokmak S, Belghiti J, Bedossa P, Paradis V. Changing trends in malignant transformation of hepatocellular adenoma. Gut. 2011;60(1):85-9.
42. Tanwar S, Rhodes F, Srivastava A, Trembling PM, Rosenberg WM. Inflammation and fibrosis in chronic liver diseases including non-alcoholic fatty liver disease and hepatitis C. World J Gastroenterol. 2020;26(2):109-33.
43. Friedman SL. Mechanisms of hepatic fibrogenesis. Gastroenterology. 2008;134(6):1655-69.
44. Saffioti F, Pinzani M. Development and Regression of Cirrhosis. Dig Dis. 2016;34(4):374-81.

45. Kisseleva T, Brenner D. Molecular and cellular mechanisms of liver fibrosis and its regression. Nat Rev Gastroenterol Hepatol. 2021;18(3):151-66.
46. Bengtsson B, Widman L, Wahlin S, Stål P, Björkström NK, Hagström H. The risk of hepatocellular carcinoma in cirrhosis differs by etiology, age and sex: A Swedish nationwide population-based cohort study. United European Gastroenterol J. 2022;10(5):465-76.
47. Midorikawa Y, Yamamoto S, Tatsuno K, Renard-Guillet C, Tsuji S, Hayashi A, Ueda H, Fukuda S, Fujita T, Katoh H, Ishikawa S, Covington KR, Creighton CJ, Sugitani M, Wheeler DA, Shibata T, Nagae G, Takayama T, Aburatani H. Accumulation of Molecular Aberrations Distinctive to Hepatocellular Carcinoma Progression. Cancer Res. 2020;80(18):3810-9.
48. Nault JC, Mallet M, Pilati C, Calderaro J, Bioulac-Sage P, Laurent C, Laurent A, Cherqui D, Balabaud C, Zucman-Rossi J. High frequency of telomerase reverse-transcriptase promoter somatic mutations in hepatocellular carcinoma and preneoplastic lesions. Nat Commun. 2013;4:2218.
49. Barcena-Varela M, Lujambio A. The Endless Sources of Hepatocellular Carcinoma Heterogeneity. Cancers (Basel). 2021;13(11).
50. Pathologic diagnosis of early hepatocellular carcinoma: a report of the international consensus group for hepatocellular neoplasia. Hepatology. 2009;49(2):658-64.
51. Sato T, Kondo F, Ebara M, Sugiura N, Okabe S, Sunaga M, Yoshikawa M, Suzuki E, Ogasawara S, Shinozaki Y, Ooka Y, Chiba T, Kanai F, Kishimoto T, Nakatani Y, Fukusato T, Yokosuka O. Natural history of large regenerative nodules and dysplastic nodules in liver cirrhosis: 28-year follow-up study. Hepatol Int. 2015;9(2):330-6.
52. Zucman-Rossi J, Villanueva A, Nault JC, Llovet JM. Genetic Landscape and Biomarkers of Hepatocellular Carcinoma. Gastroenterology. 2015;149(5):1226-39.e4.
53. Louault K, Li RR, DeClerck YA. Cancer-Associated Fibroblasts: Understanding Their Heterogeneity. Cancers (Basel). 2020;12(11).
54. Witz IP, Levy-Nissenbaum O. The tumor microenvironment in the post-PAGET era. Cancer Lett. 2006;242(1):1-10.
55. Pietras K, Ostman A. Hallmarks of cancer: interactions with the tumor stroma. Exp Cell Res. 2010;316(8):1324-31.
56. Lakins MA, Ghorani E, Munir H, Martins CP, Shields JD. Cancer-associated fibroblasts induce antigen-specific deletion of CD8 (+) T Cells to protect tumour cells. Nat Commun. 2018;9(1):948.
57. Leonardi GC, Candido S, Cervello M, Nicolosi D, Raiti F, Travali S, Spandidos DA, Libra M. The tumor microenvironment in hepatocellular carcinoma (review). Int J Oncol. 2012;40(6):1733-47.
58. Selzner N, Selzner M, Odermatt B, Tian Y, Van Rooijen N, Clavien PA. ICAM-1 triggers liver regeneration through leukocyte recruitment and Kupffer cell-dependent release of TNF-alpha/IL-6 in mice. Gastroenterology. 2003;124(3):692-700.
59. Jin X, Zimmers TA, Perez EA, Pierce RH, Zhang Z, Koniaris LG. Paradoxical effects of short- and long-term interleukin-6 exposure on liver injury and repair. Hepatology. 2006;43(3):474-84.
60. Nakagawa H, Maeda S, Yoshida H, Tateishi R, Masuzaki R, Ohki T, Hayakawa Y, Kinoshita H, Yamakado M, Kato N, Shiina S, Omata M. Serum IL-6 levels and the risk for hepatocarcinogenesis in chronic hepatitis C patients: an analysis based on gender differences. Int J Cancer. 2009;125(10):2264-9.
61. Ohno H, Kaneko S, Lin Y, Kobayashi K, Murakami S. Human hepatitis B virus X protein augments the DNA binding of nuclear factor for IL-6 through its basic-leucine zipper domain. J Med Virol. 1999;58(1):11-8.
62. Prieto J. Inflammation, HCC and sex: IL-6 in the centre of the triangle. J Hepatol. 2008;48(2):380-1.
63. Hou J, Zhang H, Sun B, Karin M. The immunobiology of hepatocellular carcinoma in humans and mice: Basic concepts and therapeutic implications. J Hepatol. 2020;72(1):167-82.
64. Nault JC, Villanueva A. Intratumor molecular and phenotypic diversity in hepatocellular carcinoma. Clin Cancer Res. 2015;21(8):1786-8.
65. Hoshida Y, Villanueva A, Llovet JM. Molecular profiling to predict hepatocellular carcinoma outcome. Expert Rev Gastroenterol Hepatol. 2009;3(2):101-3.
66. Sherman M. Recurrence of hepatocellular carcinoma. N Engl J Med. 2008;359(19):2045-7.

67. Ding X, He M, Chan AWH, Song QX, Sze SC, Chen H, Man MKH, Man K, Chan SL, Lai PBS, Wang X, Wong N. Genomic and Epigenomic Features of Primary and Recurrent Hepatocellular Carcinomas. Gastroenterology. 2019;157(6):1630-45.e6.
68. Navin N, Kendall J, Troge J, Andrews P, Rodgers L, McIndoo J, Cook K, Stepansky A, Levy D, Esposito D, Muthuswamy L, Krasnitz A, McCombie WR, Hicks J, Wigler M. Tumour evolution inferred by single-cell sequencing. Nature. 2011;472(7341):90-4.
69. Burrell RA, Swanton C. Tumour heterogeneity and the evolution of polyclonal drug resistance. Mol Oncol. 2014;8(6):1095-111.
70. Suresh A, Dhanasekaran R. Implications of genetic heterogeneity in hepatocellular cancer. Adv Cancer Res. 2022;156:103-35.
71. Li L, Knutsdottir H, Hui K, Weiss MJ, He J, Philosophe B, Cameron AM, Wolfgang CL, Pawlik TM, Ghiaur G, Ewald AJ, Mezey E, Bader JS, Selaru FM. Human primary liver cancer organoids reveal intratumor and interpatient drug response heterogeneity. JCI Insight. 2019;4(2).
72. Reig M, Forner A, Rimola J, Ferrer-Fàbrega J, Burrel M, Garcia-Criado Á, Kelley RK, Galle PR, Mazzaferro V, Salem R, Sangro B, Singal AG, Vogel A, Fuster J, Ayuso C, Bruix J. BCLC strategy for prognosis prediction and treatment recommendation: The 2022 update. J Hepatol. 2022;76(3):681-93.
73. Vauthey JN, Dixon E, Abdalla EK, Helton WS, Pawlik TM, Taouli B, Brouquet A, Adams RB. Pretreatment assessment of hepatocellular carcinoma: expert consensus statement. HPB (Oxford). 2010;12(5):289-99.
74. Kudo M. Heterogeneity and Subclassification of Barcelona Clinic Liver Cancer Stage B. Liver Cancer. 2016;5(2):91-6.
75. Loy LM, Low HM, Choi JY, Rhee H, Wong CF, Tan CH. Variant Hepatocellular Carcinoma Subtypes According to the 2019 WHO Classification: An Imaging-Focused Review. AJR Am J Roentgenol. 2022;219(2):212-23.
76. Li X, Yao Q, Liu C, Wang J, Zhang H, Li S, Cai P. Macrotrabecular-Massive Hepatocellular Carcinoma: What Should We Know? J Hepatocell Carcinoma. 2022;9:379-87.
77. Bauer J, Köhler N, Maringer Y, Bucher P, Bilich T, Zwick M, Dicks S, Nelde A, Dubbelaar M, Scheid J, Wacker M, Heitmann JS, Schroeder S, Rieth J, Denk M, Richter M, Klein R, Bonzheim I, Luibrand J, Holzer U, Ebinger M, Brecht IB, Bitzer M, Boerries M, Feucht J, Salih HR, Rammensee HG, Hailfinger S, Walz JS. The oncogenic fusion protein DNAJB1-PRKACA can be specifically targeted by peptide-based immunotherapy in fibrolamellar hepatocellular carcinoma. Nat Commun. 2022;13(1):6401.
78. Calderaro J, Couchy G, Imbeaud S, Amaddeo G, Letouzé E, Blanc JF, Laurent C, Hajji Y, Azoulay D, Bioulac-Sage P, Nault JC, Zucman-Rossi J. Histological subtypes of hepatocellular carcinoma are related to gene mutations and molecular tumour classification. J Hepatol. 2017;67(4):727-38.
79. EASL Clinical Practice Guidelines: Management of hepatocellular carcinoma. J Hepatol. 2018;69(1):182-236.
80. Heimbach JK, Kulik LM, Finn RS, Sirlin CB, Abecassis MM, Roberts LR, Zhu AX, Murad MH, Marrero JA. AASLD guidelines for the treatment of hepatocellular carcinoma. Hepatology. 2018;67(1):358-80.
81. Yang C, Zhang S, Cheng Z, Liu Z, Zhang L, Jiang K, Geng H, Qian R, Wang J, Huang X, Chen M, Li Z, Qin W, Xia Q, Kang X, Wang C, Hang H. Multi-region sequencing with spatial information enables accurate heterogeneity estimation and risk stratification in liver cancer. Genome Med. 2022;14(1):142.
82. Edmondson HA, Steiner PE. Primary carcinoma of the liver: a study of 100 cases among 48,900 necropsies. Cancer. 1954;7(3):462-503.
83. Yoon JH, Choi SK, Cho SB, Kim HJ, Ko YS, Jun CH. Early extrahepatic recurrence as a pivotal factor for survival after hepatocellular carcinoma resection: A 15-year observational study. World J Gastroenterol. 2022;28(36):5351-63.
84. Zhou L, Rui JA, Zhou WX, Wang SB, Chen SG, Qu Q. Edmondson-Steiner grade: A crucial predictor of recurrence and survival in hepatocellular carcinoma without microvascular invasio. Pathol Res Pract. 2017;213(7):824-30.
85. Di Tommaso L, Franchi G, Park YN, Fiamengo B, Destro A, Morenghi E, Montorsi M, Torzilli G, Tommasini M, Terracciano L, Tornillo L, Vecchione R, Roncalli M. Diagnostic value of HSP70, glypican 3, and glutamine synthetase in hepatocellular nodules in cirrhosis. Hepatology. 2007;45(3):725-34.

86. Liu YW, Chen CL, Chen YS, Wang CC, Wang SH, Lin CC. Needle tract implantation of hepatocellular carcinoma after fine needle biopsy. Dig Dis Sci. 2007;52(1):228-31.
87. Seeff LB, Everson GT, Morgan TR, Curto TM, Lee WM, Ghany MG, Shiffman ML, Fontana RJ, Di Bisceglie AM, Bonkovsky HL, Dienstag JL. Complication rate of percutaneous liver biopsies among persons with advanced chronic liver disease in the HALT-C trial. Clin Gastroenterol Hepatol. 2010;8(10):877-83.
88. Yoneda N, Matsui O, Kobayashi S, Kitao A, Kozaka K, Inoue D, Yoshida K, Minami T, Koda W, Gabata T. Current status of imaging biomarkers predicting the biological nature of hepatocellular carcinoma. Jpn J Radiol. 2019;37(3):191-208.
89. Jha RC, Zanello PA, Nguyen XM, Pehlivanova M, Johnson LB, Fishbein T, Shetty K. Small hepatocellular carcinoma: MRI findings for predicting tumor growth rates. Acad Radiol. 2014;21(11):1455-64.
90. Liu YI, Shin LK, Jeffrey RB, Kamaya A. Quantitatively defining washout in hepatocellular carcinoma. AJR Am J Roentgenol. 2013;200(1):84-9.
91. Kamaya A, Maturen KE, Tye GA, Liu YI, Parti NN, Desser TS. Hypervascular liver lesions. Semin Ultrasound CT MR. 2009;30(5):387-407.
92. Fan PL, Xia HS, Ding H, Dong Y, Chen LL, Wang WP. Characterization of Early Hepatocellular Carcinoma and High-Grade Dysplastic Nodules on Contrast-Enhanced Ultrasound: Correlation With Histopathologic Findings. J Ultrasound Med. 2020;39(9):1799-808.
93. Kim JH, Joo I, Lee JM. Atypical Appearance of Hepatocellular Carcinoma and Its Mimickers: How to Solve Challenging Cases Using Gadoxetic Acid-Enhanced Liver Magnetic Resonance Imaging. Korean J Radiol. 2019;20(7):1019-41.
94. Jang HJ, Kim TK, Burns PN, Wilson SR. Enhancement patterns of hepatocellular carcinoma at contrast-enhanced US: comparison with histologic differentiation. Radiology. 2007;244(3):898-906.
95. Lee JH, Lee JM, Kim SJ, Baek JH, Yun SH, Kim KW, Han JK, Choi BI. Enhancement patterns of hepatocellular carcinomas on multiphasicmultidetector row CT: comparison with pathological differentiation. Br J Radiol. 2012;85(1017):e573-83.
96. Hayashi M, Matsui O, Ueda K, Kawamori Y, Kadoya M, Yoshikawa J, Gabata T, Takashima T, Nonomura A, Nakanuma Y. Correlation between the blood supply and grade of malignancy of hepatocellular nodules associated with liver cirrhosis: evaluation by CT during intraarterial injection of contrast medium. AJR Am J Roentgenol. 1999;172(4):969-76.
97. Motosugi U, Bannas P, Sano K, Reeder SB. Hepatobiliary MR contrast agents in hypovascular hepatocellular carcinoma. J Magn Reson Imaging. 2015;41(2):251-65.
98. Asayama Y, Yoshimitsu K, Nishihara Y, Irie H, Aishima S, Taketomi A, Honda H. Arterial blood supply of hepatocellular carcinoma and histologic grading: radiologic-pathologic correlation. AJR Am J Roentgenol. 2008;190(1):W28-34.
99. Nakachi K, Tamai H, Mori Y, Shingaki N, Moribata K, Deguchi H, Ueda K, Inoue I, Maekita T, Iguchi M, Kato J, Ichinose M. Prediction of poorly differentiated hepatocellular carcinoma using contrast computed tomography. Cancer Imaging. 2014;14(1):7.
100. Klintmalm GB. Liver transplantation for hepatocellular carcinoma: a registry report of the impact of tumor characteristics on outcome. Ann Surg. 1998;228(4):479-90.
101. Jonas S, Bechstein WO, Steinmüller T, Herrmann M, Radke C, Berg T, Settmacher U, Neuhaus P. Vascular invasion and histopathologic grading determine outcome after liver transplantation for hepatocellular carcinoma in cirrhosis. Hepatology. 2001;33(5):1080-6.
102. Elbanna KY, Kielar AZ. Computed Tomography Versus Magnetic Resonance Imaging for Hepatic Lesion Characterization/Diagnosis. Clin Liver Dis (Hoboken). 2021;17(3):159-64.
103. Piana G, Trinquart L, Meskine N, Barrau V, Beers BV, Vilgrain V. New MR imaging criteria with a diffusion-weighted sequence for the diagnosis of hepatocellular carcinoma in chronic liver diseases. J Hepatol. 2011;55(1):126-32.
104. Welle CL, Guglielmo FF, Venkatesh SK. MRI of the liver: choosing the right contrast agent. Abdom Radiol (NY). 2020;45(2):384-92.
105. Van Beers BE, Pastor CM, Hussain HK. Primovist, Eovist: what to expect? J Hepatol. 2012;57(2):421-9.
106. Vernuccio F, Gagliano DS, Cannella R, Ba-Ssalamah A, Tang A, Brancatelli G. Spectrum of liver lesions hyperintense on hepatobiliary phase: an approach by clinical setting. Insights Imaging. 2021;12(1):8.

107. Choi JY, Lee JM, Sirlin CB. CT and MR imaging diagnosis and staging of hepatocellular carcinoma: part I. Development, growth, and spread: key pathologic and imaging aspects. Radiology. 2014;272(3):635-54.
108. Hanna RF, Miloushev VZ, Tang A, Finklestone LA, Brejt SZ, Sandhu RS, Santillan CS, Wolfson T, Gamst A, Sirlin CB. Comparative 13-year meta-analysis of the sensitivity and positive predictive value of ultrasound, CT, and MRI for detecting hepatocellular carcinoma. Abdom Radiol (NY). 2016;41(1):71-90.
109. Joo I, Lee JM, Lee DH, Jeon JH, Han JK. Retrospective validation of a new diagnostic criterion for hepatocellular carcinoma on gadoxetic acid-enhanced MRI: can hypointensity on the hepatobiliary phase be used as an alternative to washout with the aid of ancillary features? Eur Radiol. 2019;29(4):1724-32.
110. Kierans AS, Kang SK, Rosenkrantz AB. The Diagnostic Performance of Dynamic Contrast-enhanced MR Imaging for Detection of Small Hepatocellular Carcinoma Measuring Up to 2 cm: A Meta-Analysis. Radiology. 2016;278(1):82-94.
111. Sciarra A, Schmidt S, Pellegrinelli A, Maggioni M, Dondossola D, Pasquier J, Cigala C, Tosi D, Halkic N, Bulfamante G, Viale G, Bosari S, Balabaud C, Bioulac-Sage P, Sempoux C. OATPB1/B3 and MRP3 expression in hepatocellular adenoma predicts Gd-EOB-DTPA uptake and correlates with risk of malignancy. Liver Int. 2019;39(1):158-67.
112. Suh CH, Kim KW, Kim GY, Shin YM, Kim PN, Park SH. The diagnostic value of Gd-EOB-DTPA-MRI for the diagnosis of focal nodular hyperplasia: a systematic review and meta-analysis. Eur Radiol. 2015;25(4):950-60.
113. Ba-Ssalamah A, Antunes C, Feier D, Bastati N, Hodge JC, Stift J, Cipriano MA, Wrba F, Trauner M, Herold CJ, Caseiro-Alves F. Morphologic and Molecular Features of Hepatocellular Adenoma with Gadoxetic Acid-enhanced MR Imaging. Radiology. 2015;277(1):104-13.
114. Yoneda N, Matsui O, Kitao A, Kozaka K, Gabata T, Sasaki M, Nakanuma Y, Murata K, Tani T. Beta-catenin-activated hepatocellular adenoma showing hyperintensity on hepatobiliary-phase gadoxetic-enhanced magnetic resonance imaging and overexpression of OATP8. Jpn J Radiol. 2012;30(9):777-82.
115. Auer TA, Walter-Rittel T, Geisel D, Schöning W, Schmelzle M, Müller T, Sinn B, Denecke T, Hamm B, Fehrenbach U. HBP-enhancing hepatocellular adenomas and how to discriminate them from FNH in Gd-EOB MRI. BMC Med Imaging. 2021;21(1):28.
116. Roux M, Pigneur F, Calderaro J, Baranes L, Chiaradia M, Tselikas L, Decaens T, Costentin C, Laurent A, Azoulay D, Mallat A, Zafrani ES, Rahmouni A, Luciani A. Differentiation of focal nodular hyperplasia from hepatocellular adenoma: Role of the quantitative analysis of gadobenate dimeglumine-enhanced hepatobiliary phase MRI. J Magn Reson Imaging. 2015;42(5):1249-58.
117. Auer TA, Fehrenbach U, Grieser C, Penzkofer T, Geisel D, Schmelzle M, Müller T, Bläker H, Seehofer D, Denecke T. Hepatocellular adenomas: is there additional value in using Gd-EOB-enhanced MRI for subtype differentiation? Eur Radiol. 2020;30(6):3497-506.
118. Bioulac-Sage P, Laumonier H, Couchy G, Le Bail B, Sa Cunha A, Rullier A, Laurent C, Blanc JF, Cubel G, Trillaud H, Zucman-Rossi J, Balabaud C, Saric J. Hepatocellular adenoma management and phenotypic classification: the Bordeaux experience. Hepatology. 2009;50(2):481-9.
119. Min JH, Lee MW, Park HS, Lee DH, Park HJ, Lee JE, Park SJ, Kim SS, Park SH, Ha SY, Hwang JA, Cha DI, Park B. LI-RADS Version 2018 Targetoid Appearances on Gadoxetic Acid-Enhanced MRI: Interobserver Agreement and Diagnostic Performance for the Differentiation of HCC and Non-HCC Malignancy. AJR Am J Roentgenol. 2022;219(3):421-32.
120. Cannella R, Fraum TJ, Ludwig DR, Borhani AA, Tsung A, Furlan A, Fowler KJ. Targetoid appearance on T2-weighted imaging and signs of tumor vascular involvement: diagnostic value for differentiating HCC from other primary liver carcinomas. Eur Radiol. 2021;31(9):6868-78.
121. Choi JW, Lee JM, Kim SJ, Yoon JH, Baek JH, Han JK, Choi BI. Hepatocellular carcinoma: imaging patterns on gadoxetic acid-enhanced MR Images and their value as an imaging biomarker. Radiology. 2013;267(3):776-86.
122. Kim JY, Kim MJ, Kim KA, Jeong HT, Park YN. Hyperintense HCC on hepatobiliary phase images of gadoxetic acid-enhanced MRI: correlation with clinical and pathological features. Eur J Radiol. 2012;81(12):3877-82.
123. Tabrizian P, Jibara G, Shrager B, Schwartz M, Roayaie S. Recurrence of hepatocellular cancer after resection: patterns, treatments, and prognosis. Ann Surg. 2015;261(5):947-55.

124. Tan DJH, Wong C, Ng CH, Poh CW, Jain SR, Huang DQ, Muthiah MD. A Meta-Analysis on the Rate of Hepatocellular Carcinoma Recurrence after Liver Transplant and Associations to Etiology, Alpha-Fetoprotein, Income and Ethnicity. J Clin Med. 2021;10(2).
125. Zhang XP, Wang K, Wei XB, Li LQ, Sun HC, Wen TF, Chai ZT, Chen ZH, Shi J, Guo WX, Xie D, Cong WM, Wu MC, Lau WY, Cheng SQ. An Eastern Hepatobiliary Surgery Hospital Microvascular Invasion Scoring System in Predicting Prognosis of Patients with Hepatocellular Carcinoma and Microvascular Invasion After R0 Liver Resection: A Large-Scale, Multicenter Study. Oncologist. 2019;24(12):e1476-e88.
126. Renne SL, Woo HY, Allegra S, Rudini N, Yano H, Donadon M, Viganò L, Akiba J, Lee HS, Rhee H, Park YN, Roncalli M, Di Tommaso L. Vessels Encapsulating Tumor Clusters (VETC) Is a Powerful Predictor of Aggressive Hepatocellular Carcinoma. Hepatology. 2020;71(1):183-95.
127. Rodríguez-Perálvarez M, Luong TV, Andreana L, Meyer T, Dhillon AP, Burroughs AK. A systematic review of microvascular invasion in hepatocellular carcinoma: diagnostic and prognostic variability. Ann Surg Oncol. 2013;20(1):325-39.
128. Wang L, Jia M, Wen X, Shen J, Yang H. Diagnostic value of magnetic resonance imaging features of microvascular invasion in hepatocellular carcinoma: a meta-analysis. Diagn Interv Radiol. 2022;28(5):428-40.
129. Huang J, Tian W, Zhang L, Huang Q, Lin S, Ding Y, Liang W, Zheng S. Preoperative Prediction Power of Imaging Methods for Microvascular Invasion in Hepatocellular Carcinoma: A Systemic Review and Meta-Analysis. Front Oncol. 2020;10:887.
130. Shah MR, Flusberg M, Paroder V, Rozenblit AM, Chernyak V. Transient arterial phase respiratory motion-related artifact in MR imaging of the liver: an analysis of four different gadolinium-based contrast agents. Clin Imaging. 2017;41:23-7.
131. Rimola J, Darnell A, Belmonte E, Sapena V, Caparroz C, Llarch N, Reig M, Forner A, Bruix J, Ayuso C. Does transient arterial-phase respiratory-motion-related artifact impact on diagnostic performance? An intra-patient comparison of extracellular gadolinium versus gadoxetic acid. Eur Radiol. 2020;30(12):6694-701.
132. Pietryga JA, Burke LM, Marin D, Jaffe TA, Bashir MR. Respiratory motion artifact affecting hepatic arterial phase imaging with gadoxetate disodium: examination recovery with a multiple arterial phase acquisition. Radiology. 2014;271(2):426-34.
133. Tamada T, Ito K, Sone T, Yamamoto A, Yoshida K, Kakuba K, Tanimoto D, Higashi H, Yamashita T. Dynamic contrast-enhanced magnetic resonance imaging of abdominal solid organ and major vessel: comparison of enhancement effect between Gd-EOB-DTPA and Gd-DTPA. J Magn Reson Imaging. 2009;29(3):636-40.
134. Blankenburg M, Elhamamy M, Zhang D, Corbin A, Jin G, Harris J, Knobloch G. Evaluation of the health economic impact of initial diagnostic modality selection in patients suspected of having HCC in China and the USA. J Med Econ. 2022;25(1):1015-29.
135. Chernyak V, Fowler KJ, Kamaya A, Kielar AZ, Elsayes KM, Bashir MR, Kono Y, Do RK, Mitchell DG, Singal AG, Tang A, Sirlin CB. Liver Imaging Reporting and Data System (LI-RADS) Version 2018: Imaging of Hepatocellular Carcinoma in At-Risk Patients. Radiology. 2018;289(3):816-30.
136. Marrero JA, Kulik LM, Sirlin CB, Zhu AX, Finn RS, Abecassis MM, Roberts LR, Heimbach JK. Diagnosis, Staging, and Management of Hepatocellular Carcinoma: 2018 Practice Guidance by the American Association for the Study of Liver Diseases. Hepatology. 2018;68(2):723-50.
137. Singal AG, Pillai A, Tiro J. Early detection, curative treatment, and survival rates for hepatocellular carcinoma surveillance in patients with cirrhosis: a meta-analysis. PLoS Med. 2014;11(4):e1001624.
138. Singal A, Volk ML, Waljee A, Salgia R, Higgins P, Rogers MA, Marrero JA. Meta-analysis: surveillance with ultrasound for early-stage hepatocellular carcinoma in patients with cirrhosis. Aliment Pharmacol Ther. 2009;30(1):37-47.
139. Kim DH, Choi SH, Shim JH, Kim SY, Lee SS, Byun JH, Choi JI. Meta-Analysis of the Accuracy of Abbreviated Magnetic Resonance Imaging for Hepatocellular Carcinoma Surveillance: Non-Contrast versus Hepatobiliary Phase-Abbreviated Magnetic Resonance Imaging. Cancers (Basel). 2021;13(12).
140. Salomao M, Yu WM, Brown RS, Jr., Emond JC, Lefkowitch JH. Steatohepatitic hepatocellular carcinoma (SH-HCC): a distinctive histological variant of HCC in hepatitis C virus-related cirrhosis with associated NAFLD/NASH. Am J Surg Pathol. 2010;34(11):1630-6.

141. Olofson AM, Gonzalo DH, Chang M, Liu X. Steatohepatitic Variant of Hepatocellular Carcinoma: A Focused Review. Gastroenterology Res. 2018;11(6):391-6.
142. Yeh MM, Liu Y, Torbenson M. Steatohepatitic variant of hepatocellular carcinoma in the absence of metabolic syndrome or background steatosis: a clinical, pathological, and genetic study. Hum Pathol. 2015;46(11):1769-75.
143. Mulé S, Serhal A, Pregliasco AG, Nguyen J, Vendrami CL, Reizine E, Yang GY, Calderaro J, Amaddeo G, Luciani A, Miller FH. MRI features associated with HCC histologic subtypes: a western American and European bicenter study. Eur Radiol. 2023;33(2):1342-52.
144. Cannella R, Dioguardi Burgio M, Beaufrère A, Trapani L, Paradis V, Hobeika C, Cauchy F, Bouattour M, Vilgrain V, Sartoris R, Ronot M. Imaging features of histological subtypes of hepatocellular carcinoma: Implication for LI-RADS. JHEP Rep. 2021;3(6):100380.
145. Zhang YN, Fowler KJ, Hamilton G, Cui JY, Sy EZ, Balanay M, Hooker JC, Szeverenyi N, Sirlin CB. Liver fat imaging-a clinical overview of ultrasound, CT, and MR imaging. Br J Radiol. 2018;91(1089):20170959.
146. Piekarski J, Goldberg HI, Royal SA, Axel L, Moss AA. Difference between liver and spleen CT numbers in the normal adult: its usefulness in predicting the presence of diffuse liver disease. Radiology. 1980;137(3):727-9.
147. Inui S, Kondo H, Tanahashi Y, Fukukura Y, Sano K, Morisaka H, Saito K, Kondo F, Fukusato T, Furui S, Oba H. Steatohepatitic hepatocellular carcinoma: imaging findings with clinicopathological correlation. Clin Radiol. 2021;76(2):160.e15-.e25.
148. Ziol M, Poté N, Amaddeo G, Laurent A, Nault JC, Oberti F, Costentin C, Michalak S, Bouattour M, Francoz C, Pageaux GP, Ramos J, Decaens T, Luciani A, Guiu B, Vilgrain V, Aubé C, Derman J, Charpy C, Zucman-Rossi J, Barget N, Seror O, Ganne-Carrié N, Paradis V, Calderaro J. Macrotrabecular-massive hepatocellular carcinoma: A distinctive histological subtype with clinical relevance. Hepatology. 2018;68(1):103-12.
149. Liu N, Liu M, Fu S, Wang J, Tang H, Isah AD, Chen D, Wang X. Ang2-Targeted Combination Therapy for Cancer Treatment. Front Immunol. 2022;13:949553.
150. Fang JH, Zhou HC, Zhang C, Shang LR, Zhang L, Xu J, Zheng L, Yuan Y, Guo RP, Jia WH, Yun JP, Chen MS, Zhang Y, Zhuang SM. A novel vascular pattern promotes metastasis of hepatocellular carcinoma in an epithelial-mesenchymal transition-independent manner. Hepatology. 2015;62(2):452-65.
151. Rhee H, Cho ES, Nahm JH, Jang M, Chung YE, Baek SE, Lee S, Kim MJ, Park MS, Han DH, Choi JY, Park YN. Gadoxetic acid-enhanced MRI of macrotrabecular-massive hepatocellular carcinoma and its prognostic implications. J Hepatol. 2021;74(1):109-21.
152. Mulé S, Galletto Pregliasco A, Tenenhaus A, Kharrat R, Amaddeo G, Baranes L, Laurent A, Regnault H, Sommacale D, Djabbari M, Pigneur F, Tacher V, Kobeiter H, Calderaro J, Luciani A. Multiphase Liver MRI for Identifying the Macrotrabecular-Massive Subtype of Hepatocellular Carcinoma. Radiology. 2020;295(3):562-71.
153. Zhu Y, Weng S, Li Y, Yan C, Ye R, Wen L, Zhou L, Gao L. A radiomics nomogram based on contrast-enhanced MRI for preoperative prediction of macrotrabecular-massive hepatocellular carcinoma. Abdom Radiol (NY). 2021;46(7):3139-48.
154. Cha H, Choi JY, Park YN, Han K, Jang M, Kim MJ, Park MS, Rhee H. Comparison of imaging findings of macrotrabecular-massive hepatocellular carcinoma using CT and gadoxetic acid-enhanced MRI. Eur Radiol. 2023;33(2):1364-77.
155. Feng Z, Li H, Zhao H, Jiang Y, Liu Q, Chen Q, Wang W, Rong P. Preoperative CT for Characterization of Aggressive Macrotrabecular-Massive Subtype and Vessels That Encapsulate Tumor Clusters Pattern in Hepatocellular Carcinoma. Radiology. 2021;300(1):219-29.
156. Ribback S. [Preneoplastic glycogenotic lesions of the liver and kidney : Metabolic and molecular alterations in preneoplastic clear cell lesions of the liver and the kidney in experimental and human carcinogenesis]. Pathologe. 2020;41(Suppl 2):83-90.
157. Bannasch P, Ribback S, Su Q, Mayer D. Clear cell hepatocellular carcinoma: origin, metabolic traits and fate of glycogenotic clear and ground glass cells. Hepatobiliary Pancreat Dis Int. 2017;16(6):570-94.
158. Chen X, Lu Y, Shi X, Han G, Zhang L, Ni C, Zhao J, Gao Y, Wang X. Epidemiological and Clinical Characteristics of Five Rare Pathological Subtypes of Hepatocellular Carcinoma. Front Oncol. 2022;12:864106.

159. Park BV, Gaba RC, Huang YH, Chen YF, Guzman G, Lokken RP. Histology of Hepatocellular Carcinoma: Association with Clinical Features, Radiological Findings, and Locoregional Therapy Outcomes. J Clin Imaging Sci. 2019;9:52.
160. Ji SP, Li Q, Dong H. Therapy and prognostic features of primary clear cell carcinoma of the liver. World J Gastroenterol. 2010;16(6):764-9.
161. Deng Y, Zhu S, Yan W, Qi L, Chen Z, Ma L. Influence of clear cell carcinoma on the post-hepatectomy prognosis of patients with hepatocellular carcinoma. Future Oncol. 2022;18(5):543-52.
162. Liu QY, Li HG, Gao M, Lin XF, Li Y, Chen JY. Primary clear cell carcinoma in the liver: CT and MRI findings. World J Gastroenterol. 2011;17(7):946-52.
163. Monzawa S, Omata K, Shimazu N, Yagawa A, Hosoda K, Araki T. Well-differentiated hepatocellular carcinoma: findings of US, CT, and MR imaging. Abdom Imaging. 1999;24(4):392-7.
164. Bello HR, Mahdi ZK, Lui SK, Nandwana SB, Harri PA, Davarpanah AH. Hepatocellular Carcinoma With Atypical Imaging Features: Review of the Morphologic Hepatocellular Carcinoma Subtypes With Radiology-Pathology Correlation. J Magn Reson Imaging. 2022;55(3):681-97.
165. Wood LD, Heaphy CM, Daniel HD, Naini BV, Lassman CR, Arroyo MR, Kamel IR, Cosgrove DP, Boitnott JK, Meeker AK, Torbenson MS. Chromophobe hepatocellular carcinoma with abrupt anaplasia: a proposal for a new subtype of hepatocellular carcinoma with unique morphological and molecular features. Mod Pathol. 2013;26(12):1586-93.
166. Kang HJ, Oh JH, Kim YW, Kim W, An J, Sung CO, Kim J, Shim JH, Hwang S, Yu E, Heaphy CM, Hong SM. Clinicopathological and molecular characterization of chromophobe hepatocellular carcinoma. Liver Int. 2021;41(10):2499-510.
167. Lee JH, Choi MS, Gwak GY, Lee JH, Koh KC, Paik SW, Yoo BC, Choi D, Park CK. Clinicopathologic characteristics and long-term prognosis of scirrhous hepatocellular carcinoma. Dig Dis Sci. 2012;57(6):1698-707.
168. Kurogi M, Nakashima O, Miyaaki H, Fujimoto M, Kojiro M. Clinicopathological study of scirrhous hepatocellular carcinoma. J Gastroenterol Hepatol. 2006;21(9):1470-7.
169. Murtha-Lemekhova A, Fuchs J, Schulz E, Sterkenburg AS, Mayer P, Pfeiffenberger J, Hoffmann K. Scirrhous Hepatocellular Carcinoma: Systematic Review and Pooled Data Analysis of Clinical, Radiological, and Histopathological Features. J Hepatocell Carcinoma. 2021;8:1269-79.
170. Yoshikawa J, Matsui O, Kadoya M, Gabata T, Arai K, Takashima T. Delayed enhancement of fibrotic areas in hepatic masses: CT-pathologic correlation. J Comput Assist Tomogr. 1992;16(2):206-11.
171. Chong YS, Kim YK, Lee MW, Kim SH, Lee WJ, Rhim HC, Lee SJ. Differentiating mass-forming intrahepatic cholangiocarcinoma from atypical hepatocellular carcinoma using gadoxetic acid-enhanced MRI. Clin Radiol. 2012;67(8):766-73.
172. Choi SY, Kim YK, Min JH, Kang TW, Jeong WK, Ahn S, Won H. Added value of ancillary imaging features for differentiating scirrhous hepatocellular carcinoma from intrahepatic cholangiocarcinoma on gadoxetic acid-enhanced MR imaging. Eur Radiol. 2018;28(6):2549-60.
173. Kim SH, Lim HK, Lee WJ, Choi D, Park CK. Scirrhous hepatocellular carcinoma: comparison with usual hepatocellular carcinoma based on CT-pathologic features and long-term results after curative resection. Eur J Radiol. 2009;69(1):123-30.
174. Ross HM, Daniel HD, Vivekanandan P, Kannangai R, Yeh MM, Wu TT, Makhlouf HR, Torbenson M. Fibrolamellar carcinomas are positive for CD68. Mod Pathol. 2011;24(3):390-5.
175. Eggert T, McGlynn KA, Duffy A, Manns MP, Greten TF, Altekruse SF. Fibrolamellar hepatocellular carcinoma in the USA, 2000-2010: A detailed report on frequency, treatment and outcome based on the Surveillance, Epidemiology, and End Results database. United European Gastroenterol J. 2013;1(5):351-7.
176. Honeyman JN, Simon EP, Robine N, Chiaroni-Clarke R, Darcy DG, Lim, II, Gleason CE, Murphy JM, Rosenberg BR, Teegan L, Takacs CN, Botero S, Belote R, Germer S, Emde AK, Vacic V, Bhanot U, LaQuaglia MP, Simon SM. Detection of a recurrent DNAJB1-PRKACA chimeric transcript in fibrolamellar hepatocellular carcinoma. Science. 2014;343(6174):1010-4.
177. Karamafrooz A, Brennan J, Thomas DD, Parker LL. Integrated Phosphoproteomics for Identifying Substrates of Human Protein Kinase A (PRKACA) and Its Oncogenic Mutant DNAJB1-PRKACA. J Proteome Res. 2021;20(10):4815-30.

178. Kakar S, Burgart LJ, Batts KP, Garcia J, Jain D, Ferrell LD. Clinicopathologic features and survival in fibrolamellar carcinoma: comparison with conventional hepatocellular carcinoma with and without cirrhosis. Mod Pathol. 2005;18(11):1417-23.
179. Palm V, Sheng R, Mayer P, Weiss KH, Springfeld C, Mehrabi A, Longerich T, Berger AK, Kauczor HU, Weber TF. Imaging features of fibrolamellar hepatocellular carcinoma in gadoxetic acid-enhanced MRI. Cancer Imaging. 2018;18(1):9.
180. Ganeshan D, Szklaruk J, Kaseb A, Kattan A, Elsayes KM. Fibrolamellar hepatocellular carcinoma: multiphasic CT features of the primary tumor on pre-therapy CT and pattern of distant metastases. Abdom Radiol (NY). 2018;43(12):3340-8.
181. Dong Y, Wang WP, Mao F, Zhang Q, Yang D, Tannapfel A, Meloni MF, Neye H, Clevert DA, Dietrich CF. Imaging Features of Fibrolamellar Hepatocellular Carcinoma with Contrast-Enhanced Ultrasound. Ultraschall Med. 2021;42(3):306-13.
182. Erratum to: Imaging findings of fibrolamellar hepatocellular carcinomas on ultrasonography: A comparison with conventional hepatocellular carcinomas. Clin Hemorheol Microcirc. 2021;79(2):363.
183. Kim T, Hori M, Onishi H. Liver masses with central or eccentric scar. Semin Ultrasound CT MR. 2009;30(5):418-25.
184. Torbenson MS. Hepatocellular carcinoma: making sense of morphological heterogeneity, growth patterns, and subtypes. Hum Pathol. 2021;112:86-101.
185. Omori G, Osuga T, Miyanishi K, Hamaguchi K, Tanaka S, Ohnuma H, Murase K, Takada K, Nagayama M, Kimura Y, Takemasa I, Kikuchi Y, Torigoe T, Kato J. Programmed cell death ligand 1 expression in a case of poorly differentiated lymphocyte-rich hepatocellular carcinoma. Clin Case Rep. 2021;9(9):e04764.
186. Renzulli M, Braccischi L, D'Errico A, Pecorelli A, Brandi N, Golfieri R, Albertini E, Vasuri F. State-of-the-art review on the correlations between pathological and magnetic resonance features of cirrhotic nodules. Histol Histopathol. 2022;37(12):1151-65.
187. Pathology AFIo. Torbenson MZ, Y; Yeh, M Tumors of the liver in AFIP Atlas of Tumor Pathology, 4th series, fascicle 27, American registry of Pathology 2018.
188. 2022 KLCA-NCC Korea practice guidelines for the management of hepatocellular carcinoma. Clin Mol Hepatol. 2022;28(4):583-705.
189. Auer TA, Halskov S, Fehrenbach U, Nevermann NF, Pelzer U, Mohr R, Hamm B, Schöning W, Horst D, Ihlow J, Geisel D. Gd-EOB MRI for HCC subtype differentiation in a western population according to the 5(th) edition of the World Health Organization classification. Eur Radiol. 2023.
190. Trevethan R. Sensitivity, Specificity, and Predictive Values: Foundations, Pliabilities, and Pitfalls in Research and Practice. Front Public Health. 2017;5:307.
191. Tzartzeva K, Obi J, Rich NE, Parikh ND, Marrero JA, Yopp A, Waljee AK, Singal AG. Surveillance Imaging and Alpha Fetoprotein for Early Detection of Hepatocellular Carcinoma in Patients With Cirrhosis: A Meta-analysis. Gastroenterology. 2018;154(6):1706-18.e1.
192. Deeks JJ, Altman DG. Diagnostic tests 4: likelihood ratios. Bmj. 2004;329(7458):168-9.
193. Grimes DA, Schulz KF. Refining clinical diagnosis with likelihood ratios. Lancet. 2005;365(9469):1500-5.
194. Stengel D, Bauwens K, Sehouli J, Ekkernkamp A, Porzsolt F. A likelihood ratio approach to meta-analysis of diagnostic studies. J Med Screen. 2003;10(1):47-51.
195. Steyerberg EW, Harrell FE, Jr., Borsboom GJ, Eijkemans MJ, Vergouwe Y, Habbema JD. Internal validation of predictive models: efficiency of some procedures for logistic regression analysis. J Clin Epidemiol. 2001;54(8):774-81.
196. Shan Y, Yu X, Yang Y, Sun J, Wu S, Mao S, Lu C. Nomogram for the Preoperative Prediction of the Macrotrabecular-Massive Subtype of Hepatocellular Carcinoma. J Hepatocell Carcinoma. 2022;9:717-28.
197. Liang Y, Xu F, Wang Z, Tan C, Zhang N, Wei X, Jiang X, Wu H. A gadoxetic acid-enhanced MRI-based multivariable model using LI-RADS v2018 and other imaging features for preoperative prediction of macrotrabecular-massive hepatocellular carcinoma. Eur J Radiol. 2022;153:110356.
198. Jeon Y, Benedict M, Taddei T, Jain D, Zhang X. Macrotrabecular Hepatocellular Carcinoma: An Aggressive Subtype of Hepatocellular Carcinoma. Am J Surg Pathol. 2019;43(7):943-8.

199. Ando S, Shibahara J, Hayashi A, Fukayama M. β-catenin alteration is rare in hepatocellular carcinoma with steatohepatitic features: immunohistochemical and mutational study. Virchows Arch. 2015;467(5):535-42.
200. Seok JY, Na DC, Woo HG, Roncalli M, Kwon SM, Yoo JE, Ahn EY, Kim GI, Choi JS, Kim YB, Park YN. A fibrous stromal component in hepatocellular carcinoma reveals a cholangiocarcinoma-like gene expression trait and epithelial-mesenchymal transition. Hepatology. 2012;55(6):1776-86.
201. Wang K, Zhang H, Xia Y, Liu J, Shen F. Surgical options for intrahepatic cholangiocarcinoma. Hepatobiliary Surg Nutr. 2017;6(2):79-90.
202. Tsilimigras DI, Brodt P, Clavien PA, Muschel RJ, D'Angelica MI, Endo I, Parks RW, Doyle M, de Santibañes E, Pawlik TM. Liver metastases. Nat Rev Dis Primers. 2021;7(1):27.
203. Mavros MN, Mayo SC, Hyder O, Pawlik TM. A systematic review: treatment and prognosis of patients with fibrolamellar hepatocellular carcinoma. J Am Coll Surg. 2012;215(6):820-30.
204. Kovac JD, Milovanovic T, Dugalic V, Dumic I. Pearls and pitfalls in magnetic resonance imaging of hepatocellular carcinoma. World J Gastroenterol. 2020;26(17):2012-29.
205. Eschrich J, Kobus Z, Geisel D, Halskov S, Roßner F, Roderburg C, Mohr R, Tacke F. The Diagnostic Approach towards Combined Hepatocellular-Cholangiocarcinoma-State of the Art and Future Perspectives. Cancers (Basel). 2023;15(1).
206. Forner A, Reig M, Bruix J. Hepatocellular carcinoma. Lancet. 2018;391(10127):1301-14.
207. Altekruse SF, McGlynn KA, Reichman ME. Hepatocellular carcinoma incidence, mortality, and survival trends in the United States from 1975 to 2005. J Clin Oncol. 2009;27(9):1485-91.
208. Moyé L. What can we do about exploratory analyses in clinical trials? Contemp Clin Trials. 2015;45(Pt B):302-10.
209. Guo P, Zeng F, Hu X, Zhang D, Zhu S, Deng Y, Hao Y. Improved Variable Selection Algorithm Using a LASSO-Type Penalty, with an Application to Assessing Hepatitis B Infection Relevant Factors in Community Residents. PLoS One. 2015;10(7):e0134151.
210. Chen SY, Feng Z, Yi X. A general introduction to adjustment for multiple comparisons. J Thorac Dis. 2017;9(6):1725-9.
211. Rebouissou S, Nault JC. Advances in molecular classification and precision oncology in hepatocellular carcinoma. J Hepatol. 2020;72(2):215-29.
212. Ruiz de Galarreta M, Bresnahan E, Molina-Sánchez P, Lindblad KE, Maier B, Sia D, Puigvehi M, Miguela V, Casanova-Acebes M, Dhainaut M, Villacorta-Martin C, Singhi AD, Moghe A, von Felden J, Tal Grinspan L, Wang S, Kamphorst AO, Monga SP, Brown BD, Villanueva A, Llovet JM, Merad M, Lujambio A. β-Catenin Activation Promotes Immune Escape and Resistance to Anti-PD-1 Therapy in Hepatocellular Carcinoma. Cancer Discov. 2019;9(8):1124-41.
213. Padhani AR, Liu G, Koh DM, Chenevert TL, Thoeny HC, Takahara T, Dzik-Jurasz A, Ross BD, Van Cauteren M, Collins D, Hammoud DA, Rustin GJ, Taouli B, Choyke PL. Diffusion-weighted magnetic resonance imaging as a cancer biomarker: consensus and recommendations. Neoplasia. 2009;11(2):102-25.
214. Calderaro J, Ziol M, Paradis V, Zucman-Rossi J. Molecular and histological correlations in liver cancer. J Hepatol. 2019;71(3):616-30.
215. Campani C, Zucman-Rossi J, Nault JC. Genetics of Hepatocellular Carcinoma: From Tumor to Circulating DNA. Cancers (Basel). 2023;15(3).
216. Crowley E, Di Nicolantonio F, Loupakis F, Bardelli A. Liquid biopsy: monitoring cancer-genetics in the blood. Nat Rev Clin Oncol. 2013;10(8):472-84.

12 Statutory declaration

“I, Sebastian Halskov, by personally signing this document in lieu of an oath, hereby affirm that I prepared the submitted dissertation on the topic “Hepatocellular carcinoma: establishing imaging biomarkers for non-invasive subtype differentiation with Gd-EOB-enhanced MRI”, “Hepatozelluläres Karzinom: Etablierung bildbasierter Biomarker für nicht-invasive Subtypendifferenzierung mittels Gd-EOB-verstärktem MRT” independently and without the support of third parties, and that I used no other sources and aids than those stated.

All parts which are based on the publications or presentations of other authors, either in letter or in spirit, are specified as such in accordance with the citing guidelines. The sections on methodology (in particular regarding practical work, laboratory regulations, statistical processing) and results (in particular regarding figures, charts and tables) are exclusively my responsibility.

Furthermore, I declare that I have correctly marked all of the data, the analyses, and the conclusions generated from data obtained in collaboration with other persons, and that I have correctly marked my own contribution and the contributions of other persons (cf. declaration of contribution). I have correctly marked all texts or parts of texts that were generated in collaboration with other persons.

My contributions to any publications to this dissertation correspond to those stated in the below joint declaration made together with the supervisor. All publications created within the scope of the dissertation comply with the guidelines of the ICMJE (International Committee of Medical Journal Editors, www.icmje.org) on authorship. In addition, I declare that I shall comply with the regulations of Charité – Universitätsmedizin Berlin on ensuring good scientific practice.

I declare that I have not yet submitted this dissertation in identical or similar form to another Faculty.

The significance of this statutory declaration and the consequences of a false statutory declaration under criminal law (Sections 156, 161 of the German Criminal Code) are known to me.”

Date	Signature

13 Declaration of contributions to publications

Sebastian Halskov made the following contributions to a publication that is related to this dissertation:

Publication #1: Auer TA, Halskov S, Fehrenbach U, Nevermann NF, Pelzer U, Mohr R, Hamm B, Schöning W, Horst D, Ihlow J, Geisel D. Gd-EOB MRI for HCC subtype differentiation in a western population according to the 5th edition of the World Health Organization classification. Eur Radiol. 2023 Apr 28. doi: 10.1007/s00330-023-09669-y. Epub ahead of print. PMID: 37115216.

- Literature research
- Retrospective recruitment of patients
- Acquisition of radiological and clinical data
- Cooperation with Health Data Platform, Berlin Institute of Health, for acquiring laboratory data
- Data management
- Analysis and interpretation of data
- Drafting of the “Methods” and “Results” sections
- Generation of tables (1 to 4) and figures (1 to 6)
- Revision and editing of the manuscript in accordance with reviewer feedback: two major revisions and one minor revision
- Research abstract presentation at the 2023 European Congress of Radiology in Vienna, Austria, for which Sebastian Halskov received the “Best Research Abstract Presentation Award” within the topic “Abdominal and Gastrointestinal”.

Signature and stamp of the primary supervisor

Signature of the doctoral student

14 Curriculum vitae

My curriculum vitae is not included in the electronic version of my dissertation for data protection reasons.

15 List of publications by Sebastian Halskov

Papers:

04/2023	Gd-EOB MRI for HCC subtype differentiation in a western population according to the 5th edition of the World Health Organization classification. Auer TA, **Halskov S**, Fehrenbach U, Nevermann NF, Pelzer U, Mohr R, Hamm B, Schöning W, Horst D, Ihlow J, Geisel D. Eur Radiol. 2023 Apr 28. doi: 10.1007/s00330-023-09669-y. Epub ahead of print. PMID: 37115216.
01/2023	The Diagnostic Approach towards Combined Hepatocellular-Cholangiocarcinoma—State of the Art and Future Perspectives. Eschrich J; Kobus Z; Geisel D; **Halskov S;** Roßner F; Roderburg C; Mohr R; Tacke F. Cancers 2023, 15, 301. https://doi.org/10.3390/cancers15010301

Presentations:

03/2023	The value of Gd-EOB MRI for HCC subtype differentiation in a western population according to the 5th edition of the World Health Organization (WHO) classification. European Congress of Radiology 2023, Vienna, Austria. Awarded "Best Research Presentation Abstract Award" within the topic "Abdominal and Gastrointestinal".

16 Acknowledgements

I would like to thank Prof. Dr. med. Bernd Hamm, Director of the Charité Department of Radiology, for giving me the opportunity to work within the excellent clinical and academic framework of the Department.

I also would like to thank my supervisors PD Dr. med. Dominik Geisel, head of the Charité MRI section, and PD Dr. med. Timo Auer, head of the “Hepatocellular Carcinoma Subtyping” program, for their outstanding guidance and readily available support. They were a strong source of encouragement throughout and well beyond the project, fostering my enthusiasm for radiology and research.

Furthermore, I would like to thank my colleagues from the Charité Departments of Surgery and of Pathology, in particular Dr. med. Jana Ihlow, for their valuable cooperation. I also thank the Health Data Platform for providing support in data extraction.

Finally, thank you to my parents for their unwavering material and moral support throughout my studies and my work with this dissertation.

17 Certification of statistics

CHARITÉ

CharitéCentrum für Human- und Gesundheitswissenschaften

Charité | Campus Charité Mitte | 10117 Berlin

Institut für Biometrie und klinische Epidemiologie (iBikE)

Direktor: Prof. Dr. Frank Konietschke

Postantschrift:
Charitéplatz 1 | 10117 Berlin
Besucheranschrift:
Reinhardtstr. 58 | 10117 Berlin

Tel. +49 (0)30 450 562 161
frank.konietschke@charite.de
https://biometrie.charite.de/

Name, Vorname: Halskov, Sebastian

Emailadresse: sebastian.halskov@charite.de

Matrikelnummer: 218957

PromotionsbetreuerIn: PD Dr. Geisel, PD Dr. Auer

Promotionsinstitution / Klinik: Klinik für Radiologie der Charité

Bescheinigung

Hiermit bescheinige ich, dass Herr Halskov innerhalb der Service Unit Biometrie des Instituts für Biometrie und klinische Epidemiologie (iBikE) bei mir eine statistische Beratung zu einem Promotionsvorhaben wahrgenommen hat. Folgende Beratungstermine wurden wahrgenommen:

- Termin 1: 13.06.2022

Folgende wesentliche Ratschläge hinsichtlich einer sinnvollen Auswertung und Interpretation der Daten wurden während der Beratung erteilt:

- Deskriptive Analysen durchführen; Ergebnisse z.B. in einer Tabelle zusammenfassen, eine Ordinalvariable mit 5 Kategorien (0: 0-5%, 1: 5-25%, 2: 25-50%, 3: 50-75%, 4: 75-100%) gegen 8 Subtypen von Leberkrebs (eine Nominalvariable)
- Passende Teststatistiken: pro Zelle mindestens 5 Einträge vorhanden, dann Chi-Quadrat Test nutzen, ansonsten Fisher's Exact Test
- Regression aufgrund der kleinen Fallzahl in einigen Gruppen nicht empfehlenswert

Diese Bescheinigung garantiert nicht die richtige Umsetzung der in der Beratung gemachten Vorschläge, die korrekte Durchführung der empfohlenen statistischen Verfahren und die richtige Darstellung und Interpretation der Ergebnisse. Die Verantwortung hierfür obliegt allein dem Promovierenden. Das Institut für Biometrie und klinische Epidemiologie übernimmt hierfür keine Haftung.

Datum: 14.04.2023

CHARITÉ Name der Beraterin: Nilufar Akbari

[redacted]

UNIVERSITÄTSMEDIZIN BERLIN
Institut für Biometrie und
Klinische Epidemiologie
Campus Charité Mitte
Charitéplatz 1 | D-10117 Berlin
SitZ: Reinhardtstr. 58

Unterschrift BeraterIn, Institutsstempel